austenite, so that at any stage of the reaction, the carbon concentration of the residual austenite x_γ changes with the fraction of transformation. Thus, the growth condition depends on the instantaneous value of x_γ, so that an increment of volume fraction is only permitted if:

$$x_\gamma^{ij} < x_{To}^i \tag{4.8}$$

where x_{To}^i is the concentration of carbon in slice i at temperature T_i where austenite and ferrite of the same composition have the same free energy. It is given by the T_o curve computed for the particular slice concerned.

The calculation begins with all slices being fully austenitic. For the first step ($j = 1$) B_s temperatures are calculated for all the slices. If for any slice, $B_s^i < T_i$ then that slice remains untransformed throughout the experiment. For slices which are below their B_s^i temperatures, a small amount of bainite is permitted to form, giving a volume fraction increment of ΔV. This increment of transformation changes the carbon concentration in the unreacted regions of the slices according to the equation

$$x_\gamma^{ij} = \overline{x} + \frac{V_{ij}(\overline{x} - x_\alpha)}{(1 - V_{ij})} \tag{4.9}$$

where V_{ij} and x_γ^{ij} are, respectively, the total volume fraction of bainitic ferrite, and the total carbon concentration of the residual austenite in slice i at stage j of the calculation. x_α is the amount of carbon which is left in the bainitic ferrite, either in solid solution or in the form of carbides precipitated from supersaturated ferrite. Hence, for $j > 1$, an increment of transformation is only allowed in any given slice if for that slice $x_\gamma^{ij} < x_{To}^i$. The mean volume fraction of transformation in the alloy as a whole at stage j is given by:

$$\overline{V}_j = \sum_i V_{ij}/N. \tag{4.10}$$

The calculation is stopped when all slices cease to transform; $x_\gamma^{ij} = x_{To}^i$ for all i.

We consider first the case where the slices transform independent of each other, i.e., without any diffusion of carbon between slices. This is the more likely circumstance because the sheaf morphology of bainite in general ensures that regions of residual austenite are isolated from one another, so that carbon does not homogenise over large distances.

To decide on the number of slices into which the alloy should be divided, the calculations were carried out for several values of N (Fig. 4.14). The results of the calculations converged as N tended towards 100 (the curves for $N = 80$ and $N = 100$ are virtually identical in Fig. 4.14), so that all subsequent computations were carried out with $N = 100$. Fig. 4.15a illustrates how the number of non-transforming slices varies as a function of transformation temperature and the stage of the calculation. At higher transformation temperatures (i.e., lower driving forces), a large number of the substitutional-solute enriched slices are above the B_s temperature and do not participate at all in the transformation process. This is consistent with the observation of untransformed bands in the samples reacted at higher temperatures (Figs. 4.1 and 4.9). As the carbon concentration of the residual austenite increases during transformation and approaches the appropriate x_{T_o} value, there is for each transformation temperature an abrupt increase in the number of non-transforming slices (Fig. 4.15a). The slope of the last part of each curve in Fig. 4.15 is determined by the degree of inhomogeneity in the alloy; for a homogenous alloy it is expected to be infinite in slope.

The calculations use a finite increment ΔV of transformation for successive stages of the reaction. Clearly, the precision of the method is expected to deteriorate as ΔV increases; Fig. 4.15b illustrates how the calculated maximum volume fraction of transformation to upper bainite depends on the magnitude of the increment used. The variations in the calculated results are not large, but are significant at higher transformation temperatures where the absolute maximum volume fraction is in any case rather low, and the use of a large ΔV also seems to give a lower degree of discrimination between the different transformation temperatures. For these reasons, all subsequent calculations were carried out using $\Delta V = 0.00005$.

The increase average carbon concentration of the residual austenite during the reaction is illustrated in Fig. 4.16, where the maximum value in each case is determined *approximately* by the T_o curve of the phase diagram; the values are not exactly determined by the T_o curve because each slice has a different substitutional alloy content (and hence a different T_o curve), so that the maximum value reflects an averaged effect.

4.2.3 Comparison between experiment and theory

Calculations of the maximum volume fractions of bainitic ferrite expected by isothermal transformation were carried out using the computer model described above, and compared with experimental data (Table 4.1) in Figs. 4.17a, b, c. The agreement is found to be reasonable, both in an absolute sense (Figs. 4.17a, b), and in predicting the different behaviours of the as-received and homogenised samples (Fig. 4.17c). For example, for most of the data, both theory and experiment show a higher degree of transformation in the homogenised samples, and both show a reversal of trend as the transformation temperature approaches the B_s temperature of the homogenised alloy.

The fact that the homogenised samples in general show a higher degree of transformation when compared with the more heterogeneous samples was explained earlier on two grounds. Firstly, the nucleation of bainite occurs uniformly throughout the homogeneous samples, while it is restricted to the substitutional-solute depleted regions in the segregated samples. Secondly, since the carbon that partitions from the bainitic ferrite essentially remains trapped locally between the ferrite subunits, the untransformed regions of the heterogeneous sample which are rich in substitutional alloy content are unable to act as sinks for the excess carbon, so as to allow further transformation in the substitutional-solute depleted regions.

The significance of this last effect can be examined theoretically using the computer model with the additional condition that after every increment ΔV of transformation, the carbon is allowed to redistribute and homogenise between the slices. This should allow the substitutionally-enriched regions to act as sinks for excess carbon, thereby promoting further reaction in the substitutionally-depleted regions. The fact that the carbon does not homogenise during transformation is emphasised by the results presented in Figs. 4.17d and 4.17e, where the calculated data (assuming that carbon homogenises between the slices) are seen to overestimate the volume fraction of bainite.

The results (Fig. 4.17f) also show that if carbon *is* permitted to homogenise in the residual austenite after every increment of transformation, the volume fraction of transformation in the heterogeneous samples should always exceed that in the homogenised samples. This idea is difficult to test experimentally, because the nature of a bainite sheaf is such that film-like regions of austenite become trapped between the subunits of

bainite. This isolates them from the other regions of austenite, thereby preventing the long-range homogenisation of carbon. On the other hand, if the transformation could be forced to proceed at a very slow rate, such that the time between the formation of successive subunits is large enough to allow the carbon to diffuse over long distances, then it would be experimentally possible to allow the substitutionally-enriched regions to act as sinks for the excess carbon. This was done by studying transformation behaviour, for both as-received and homogenised samples, during continuous cooling experiments. The experiments were based on the idea that as the samples cool through the transformation temperature range, they should experience small increments in transformation. If the cooling rate is sufficiently slow, it should permit substantial, if not complete, homogenisation of the rejected carbon.

The results of the continuous cooling experiments are presented in Figs. 4.18 and 4.19. The experiments were carried out at cooling rates between $6 - 215^{\circ}C\,\mathrm{hr}^{-1}$. The results from the slowest cooling rate used confirm the theoretical prediction (Fig. 4.20) that if an opportunity is provided for carbon to homogenise in the residual austenite during transformation, then the heterogeneous samples should transform to a greater extent then those which are homogenised (Fig. 4.19). As the cooling rate increases, the possibility of long-range carbon diffusion diminishes and Fig. 4.19 shows that the results tend towards those obtained during isothermal transformation, i.e., the degree of transformation in higher in the homogenised samples at high undercoolings, the reverse being true at low undercoolings.

4.3 Conclusions

It has been demonstrated that when 300M steel is isothermally transformed to bainite, the kinetics and maximum extent of transformation are sensitive to the presence of relatively small levels of chemical segregation, of the kind commonly associated with commercial samples. During isothermal transformation at high undercoolings, the maximum degree of bainitic ferrite obtained is found to be larger for homogenised samples because bainite is able to nucleate uniformly throughout the samples and because the carbon that is rejected into the residual austenite after transformation is trapped by isolated regions of austenite. In the heterogeneous samples, the bainite nucleates mainly in the substitutional-solute depleted regions and furthermore, the

untransformed subtitutional-solute enriched regions are unable to act as effectively as sinks for excess carbon, as would be the case if all regions of austenite were freely connected.

At very low undercoolings, the extent of isothermal transformation is found to be larger in the heterogeneous samples, since at such undercoolings, the transformation is nucleation dominated. Thus, regions of the heterogeneous samples are able to transform at temperatures above the bainite-start temperature of the homogenised alloy.

It has been shown that if an opportunity is provided for carbon to distribute evenly throughout the residual austenite during the development of the bainitic microstructure, then the extent of transformation is always larger for the heterogeneous samples when compared with the homogenised samples.

The experimental results have been rationalised using a theoretical model for the bainite reaction in heterogeneous steels. The model is based on the hypothesis that the growth of bainite is diffusionless, but that the excess carbon in the bainitic ferrite is immediately afterwards partitioned into the residual austenite.

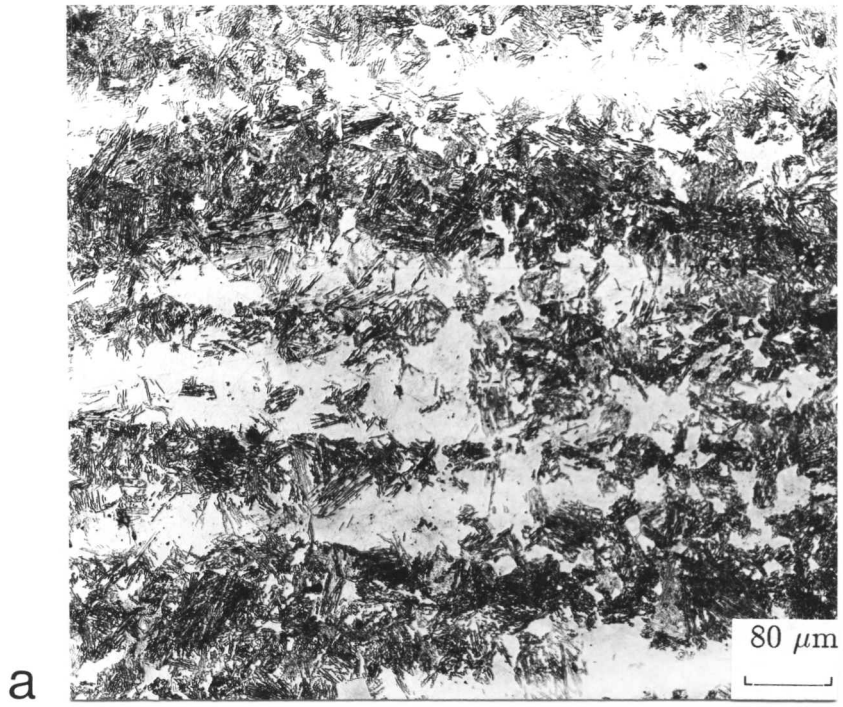

a

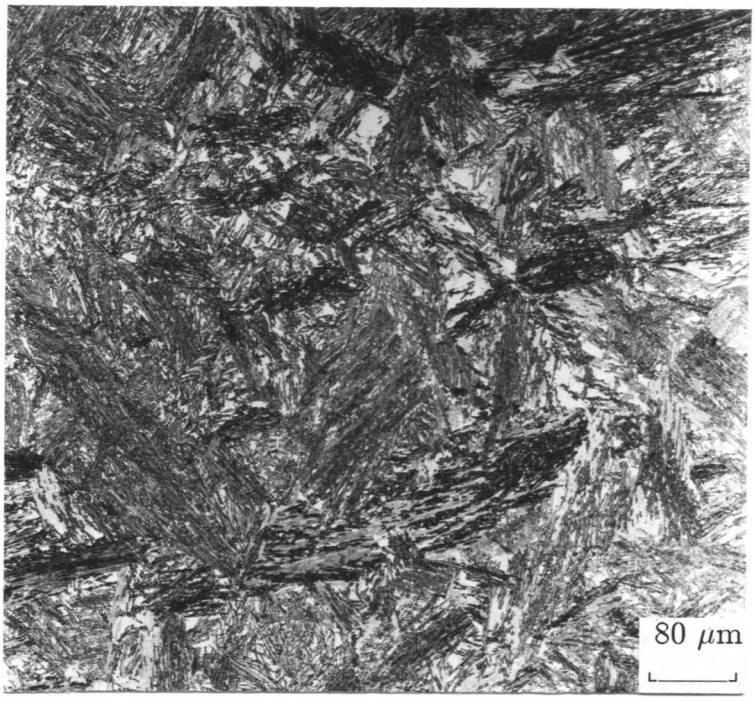

b

Fig. 4.1: *(a) Optical micrographs illustrating the banded microstructure obtained in the heterogeneous 300M steel after isothermal transformation at 400 °C (for 90 minutes) until reaction completion. (b) Corresponding optical micrograph for the homogenised sample of isothermally transformed 300M steel. For both samples, the dark etching regions are mainly bainitic and the lighter etching regions contain mainly untempered martensite, obtained during the quench from the isothermal transformation temperature.*

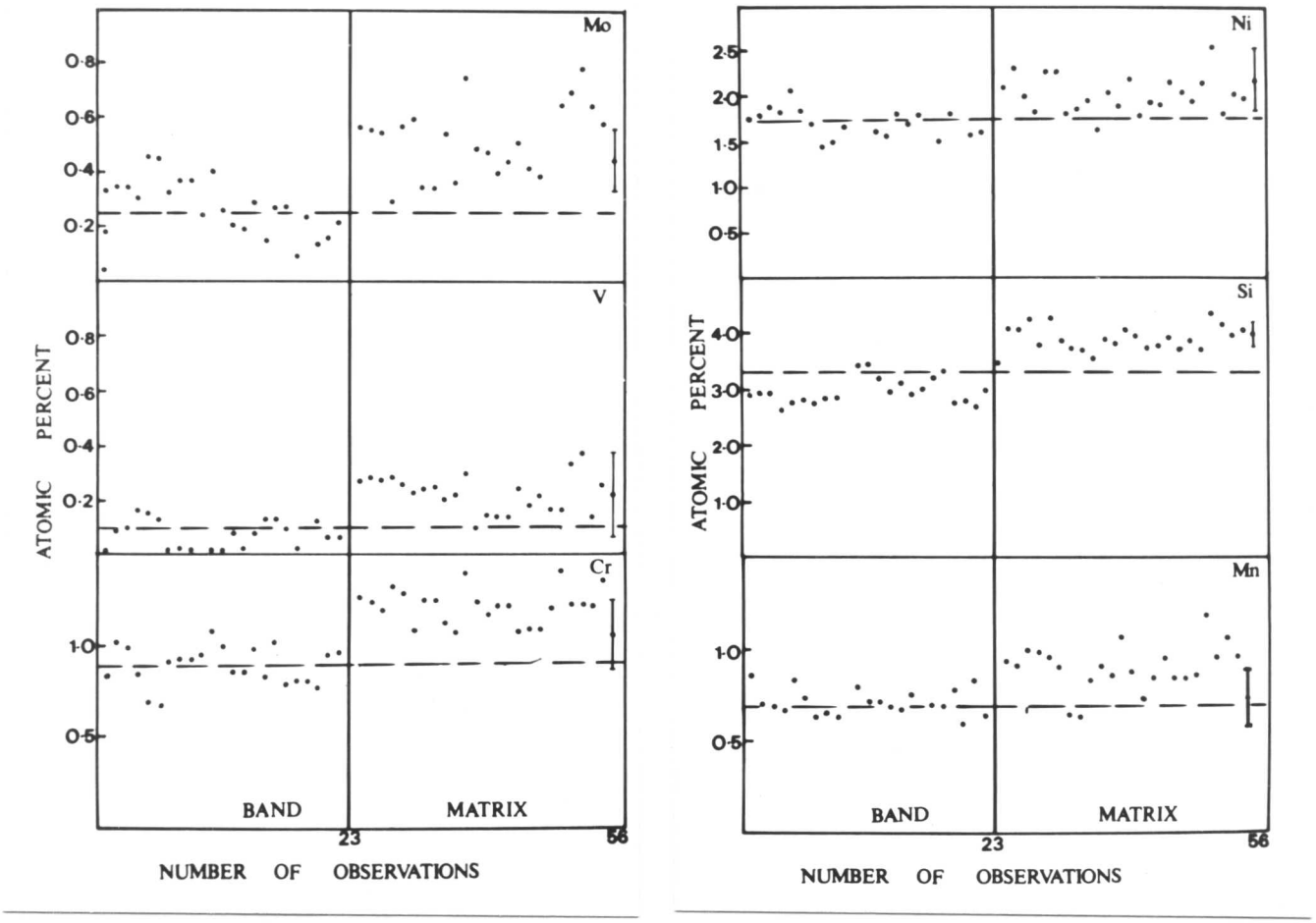

Fig. 4.2: *Microanalysis data from heterogeneous samples of 300M steel which were austenitised at 950 °C and then isothermally transformed at 400 °C (for 90 minutes) until reaction ceased. The regions designated "matrix" were essentially untransformed at the isothermal transformation temperature, whereas those designated "band" consisted predominantly of bainitic ferrite. The error bars indicate the typical 95% confidence statistical error and the average composition is in each case indicated by the dashed horizontal line.*

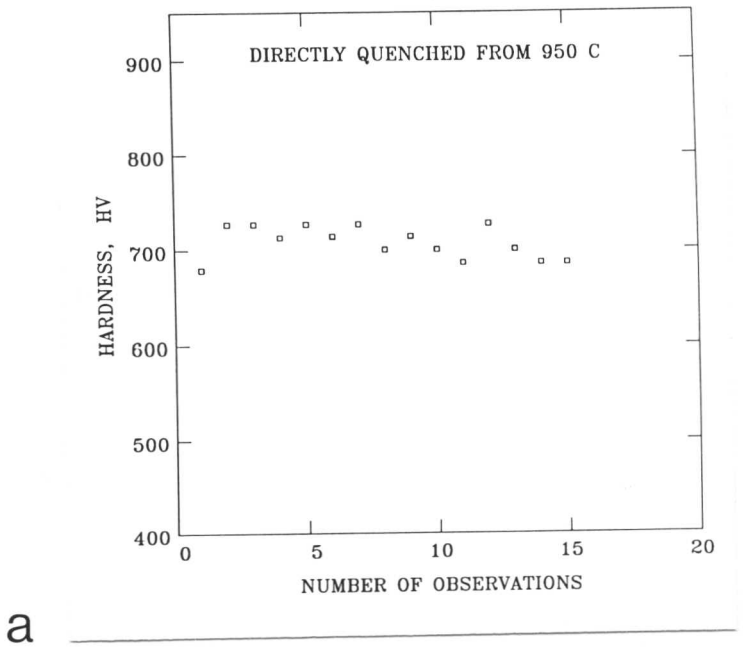

a

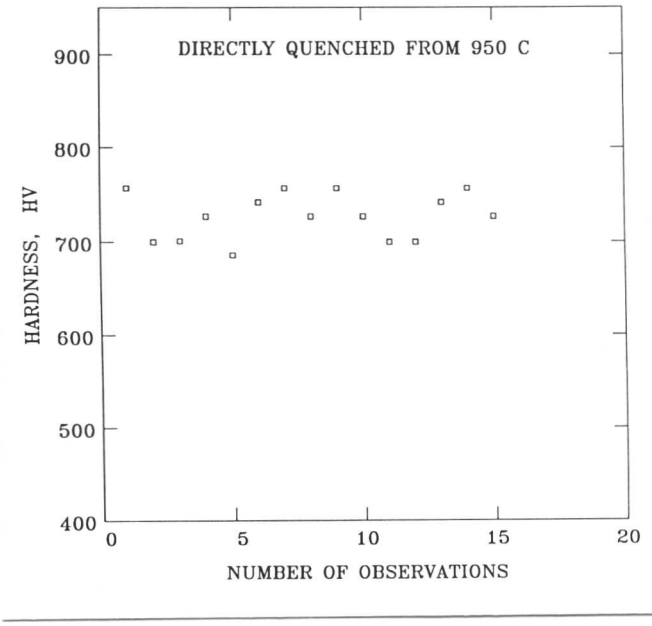

b

Fig. 4.3: *(a) Vickers Hardness tests (50g load) from a fully martensitic sample of homogenised 300M steel. (b) Vickers hardness tests (50g load) from a fully martensitic sample of heterogeneous 300M steel.*

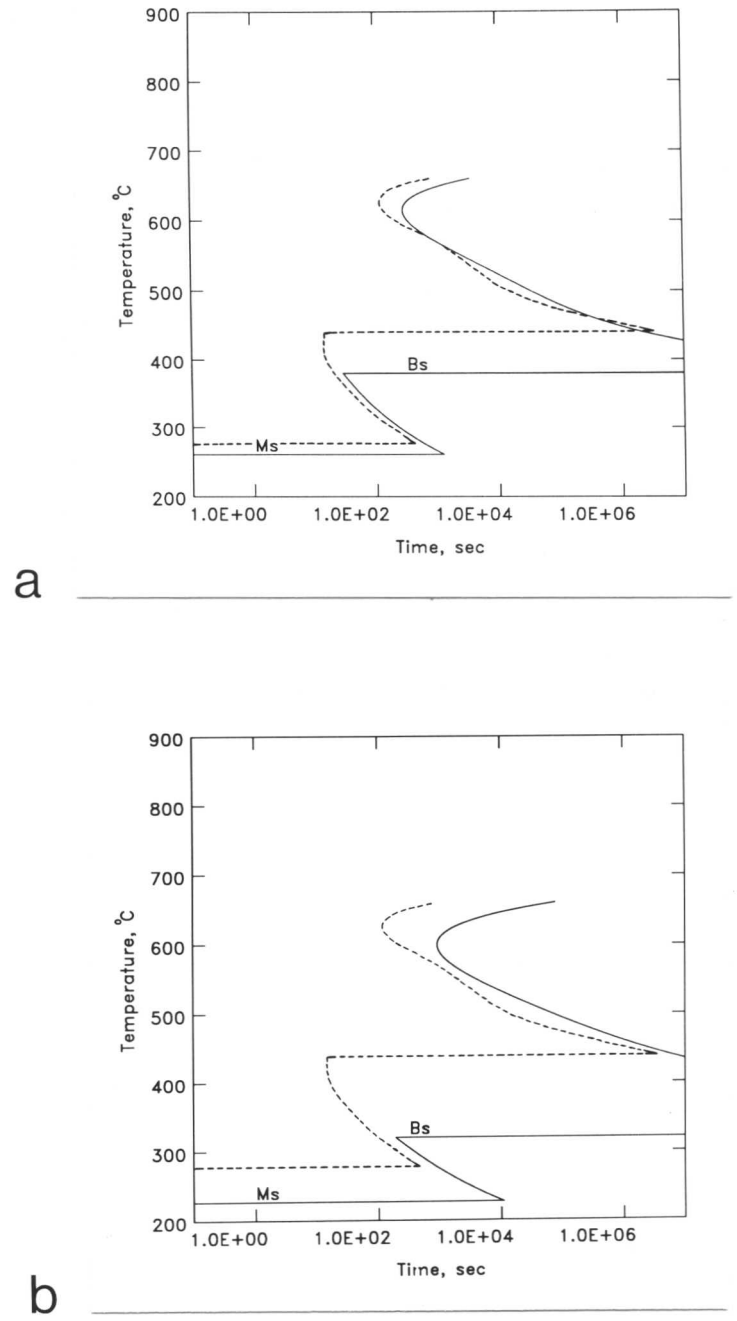

Fig. 4.4: *Calculated time-temperature-transformation (TTT) diagrams (for reaction initiation) showing the influence of adding an excess of solute to the 300M steel of average composition as used in the present work. (a) Ni; (b) V; (c) Cr; (d) Mn; (e) Mo; (f) Si. The dashed curves represent the time taken to initiate transformation in 300M steel of the base composition, and the continuous curves for the steel with the relevant excess solute addition. The concentration of excess solute added is 1wt.% in all cases except Si, where a 2wt.% excess has been added in order to produce a discernable effect. Notice that in all cases (except Si), the bainite and martensite reaction are retarded by the extra solute addition.*

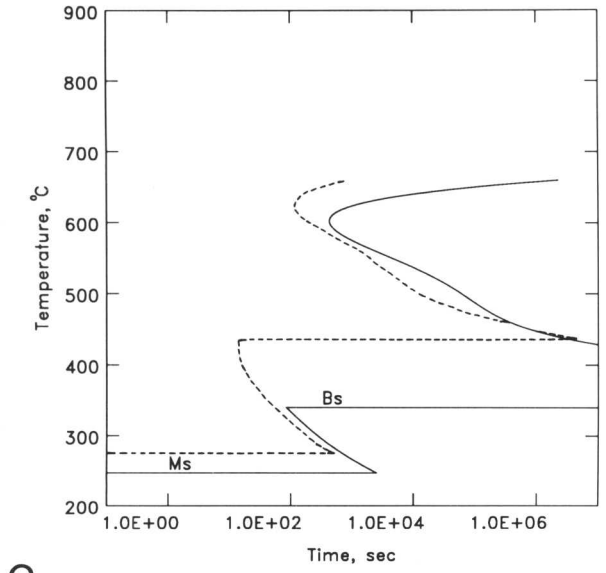

c

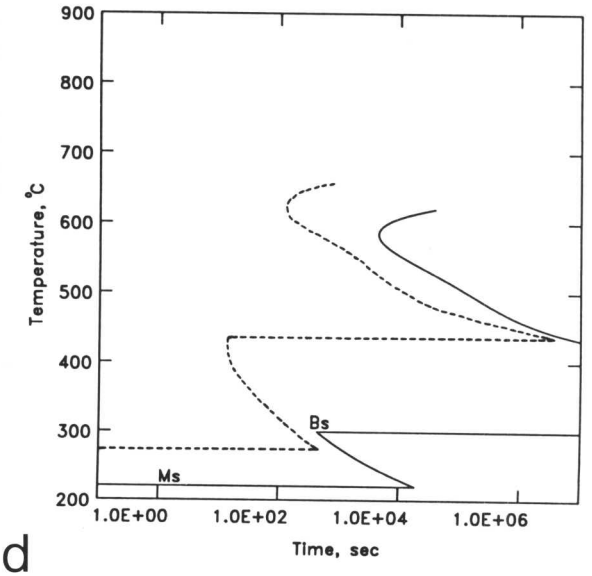

d

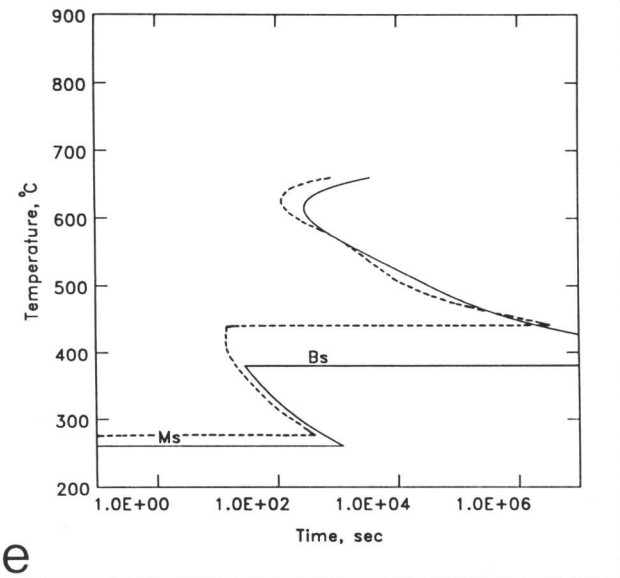

e

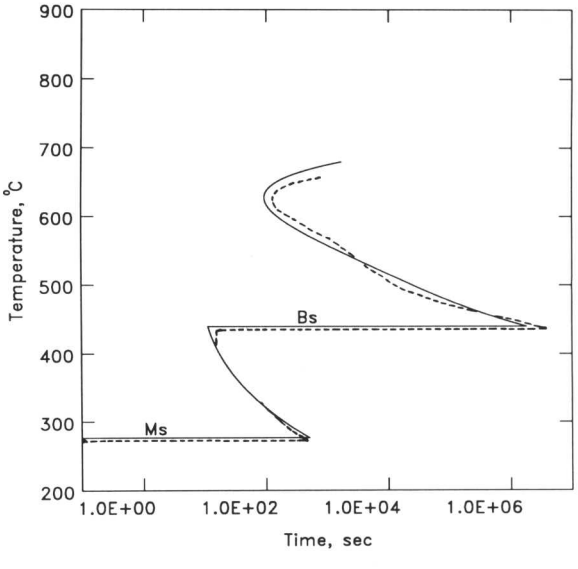

f

Fig. 4.4:*(continued .....) (c) Cr; (d) Mn; (e) Mo; (f) Si.*

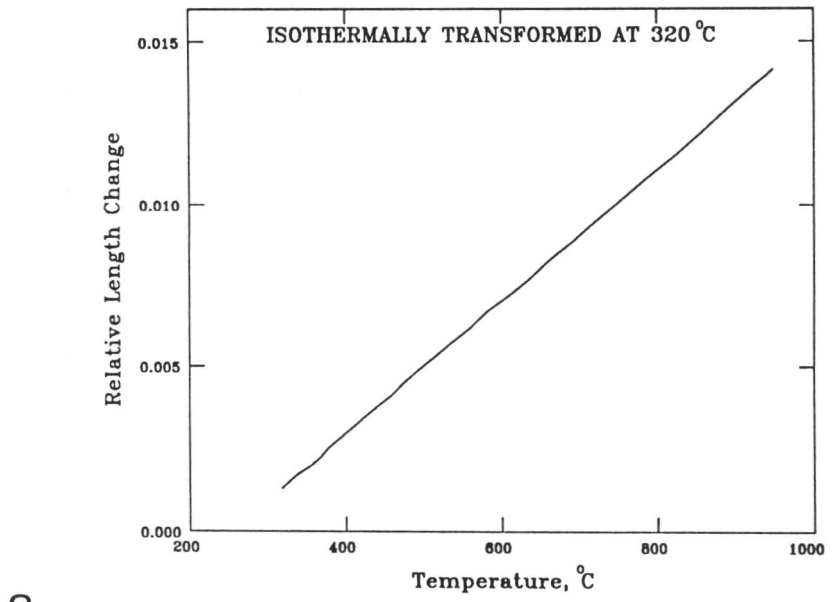

a

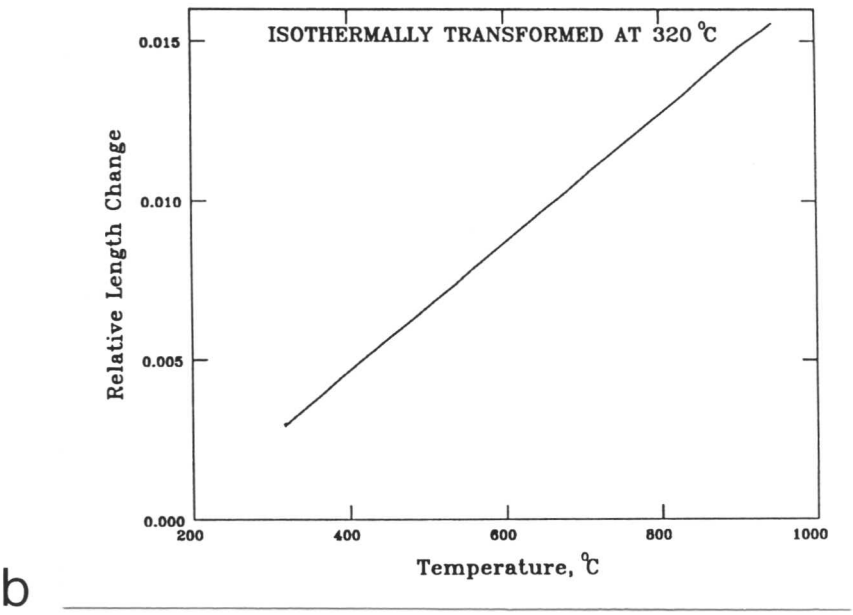

b

Fig. 4.5: *Dilatometric curves showing the linear variation of relative specimen length as a function of temperature during cooling from the austenitising temperature to the isothermal transformation temperature. (a) Homogenised sample; (b) Heterogeneous sample.*

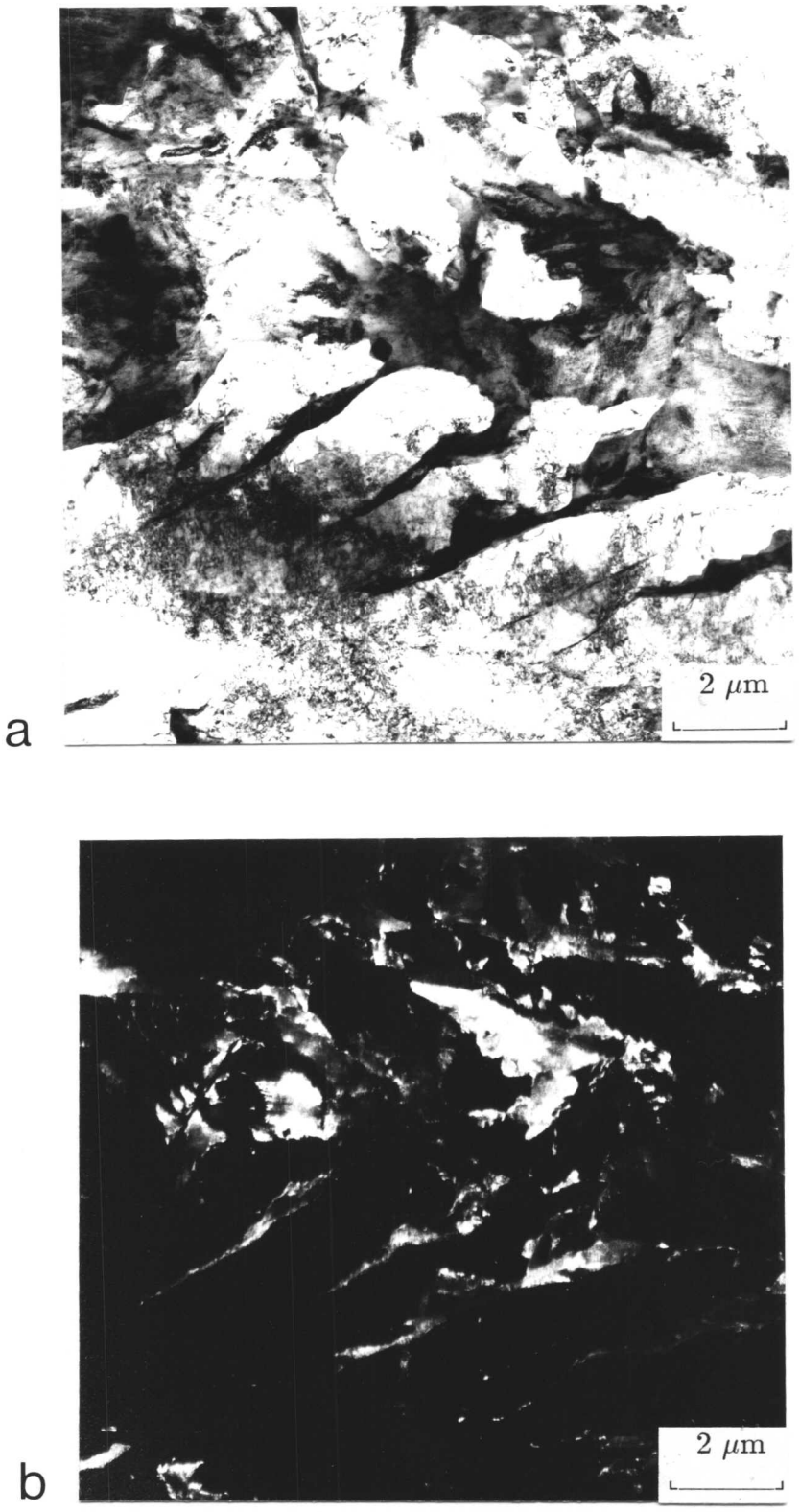

Fig. 4.6: *(a) Bright field transmission electron micrograph from a homogeneous sample of 300M steel, isothermally transformed to upper bainite at 400 °C for 90 minutes before quenching to ambient temperature. Shows sheaves of bainite consisting of subunits of bainitic ferrite separated by regions of retained austenite (and martensite); (b) corresponding retained austenite dark-field image.*

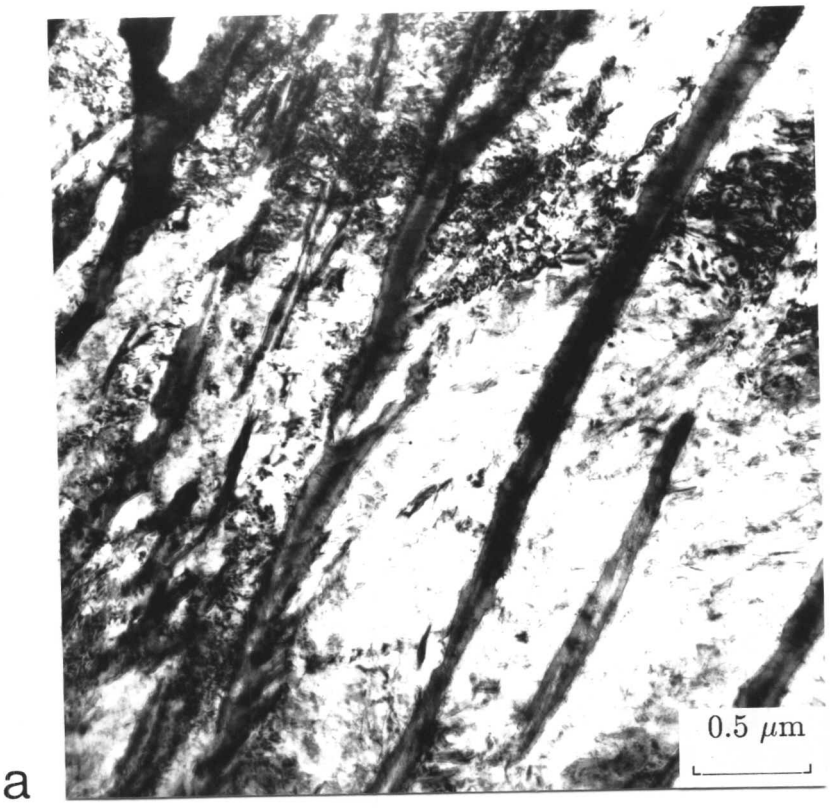

a

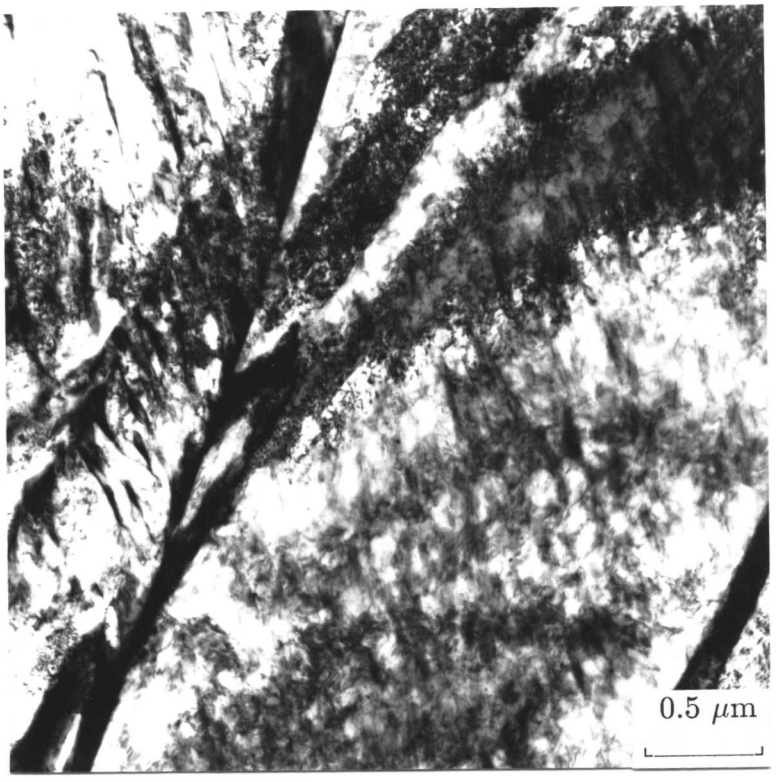

b

Fig. 4.7: *Mixed microstructure of upper and lower bainite obtained by isothermal transformation of homogeneous 300M steel at 320 °C for 60 minutes before quenching to ambient temperature. (a) Bright field image of upper bainite; (b) same sample, but showing lower bainite.*

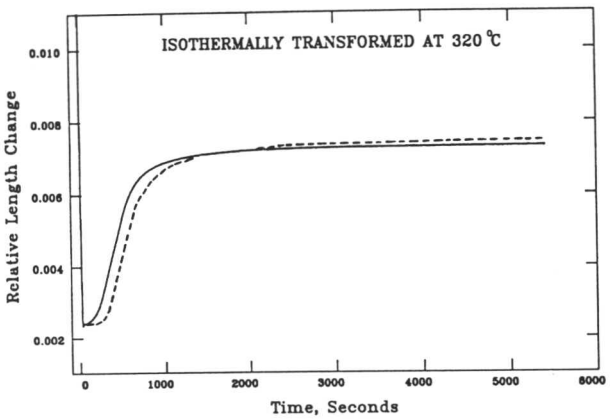

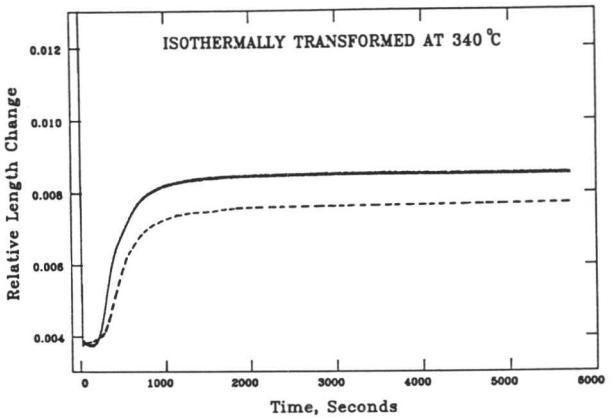

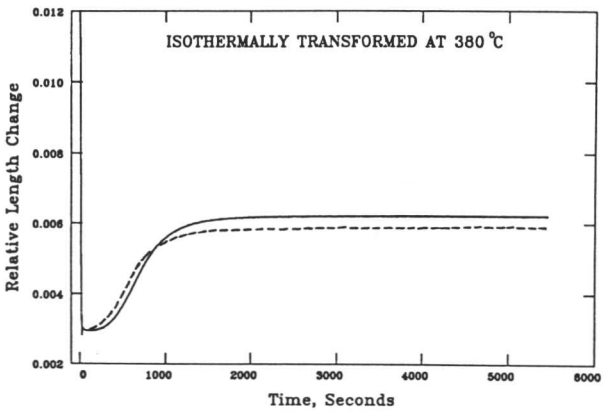

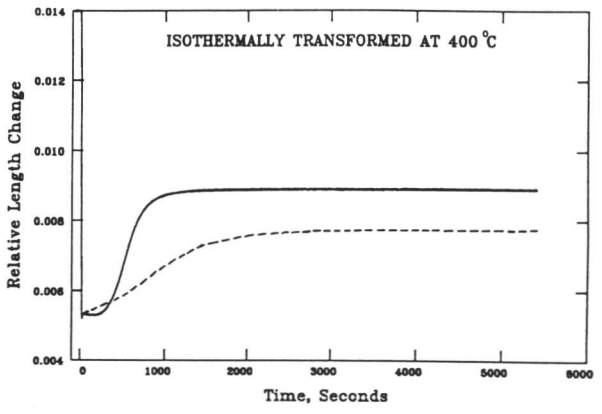

Fig. 4.8: *Dilatometric curves for samples of 300M steel isothermally transformed at the temperatures indicated. The continuous curves are for the homogenised samples and the dashed curves for the heterogeneous samples. Data on the limiting volume fractions obtained are given in Table 4.1.*

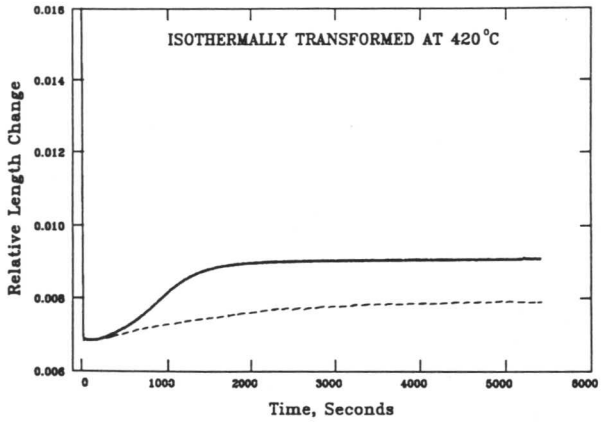

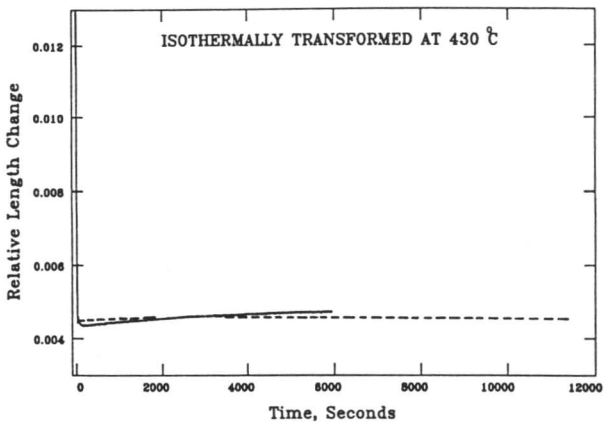

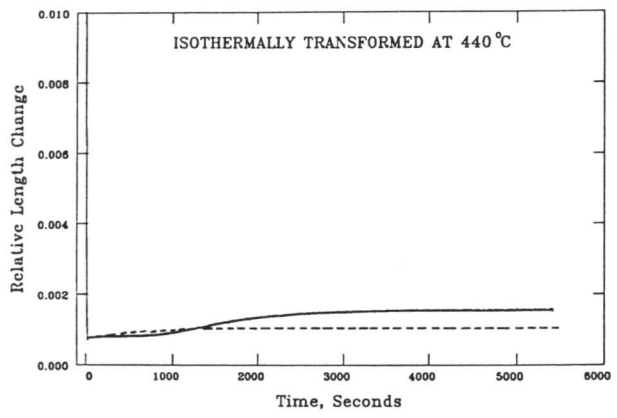

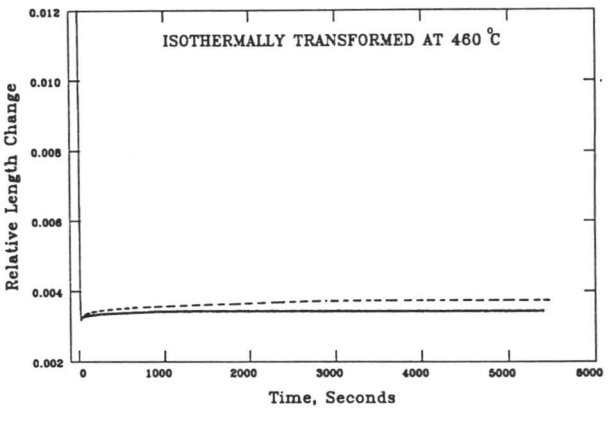

Fig. 4.8: *(continued .....)*

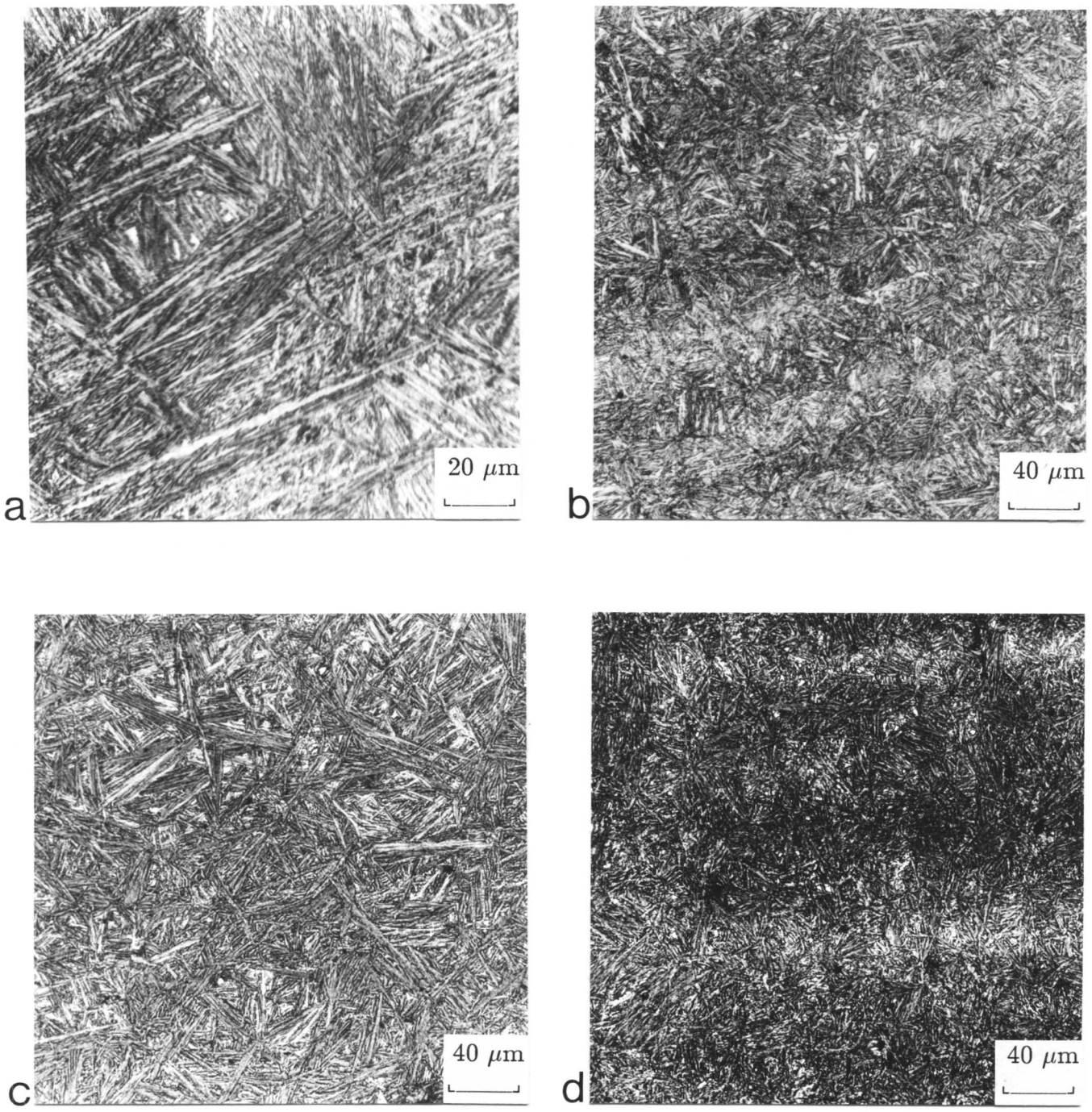

Fig. 4.9: Metallographic confirmation of the curves shown in Fig. 4.8.

(a) Optical micrograph of the homogeneous specimen isothermally transformed at 320 °C.

(b) Optical micrograph of the heterogeneous specimen isothermally transformed at 320 °C.

(c) Optical micrograph of the homogeneous specimen isothermally transformed at 340 °C.

(d) Optical micrograph of the heterogeneous specimen isothermally transformed at 340 °C.

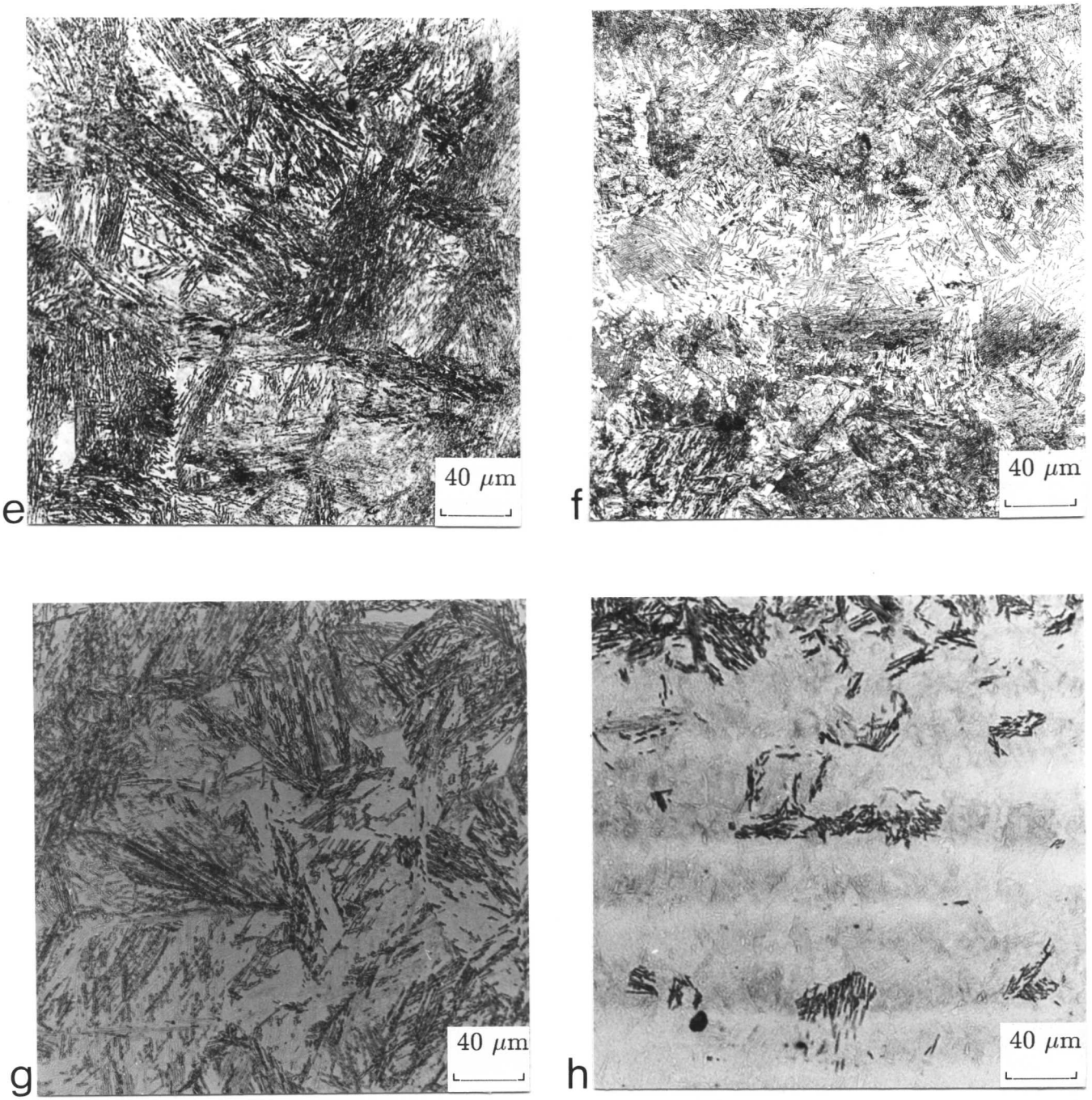

Fig. 4.9: (continued .....)

(e) Optical micrograph of the homogeneous specimen isothermally transformed at 380 °C.

(f) Optical micrograph of the heterogeneous specimen isothermally transformed at 380 °C.

(g) Optical micrograph of the homogeneous specimen isothermally transformed at 420 °C.

(h) Optical micrograph of the heterogeneous specimen isothermally transformed at 420 °C.

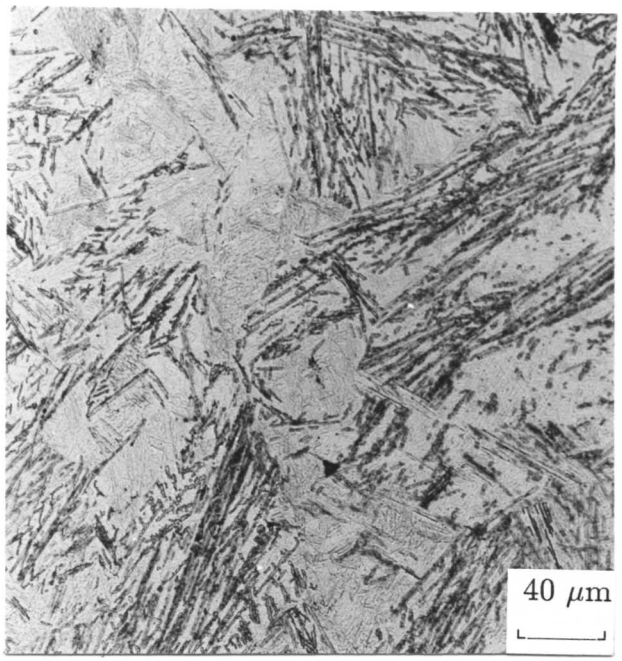

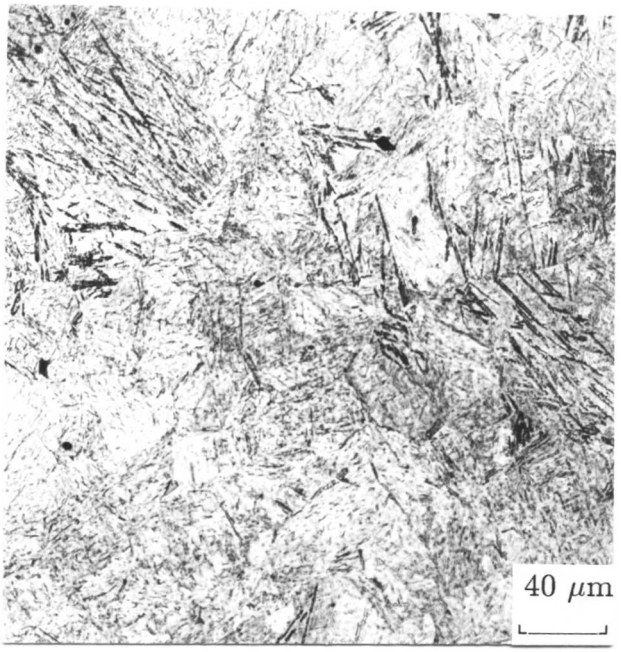

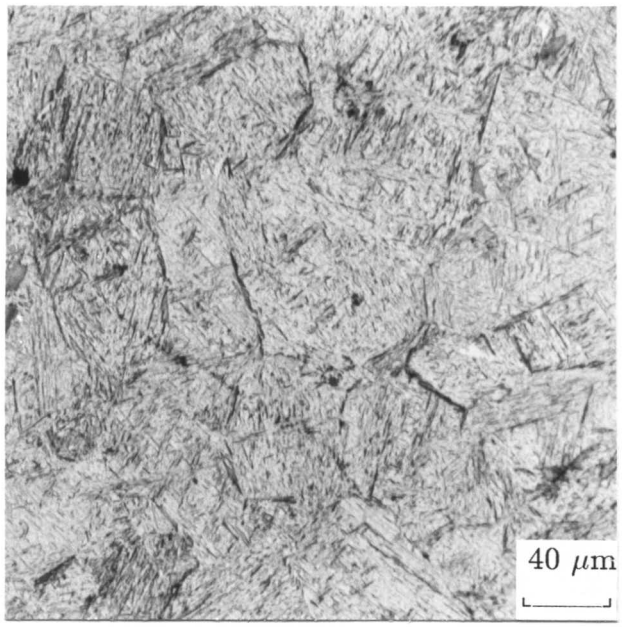

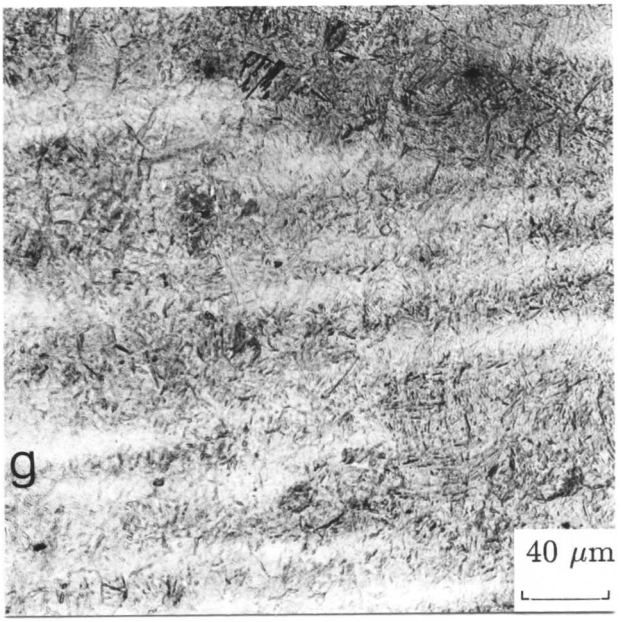

Fig. 4.9: (continued .....)

(i) Optical micrograph of the homogeneous specimen isothermally transformed at 440 °C.

(j) Optical micrograph of the heterogeneous specimen isothermally transformed at 440 °C.

(k) Optical micrograph of the homogeneous specimen isothermally transformed at 460 °C.

(l) Optical micrograph of the heterogeneous specimen isothermally transformed at 460 °C.

Isothermal Transformation Temperature °C	Experimental Volume Fraction	
	Homogeneous	Heterogeneous
320	0.63	0.64
340	0.60	0.48
380	0.45	0.40
400	0.50	0.33
420	0.34	0.14
430	0.06	0.04
440	0.11	0.07
450	0.02	0.03
460	0.03	0.05

Table. 4.1: *Dilatometrically determined maximum volume fractions of bainitic ferrite obtained by isothermal transformation at the temperatures indicated, for both the as-received and homogenised samples of 300M steel.*

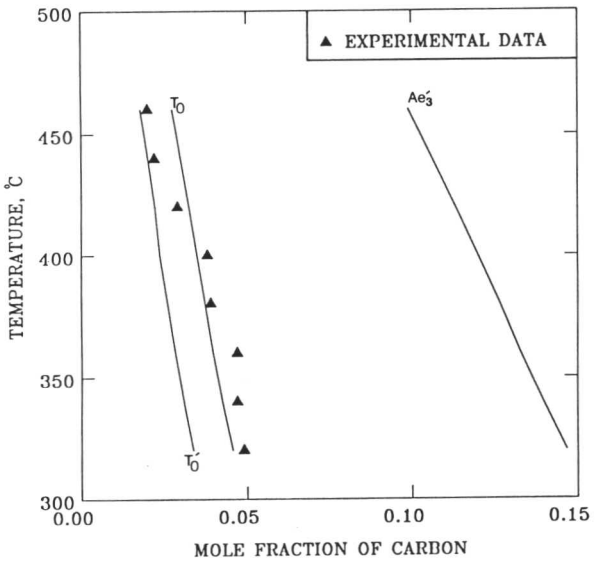

Fig. 4.10: *Calculated T_o, T'_o, and A'_{e3} phase boundaries for 300M steel. The experimental data are for samples transformed isothermally to upper bainite until reaction ceases.*

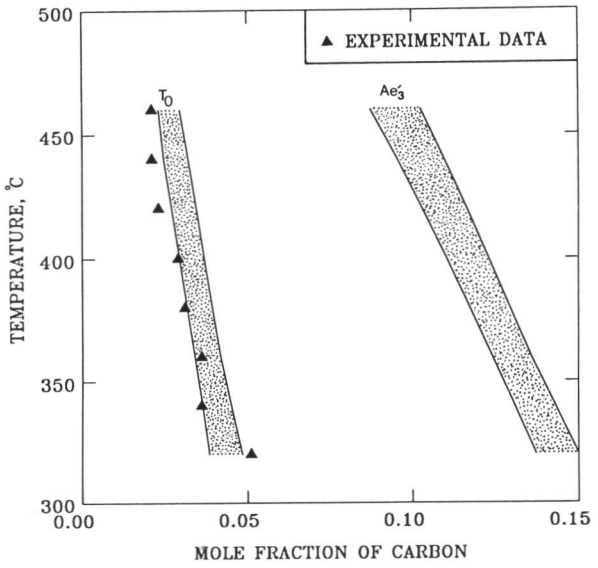

Fig. 4.11: *Calculated T_o and A'_{e3} phase boundaries for heterogeneous 300M steel, covering the range of chemical compositions detected experimentally. The experimental data are for samples transformed isothermally to upper bainite until reaction ceases.*

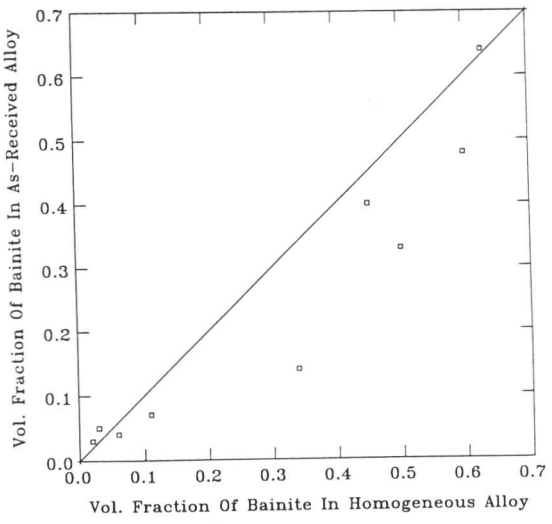

Fig. 4.12: *A plot of the maximum volume fraction of bainitic ferrite obtained by isothermal transformation in homogenised 300M steel, versus the corresponding volume fraction for as-received 300M steel. The line has a slope of unity, and serves to illustrate that except at transformation temperatures near B_s (where the degree of transformation possible is minimal), the extent of the transformation is larger in the homogenised samples.*

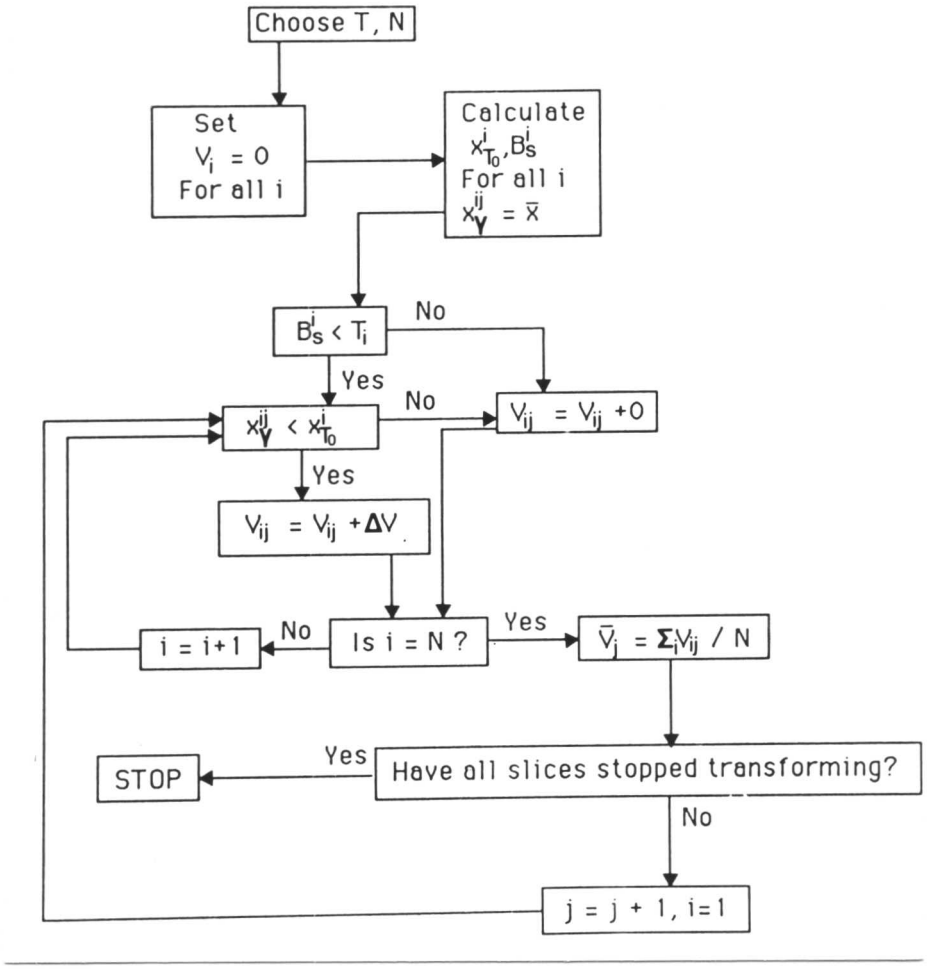

Fig. 4.13: *Flow chart illustrating the calculation procedure used to simulate the development of transformation in heterogeneous 300M steel.* T_i *represents the isothermal transformation temperature and the subscript* i *identifies the slice number and composition; the total number of slices is* N *The calculation is carried out in stages, with each stage identified by the subscript* j*. For each value of* j *(i.e., at each stage of the calculation), the volume fraction* V_{ij} *of bainite in each slice is incremented by a small fraction* ΔV *if transformation is feasible in that slice. The total volume fraction of bainite at stage* j *is thus given by* $\Sigma_i V_{ij}/N$*.*

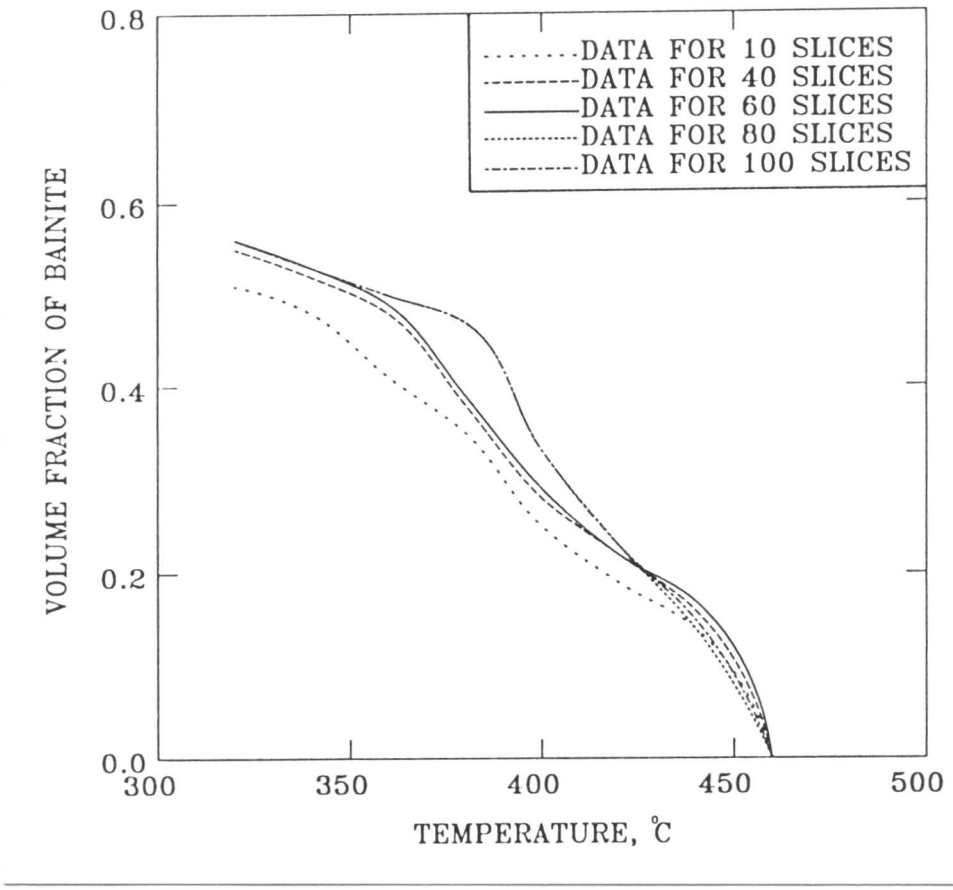

Fig. 4.14: *Variation in the calculated maximum volume fraction of upper bainitic ferrite as a function of transformation temperature and the number of slices N into which the heterogeneous alloy was rationally divided. Note that the calculations for N values of 80 and 100 are virtually superimposed.*

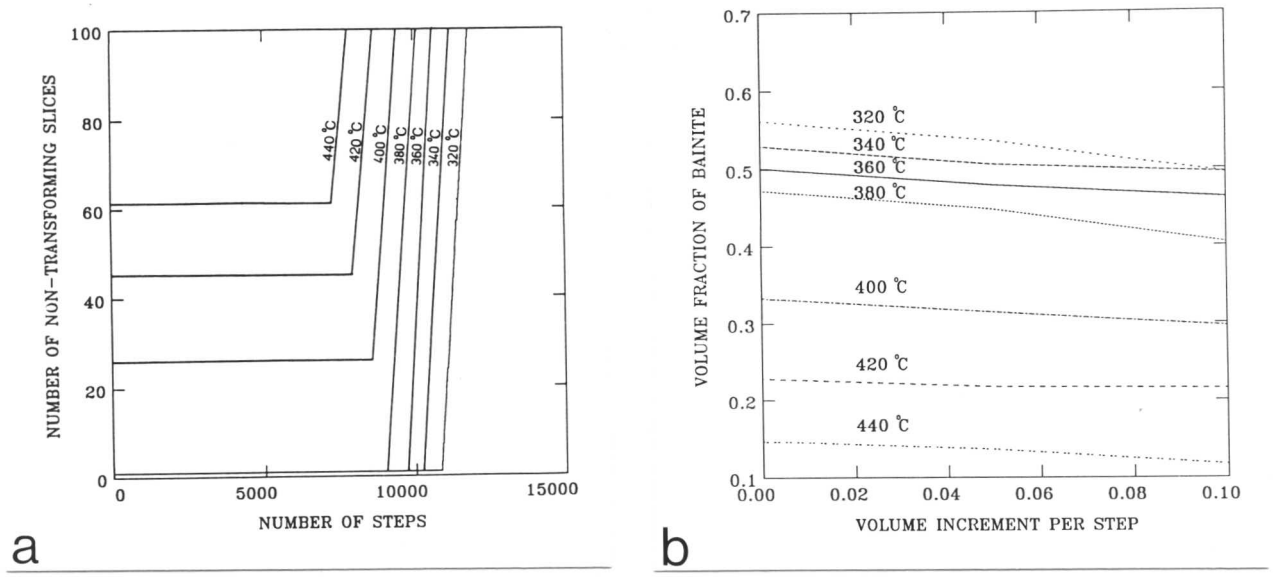

Fig. 4.15: *(a) Variation in the calculated number of non-transforming slices as a function of the stage of calculation (j). (b) Variation in the calculated maximum volume fraction of upper bainite as a function of the size of the increment ΔV of transformation.*

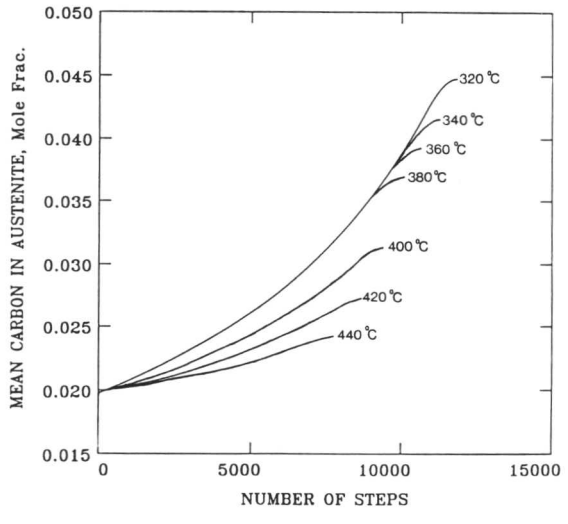

Fig. 4.16: *Variation in the calculated average carbon concentration of the residual austenite as a function of the stage of the calculation (j) and the isothermal transformation temperature, assuming that the transformation product is upper bainitic ferrite.*

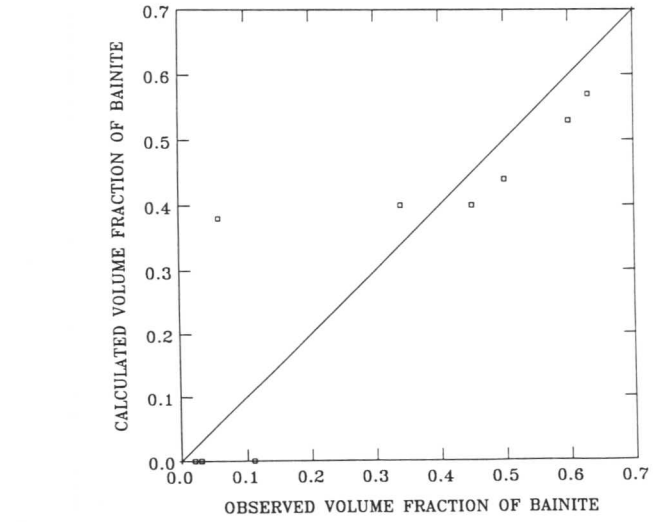

a

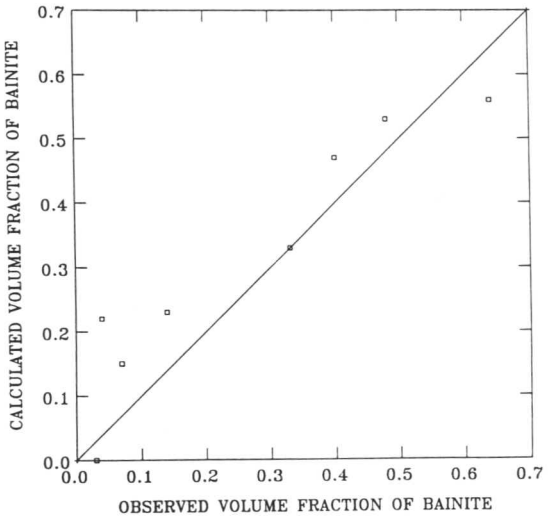

b

Fig. 4.17: *Comparison of the calculated (under circumstances when carbon is not allowed to homogenise in the residual austenite after each increment of transformation) and experimental maximum volume fractions of bainitic ferrite for (a) the homogenised alloy; (b) for the as-received alloy; (c) comparison of the homogenised and as-received alloys, for both the calculated (no homogenisation of carbon) and experimental data. Comparison of the calculated (under circumstances when carbon is allowed to homogenise in the residual austenite after each increment of transformation) and experimental maximum volume fractions of bainitic ferrite for (d) the homogenised alloy; (e) for the as-received alloy; (f) comparison of the homogenised and as-received alloys, for both the calculated (homogenisation of carbon) and experimental data. For all the above data, the transformation temperatures are as listed in Table 4.1; note however that small maximum volume fractions correspond to transformation temperatures near to the B_s temperature.*

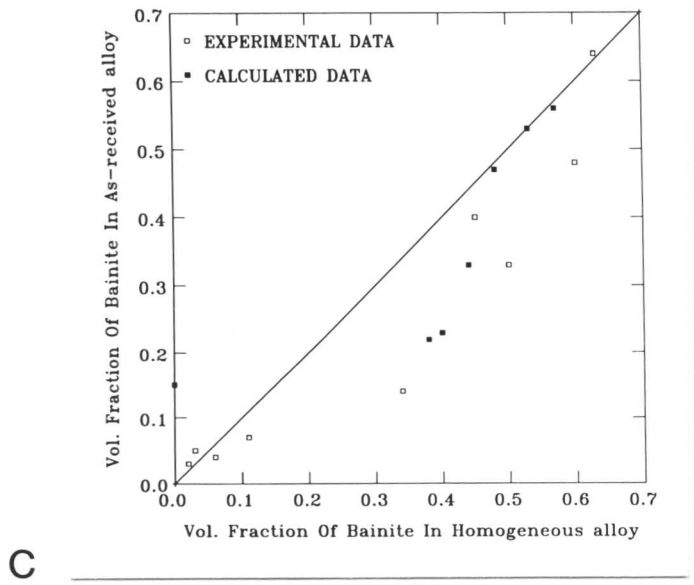

c

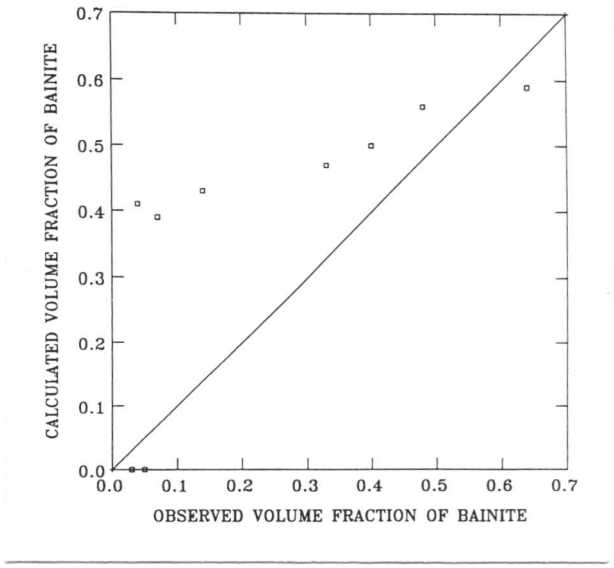

d

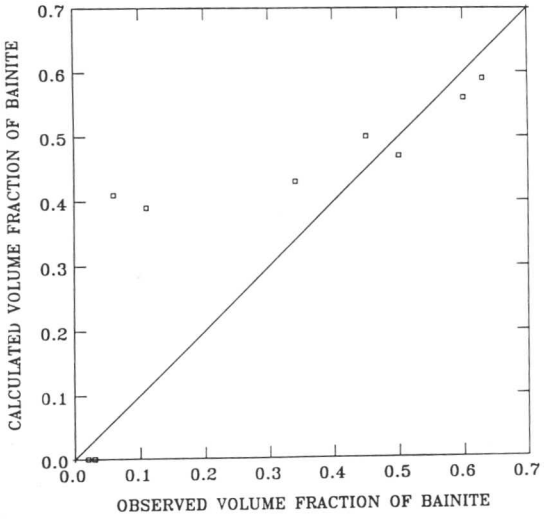

e

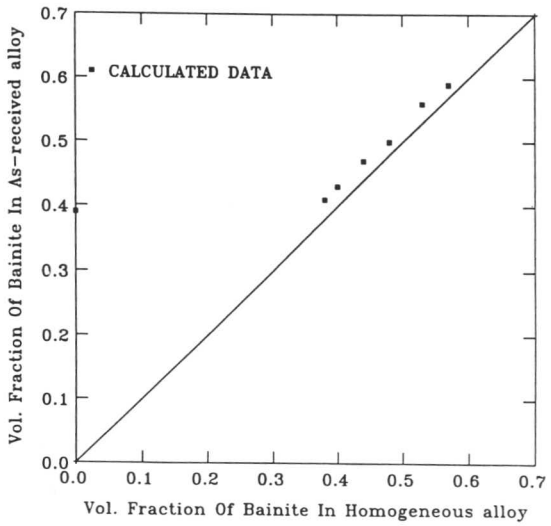

f

Fig. 4.17: *(continued .....)*

(c) comparison of the homogenised and as-received alloys, for both the calculated (no homogenisation of carbon) and experimental data. Comparison of the calculated (under circumstances when carbon is allowed to homogenise in the residual austenite after each increment of transformation) and experimental maximum volume fractions of bainitic ferrite for (d) the homogenised alloy; (e) for the as-received alloy; (f) comparison of the homogenised and as-received alloys, for both the calculated (homogenisation of carbon) and experimental data.

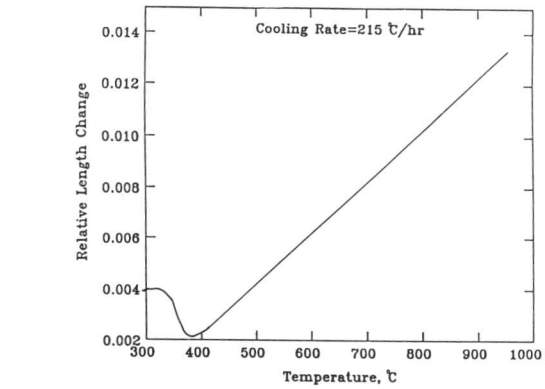

a

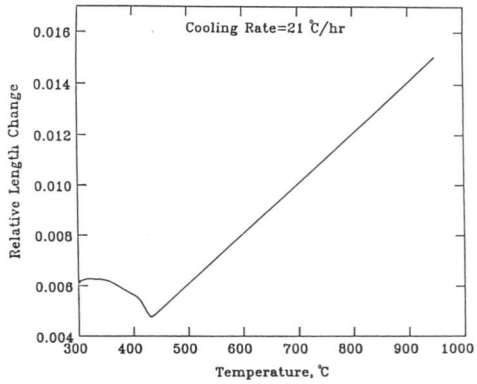

b

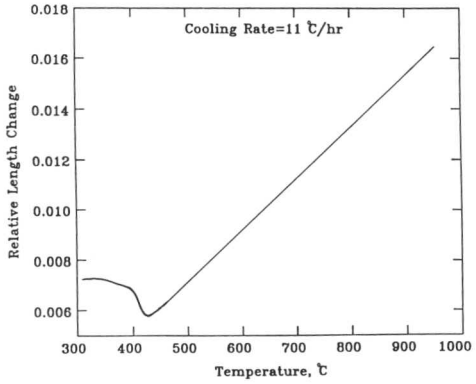

c

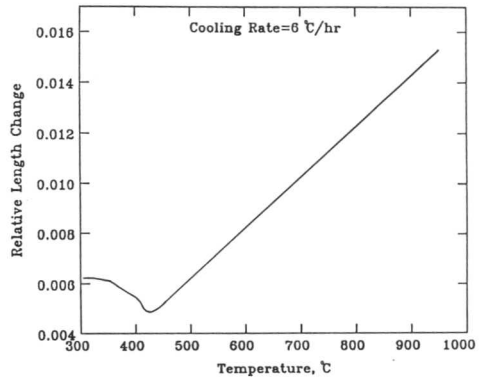

d

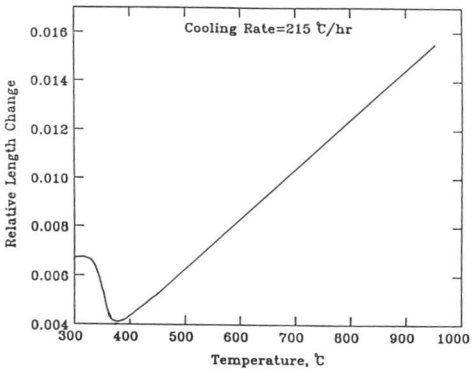

e

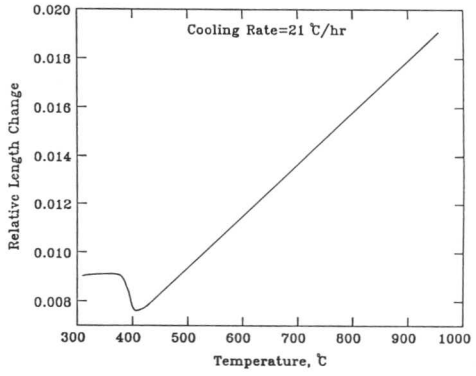

f

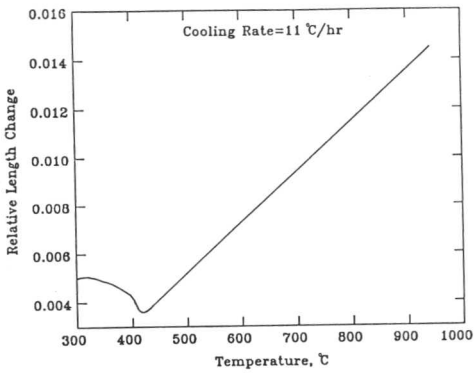

g

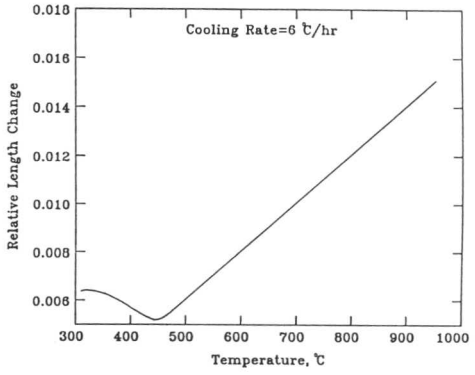

h

Fig. 4.18: *Continuous cooling transformation curves obtained using dilatometry, on the homogenised (a-d) and as-received (e-h) samples of 300M steel.*

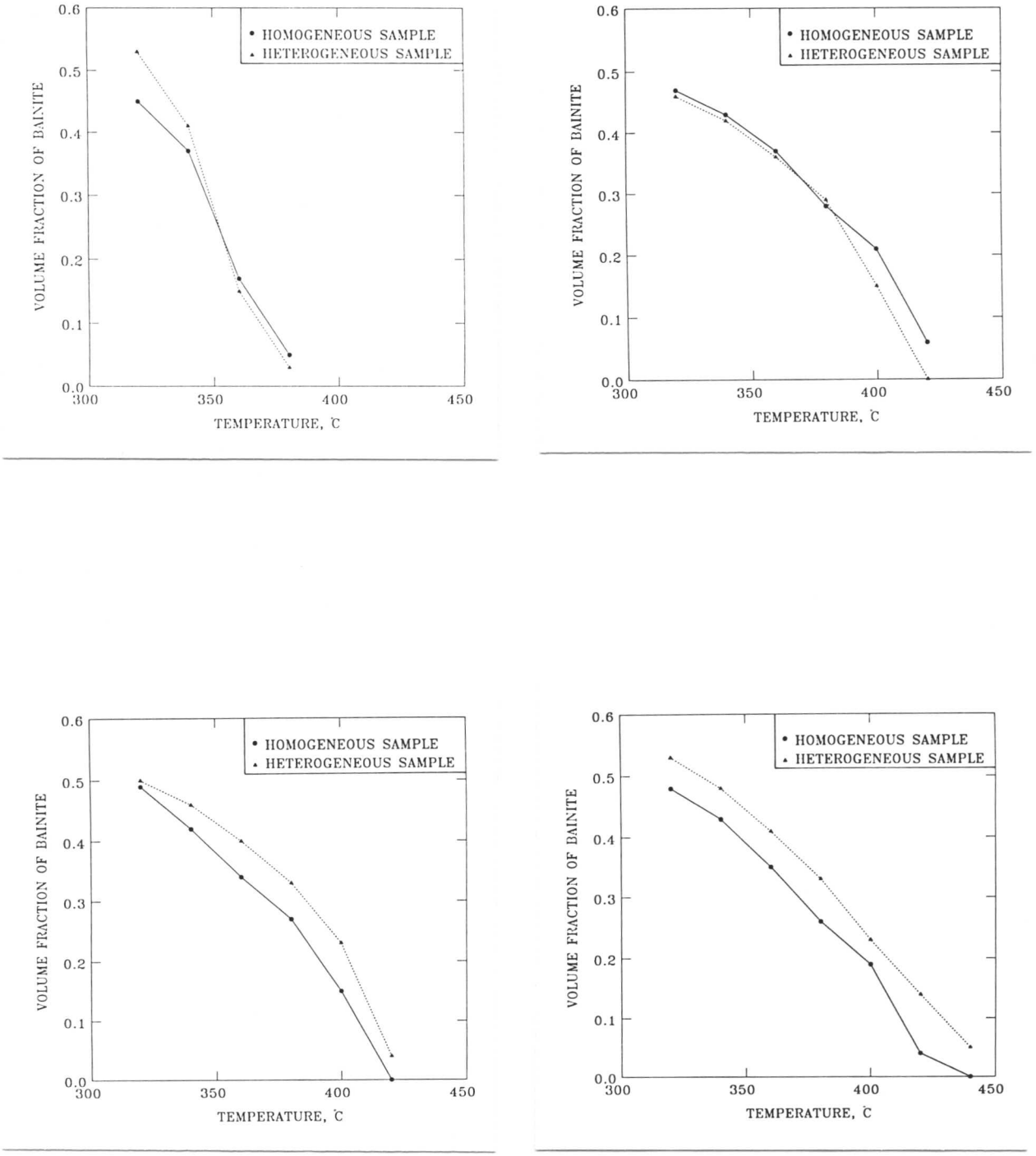

Fig. 4.19: *The information extracted from the data presented in Fig. 4.18, for the cooling rates 4, 0.35, 0.1833, 0.1 °C/min.*

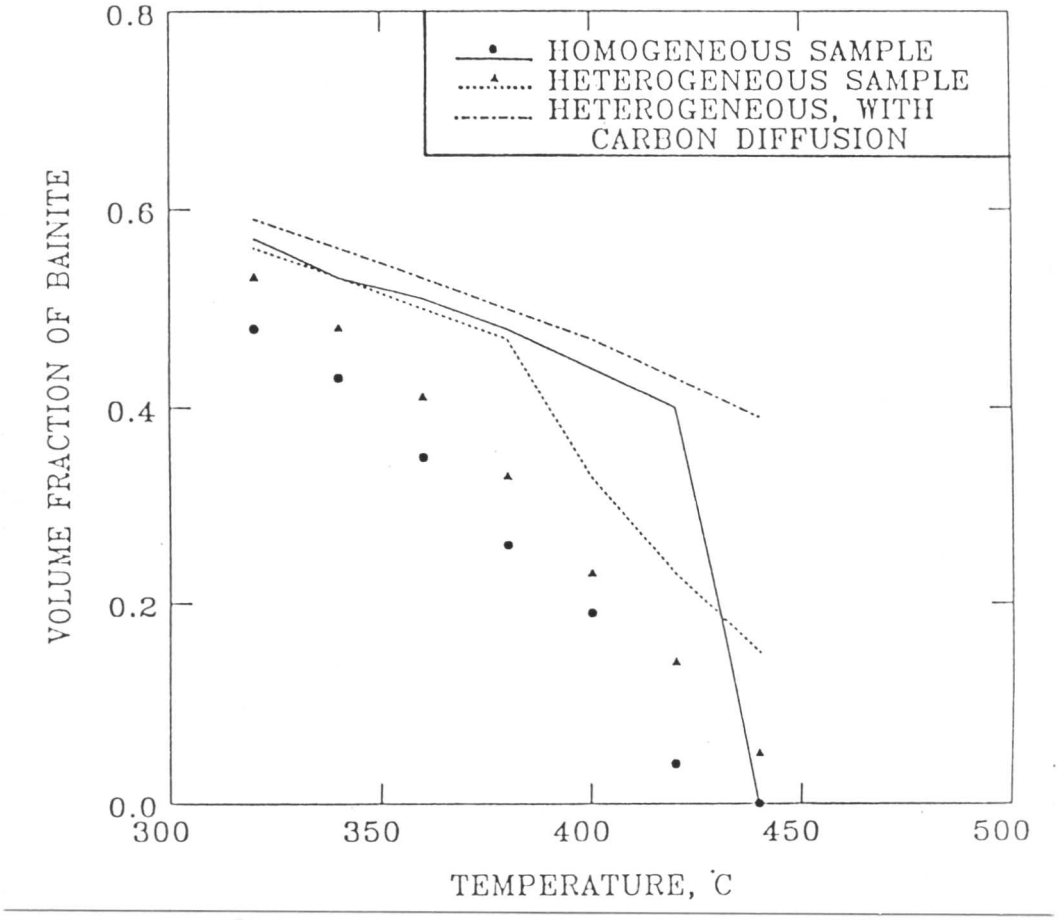

Fig. 4.20: *Results from continuous cooling transformation experiments on as-received and homogenised samples of 300M. The graphs represent the total volume fraction of bainite (calculated using the experimental data presented in Fig. 4.18) accumulated by continuous cooling transformation, as a function of the temperature to which the samples have cooled.*

REFERENCES

1. W. C. Leslie:*The Physical Metallurgy of Steels,* p. 289, McGraw-Hill Int. Book Company, New York, 1982.
2. F. B. Pickering:*Phase Transformations,* Series 3, Volume 2, p. VI-7, Institution of Metallurgists, London, 1979.
3. F. B Pickering:*Physical Metallurgy and the Design of Steels,* pp. 127, Applied Science Publishers Limited, London, 1978.
4. E. R. Parker:*Metall. Trans. A,* 1978, vol. 8A, p. 1025.
5. R. O Ritchie and R. M. Horn:*Metall. Trans. A,* 1977, vol. 9A, p. 331.
6. R. M. Horn and R. O. Ritchie:*Lawrence Berkley Laboratory Report LBL 6607,* November 1977.
7. H. K. D. H. Bhadeshia and D. V. Edmonds:*Metal Science,* 1983, vol. 17, p. 411.
8. H. K. D. H. Bhadeshia and D. V. Edmonds:*Metal Science,* 1983, vol. 17, p. 420.
9. V. T. T. Miihkinen and D. V. Edmonds:*Materials Science and Technology,* 1987, vol. 3, p. 422.
10. V. T. T. Miihkinen and D. V. Edmonds:*Materials Science and Technology,* 1987, vol. 3, p. 432.
11. V. T. T. Miihkinen and D. V. Edmonds:*Materials Science and Technology,* 1987, vol. 3, p.441.
12. J. W. Christian and D. V. Edmonds:*Phase Transformations in Ferrous Alloys,* p. 293, editors A. R. Marder and J. I. Goldstein, The Metallurgical Society of AIME, Warrendale, Pennsylvania, 1983.
13. H. K. D. H. Bhadeshia and D. V. Edmonds:*Acta Metallurgica,* 1980, vol. 28, p. 1265.
14. H. K. D. H. Bhadeshia:*Metal Science,* 1981, vol. 15, p. 175.
15. H. K. D. H. Bhadeshia:*Metal Science,* 1982, vol. 16, p. 159.
16. H. K. D. H. Bhadeshia:*Journal de Physique,* 1982, vol. 43, p. 435.
17. D. J. Dyson and B. Holmes:*Journal of the Iron and Steel Institute*, 1970, vol. 277, pp. 469.
18. H. K. D. H. Bhadeshia:*Acta Metallurgica,* 1981, vol.29, p. 1117.

Chapter 5

KINETICS OF MARTENSITIC TRANSFORMATION IN PARTIALLY BAINITIC 300M STEEL

NOMENCLATURE AND ABBREVIATIONS

a_γ	Lattice parameter of the carbon-enriched residual austenite
a_α, c_α	Lattice parameters of tetragonal martensite
B_s	Bainite–start temperature
f	Fraction of austenite transformed to martensite
M_S	Martensite–start temperature
M_F	Martensite–finish temperature
N_i	Number of original nucleation sites for martensite per unit volume of sample
N	Number of new martensite plates per unit volume of austenite
N_v	Number of new martensite plates per unit volume of sample
T_B	Temperature at which sample is transformed to bainitic ferrite and carbon enriched residual austenite
T_Q	Temperature to which the sample is cooled below M_S
$\Delta G^{\gamma\alpha'}$	Driving force for diffusionless transformation
$\overline{V}$	Average volume per newly formed plate
$V_{\alpha'}$	Absolute volume fraction of martensite
V_γ	Volume fraction of austenite present in the sample prior to martensitic transformation
V_{γ_r}	Volume fraction of austenite retained at room temperature
V_{α_b}	Volume fraction of bainitic ferrite

5.1 Introduction

Mixed microstructures consisting of bainite and martensite are usually a consequence of inadequate heat–treatment or the use of steels with insufficient martensite–hardenability in applications involving heavy sections. Early research [1–3] suggested that the presence of bainite in an otherwise martensitic microstructure generally leads to a deterioration in ductility, toughness and strength.

Contrary to these generally pessimistic indications of the properties of mixed microstructures, more recent work by Tomita and Okabayashi[4,5] has tended to indicate that in some circumstances, the presence of bainite in a predominantly martensitic microstructure enhances both strength and toughness relative to the single phase samples. They explained their results by postulating that as the lower bainite subdivides regions of austenite, there is in effect a refinement of the austenite grain size and consequently a refinement of the martensite packet size on the subsequent transformation of austenite. This leads to a strengthening of the martensite via a grain size effect. In addition, the strength of the bainite is supposed to be enhanced by the constraint provided to its deformation by the stronger martensite.

Thus, mixed microstructures of bainite and martensite are bound to become more prominent commercially, but are also of interest from a fundamental point of view, to reveal the influence of partial bainitic reaction on the subsequent formation of martensite. An attempt is therefore made here to model the development of martensitic transformation in a high–silicon, medium carbon steel, with the commercial designation "300M", with the particular aim of rationalising the formation of martensite in samples which already contain some bainitic ferrite. For this reason, some of the samples studied were quenched directly from the austenitisation temperature, while others were first transformed isothermally to bainitic ferrite, before cooling to ambient temperature to allow some of the residual austenite to decompose to martensite. The studies were carried out both on chemically segregated, "as–received" samples, and for comparison purposes, on samples homogenised by prolonged heat–treatement at a high temperature.

The work presented here extends earlier research [6,7], which focused on the development of the bainite reaction, to the modelling of the subsequent transformation of some of the residual austenite into martensite. The ultimate aim of this research

program is to develop phase transformation theory which will permit the prediction of microstructural evolution in commercial steels which contain high silicon concentrations. Such steels have a demonstrated potential as far as good combinations of strength and toughness are concerned [8–12]. Commercial steels are usually chemically heterogeneous, and such segregation is known [13–21] to cause significant changes in the kinetics and thermodynamics of the phase transformations; it was also intended to investigate the effect of the segregation on martensitic transformation.

5.2 Dilatometry

The dilatometric specimens were quenched to room temperature after an appropriately long time at the isothermal temperatures T_B (until the bainite reaction ceased), for a variety of temperatures below the bainite–start temperature (B_s). Dilatometric curves showing the relative length change due to transformation as a function of temperature are shown in Fig. 5.1

In these curves, any deviation from a straight line as the specimen cools represents the onset of martensitic transformation, so that a martensitic–start temperature (M_S) can be determined. This relies on the experimental observation that the austenite in the 300M steel used has a constant thermal expansivity over the temperature range of interest[6,7]. The expansion that occurs when austenite transforms to martensite is then detected as the deviation described earlier.

As expected, a higher martensite–start temperature was observed when the sample had been transformed partially to bainite at a higher temperature (T_B), since a lower maximum volume fraction of bainite is obtained as T_B is raised. It is also evident that the M_S temperature of the residual austenite♣ is higher for heterogeneous specimens when compared with the chemically homogeneous samples (Fig. 5.2). This is consistent with the fact that relatively less bainite forms in heterogeneous samples, so that the residual austenite then contains a lower carbon concentration relative to homogeneous specimens heat–treated in an identical manner [7]. As a result, the tendency to form martensite is more pronounced in heterogeneous samples. This is also reflected in the

♣ *The term "residual austenite" refers to that which exists at the reaction temperature during isothermal transformation to bainite. "Retained austenite" refers to the austenite which remains untransformed after cooling the specimen to ambient temperature.*

calculated data presented in Fig. 5.2, since for identical transformation conditions, it is established that more bainitic ferrite can be obtained in the homogeneous samples, giving a higher degree of carbon–enrichment in the residual austenite in those samples, and hence lowering the martensite–start temperature of the residual austenite. The carbon concentration of the residual austenite (x_γ) was calculated from the volume fraction of bainite, assuming a homogeneous distribution of carbon in austenite.

$$x_\gamma \simeq \overline{x} + \frac{V_{\alpha_b}(\overline{x} - x_\alpha)}{1 - V_{\alpha_b}}. \tag{5.1}$$

where $\overline{x}$ is the average carbon concentration of the alloy and x_α is the carbon concentration of the bainitic ferrite. Since the latter is always rather small when compared with $\overline{x}$, it is assumed here to be given by the carbon concentration of ferrite which is in equilibrium with austenite in a Fe–C alloy, as calculated[22] using the McLellan and Dunn quasichemical thermodynamic model [23].

The calculations assume a homogeneous distribution of carbon in the residual austenite, and hence underestimate the martensite–start temperature (Fig. 5.2). The real distribution of carbon is known to be inhomogeneous following bainitic ferrite growth [24–27], so that the relatively dilute regions will tend to transform martensitically at higher temperature. Consistent with this, the degree of underestimation is found to decrease as the volume fraction of bainitic ferrite decreases (*i.e.*, T_B increases). Observation of occasional pockets of twinned martensite through electron microscopy confirms the presence of high carbon regions (Fig. 5.3).

As a check on the M_S calculations, a homogeneised sample was quenched directly to ambient temperature; a martensite–start temperature (M_S) of 280 °C was observed, and this agrees reasonably with the thermodynamically calculated [28,29] M_S temperature of 276 °C.

As expected, further length changes were observed as the samples were cooled below the M_S temperature, as more of the residual austenite decomposed martensitically. The relationship between the amount of martensite formed as a function of undercooling below the M_S temperature was, as expected, found to be nonlinear. The volume fraction of martensite produced at first is small; the extent of transformation as a function of undercooling below M_S then increases, although it eventually begins to decrease towards zero as the amount of unreacted austenite decreases towards zero, or as the small quantity left untransformed stabilises to further decomposition.

The "martensite–finish temperature" (M_F) is not a meaningful concept from a fundamental point of view, because the reaction progresses with further and eventually, decreasing increments of volume fraction as the temperature is reduced below M_S, in principle never reaching completion. Small amounts of retained austenite thus remain stable even at very low temperatures. The transformation of the last traces of austenite becomes more and more difficult as the amount of austenite decreases probably due to mechanical stabilisation[30,31] (Fig. 5.1).

The temperature range over which martensite forms is usually a characteristic of the specific alloy composition and particularly, the carbon concentration. The range is generally greater when the residual austenite has a lower carbon content. It can be seen from Fig. 5.1 that the range $M_S - M_F$ is always greater in the heterogeneous specimens when compared with the homogeneous samples, especially for low values of T_B. This is to be expected since each of the heterogeneous samples in effect consists of a composite of different alloys, each of which will have its own transformation range. The superposition of these ranges should consequently give a larger overall value of $(M_S - M_F)$ when compared with the homogeneous samples. Figure 5. 1 shows that martensite formation starts at lower temperatures in the homogeneous samples and reaches apparent "completion" sooner than the corresponding heterogeneous samples.

5.2.1 Calculation of Volume Fraction

Dilatometric data in the form of the relative length change $\Delta L/L$ (where L is the length of the sample at ambient temperature, and ΔL is the change in length due to transformation) were converted into the fraction (f) of austenite which is transformed to martensite using the following relationship:

$$f = \frac{3\Delta L a_\gamma^3}{V_\gamma L(2a_\alpha^2 c_\alpha - a_\gamma^3)} \tag{5.2}$$

where a_γ is the lattice parameter of the the carbon–enriched residual austenite, a_α and c_α are the lattice parameters of tetragonal martensite, and V_γ is the volume fraction of austenite present in the sample prior to martensitic transformation. The absolute volume fraction of martensite ($V_{\alpha'}$) can be obtained by multiplying the fraction of austenite transformed to martensite (f) with the actual volume fraction of austenite (V_γ) initially present at T_B, *i.e.*,

$$V_{\alpha'} = fV_\gamma \tag{5.3}$$

A computer program was written and used for these calculations. The program takes full account of the changes in lattice parameters as a function of alloy composition and temperature, as described elsewhere [7,32]. Figure 5.4 shows the volume fractions of martensite, obtained for homogeneous and heterogeneous specimens after the specimens had been transformed isothermally to bainite at the temperatures indicated, with enough time at the isothermal transformation temperatures to ensure the cessation of bainite formation.

There is a rapid increase in the volume fraction of martensite ($V_{\alpha'}$) with an increase in the isothermal transformation temperature T_B, which is consistent with the respective measured and calculated M_S temperature data (Fig. 5.2).

5.2.2 Retained Austenite

Given that the volume fractions of bainite and martensite were determined by dilatometry, it is relatively easy to calculate the volume fraction of austenite retained (V_{γ_r}) at room temperature by difference:

$$V_{\gamma_r} = 1 - V_{\alpha_b} - V_{\alpha'} \tag{5.4}$$

It was found that for both the homogeneous and heterogeneous specimens, the volume fraction of retained austenite decreased at first, and then increased with the isothermal transformation temperature T_B. At T_B = 400 °C, a relatively larger quantity of retained austenite was obtained for the homogeneous specimen (Fig. 5.5).

It is to be noted (Fig. 5.5) that in previous experiments, a relatively higher volume fraction of bainite was obtained in the case of the homogeneous specimen relative to the heterogeneous sample transformed at 400 °C. This means that more film austenite♣ can be expected than the blocky morphology after the formation of bainite in homogeneous sample. This film austenite, since it is trapped in the immediate vicinity of bainite subunits, is known to contain a higher carbon content than the blocky austenite[33,34] and is difficult to transform to martensite. There is as a result, a sudden rise in the volume fraction of austenite retained for the samples transformed to bainite at 400 °C.

♣ *Film austenite is that retained between the subunits within a given sheaf of bainite while "blocky austenite" is the retained austenite, exhibiting a triangular shape in two dimensional sections, bounded by different crystallographic variants of bainite sheaves* [8,9].

This also explains the marked drop in the volume fraction of martensite ($V_{\alpha'}$) (Fig. 5.4). An increase in the calculated volume fraction of retained austenite with an increase in isothermal transformation temperature results as higher amount of residual austenite with lower carbon content is being produced.

5.2.3 Instability of Residual Austenite

A parameter representing the stability of residual austenite can be defined by the ratio of volume fraction of martensite to the volume fraction of residual austenite at the isothermal bainite transformation temperature [8,9], *i.e.*, $\frac{V_{\alpha'}}{(1-V_{\alpha_b})}$. Figure 5.6 shows a plot of the stability parameter as a function of carbon content of residual austenite (x_γ) for the homogeneous and heterogeneous specimens.

The instability of residual austenite at any isothermal transformation temperature is higher for the heterogeneous material presumably because in all cases, the degree of reaction to bainite was lower than in comparative homogeneous samples. As has been noted previously [8,9], the observations also indicate that the enhanced stability arises from the finely divided state of the bainitic residual austenite whose carbon content is usually higher when compared with the rest of the austenite. The differences in instabilities between homogeneous and heterogeneous specimens increase with increases in the maximum degree of bainitic transformation (*i.e.*, with decrease in transformation temperature). It is interesting to note that the bainitic residual austenite becomes increasingly stable as the degree of transformation of bainitic ferrite becomes greater. The films of retained austenite separating the bainitic lenticular plates lead to high strength and they additionally break up the path of propagating cracks since the crack not only has to traverse interphase interfaces and varying crystal structures but its motion can also be dampened by transformation at the crack tip[35].

5.3 Kinetics of Athermal Martensitic Transformation

Any assessment of the overall kinetics of transformations which are thermodynamically of first order in the Ehrenfest classification scheme, must include a consideration of both the nucleation and growth rates of the product phase. On the other hand, for martensitic transformation in steels, the growth rate of the plates can be very high, often limited by the speed of sound in the steel. Furthermore, because of the displacive character of the transformation, the martensite grows in the form of thin plates whose

aspect ratio may be determined by the minimisation of strain energy if the plates are elastically accommodated. Since the coordinated movement of atoms characteristic of displacive reactions cannot in general be sustained across austenite grains which are in different crystallographic orientations, the maximum dimension of each plate must in some way be limited by the austenite grain size. Considering all these factors together, it may as a first approximation be assumed that the volume of material transformed by each plate or lath of martensite is a constant value $\overline{V}$. In these circumstances, the growth part of the overall kinetics may be neglected, since each nucleus will transform $\overline{V}$ of the parent phase.

It has been known for a long time[36], that the progress of the athermal martensitic transformation in a sample which is initially fully austenitic, can be described empirically by an equation of the form:

$$1 - f = \exp\{-C_1(\mathrm{M}_S - \mathrm{T}_Q)\} \tag{5.5}$$

where f is the volume fraction of martensite divided by the volume fraction of austenite prior to the formation of martensite, T_Q is a temperature to which the sample is cooled below M_S; C_1 is a constant obtained originally [36] by fitting to experimental data.

Magee[37] demonstrated that this relationship can be justified theoretically if it is assumed that the number of new plates of martensite that form per unit volume of austenite (*i.e.*, dN) due to the lowering of temperature below M_S is a positive proportional to the consequential change in the driving force $\Delta G^{\gamma\alpha'}$ for diffusionless transformation:

$$dN = -C_2\, d(\Delta G^{\gamma\alpha'}) \tag{5.6}$$

where C_2 is a proportionality constant. Note that $\Delta G^{\gamma\alpha'}$ is given by $G^{\alpha'} - G^{\gamma}$, where $G^{\alpha'}$ and G^{γ} refer to the Gibbs free energies of unit volumes of martensite and austenite respectively. The change in the volume fraction of martensite is therefore given by:

$$df = \overline{V}\, dN_V \tag{5.7}$$

where dN_V is the change in the number of new plates of martensite formed per unit volume of sample, with $dN_V = (1 - f)dN$ and $\overline{V}$ is the average volume per newly formed plate. On combining equations 5.6 & 5.7, and substituting $[d(\Delta G^{\gamma\alpha'})/dT]dT$ for $d(\Delta G^{\gamma\alpha'})$, Magee showed that

$$df = -\overline{V}(1 - f)C_2\, [d(\Delta G^{\gamma\alpha'})/dT]dT$$

which on integration between the limits M_S and T_Q gives

$$\ln\{1-f\} = \overline{V}C_2[d(\Delta G^{\gamma\alpha'})/dT](M_S - T_Q)$$

or

$$1 - f = \exp\{\overline{V}C_2[d(\Delta G^{\gamma\alpha'})/dT](M_S - T_Q)\}. \tag{5.8}$$

The integration procedure used above assumes that the term $[d(\Delta G^{\gamma\alpha'})/dT]$ is constant with temperature. The form of the above equation is similar to that of the empirical relation used by Koistinen and Marburger[36], so that

$$C_1 = -\overline{V}C_2[d(\Delta G^{\gamma\alpha'})/dT]. \tag{5.9}$$

Graphs illustrating the variation of $\Delta G^{\gamma\alpha'}$ as a function of undercooling below M_S are illustrated in Fig. 5.7; they show that it is a good approximation to assume that the variation is linear so that C_1 should be approximately constant over the range of interest.

Data are presented in Fig. 5.7 for 300M steel containing a range of carbon concentrations, to simulate martensitic decomposition following partial transformation to bainite. The formation of bainite leads to an enrichment of carbon in the residual austenite. The calculations use the thermodynamic theory and data detailed in references [38, 39].

5.3.1 Results of Kinetic Analysis

An attempt was made to fit the data from dilatometric experiments to an empirical equation of the form:

$$1 - f = \exp\{-C_1(M_S - T_Q)\} \tag{5.10}$$

Graphs of $(M_S - T_Q)$ versus $\ln(1-f)$ are shown in the Fig. 5.8. Comparison of the as–received heterorgeneous and the homogenised samples revealed no obvious or systematic differences in the plots (Fig. 5.8). Results of the regression analysis, in which a line passing through the origin was best fitted to the data in each case, are given in the Table 5.1.

The data, when plotted according to equation 5.8 were usually found to deviate from linearity at the very early stages of reaction (Fig. 5.9). It was considered that this failure of the theory may be a consequence of the act that it neglects the autocatalysis

effect. When plates of martensite form, they induce new embryos which are then available for further transformation, this is autocatalysis. Even Magee's interpretation (equations 5.6–5.8) does not explicitly include the autocatalysis factor, although he clearly recognised and discussed the implications of autocatalytic nucleation. Table 5.1 also shows that while the data corresponding to each isothermal transformation temperature, can be correlated well using equation 5.7, the values of C_1 calculated from the regression analysis vary significantly when all the experimental data are considered together, again emphasising the failure of the model. It is nevertheless found (Fig. 5.9) that the volume fraction of martensite at ambient temperature as predicted by an empirical application of Koistinen and Marburger's equation is in good agreement with the experimental results, provided that a suitable value of the constant C_1 is used. However, the need to use a different value of C_1 in each case makes the procedure of little use for predictive purposes.

5.3.2 The Role of Autocatalysis

As pointed out earlier, the model discussed above does not include the effects of autocatalysis. The nucleation of martensite is believed to begin at structural imperfections in the parent phase, such as arrays of dislocations. These are the preexisting defects which, on cooling below the M_S temperature dissociate into suitable partial dislocations in a way which leads to the operational nucleation of martensite[40]. The defects are not identical (they vary in potency) and are stimulated to grow into plates of martensite at different degrees of undercooling below the M_S temperature. Thus the volume fraction of martensite, in general, varies only with the degree of undercooling below M_S.

Detailed analysis reveals[40–42] that the initial number density of preexisting defects typically found in austenite is not large enough to explain the kinetics of martensitic transformation. The extra defects necessary to account for the faster than expected transformation rates are attributed to autocatalysis: when plates of martensite form, they induce new embryos which are then available for further transformation. It has been proposed that the number of autocatalytic sites generated per unit volume at different temperatures can be calculated by integrating the following equation[43]:

$$dN = dN_i + d(f'p) \tag{5.11}$$

where N_i is the number of original nucleation sites per unit volume of sample, which remain after the formation of some martensite, and is given[37] by

$$N_i = (1 - f')N_i^0$$

where N_i^0 is the number of original nucleation sites per unit volume of austenite. The term p represents the number of autocatalytic sites generated per unit volume of sample. We assume here that this autocatalytic factor is related linearly to the volume fraction of martensite and hence to f',

$$p = C_3 + C_4 f' \tag{5.12}$$

then it follows that

$$dN = (-N_i^0 + C_3 + 2C_4 f')\, df'. \tag{5.13}$$

Since $\overline{V}$ is assumed to be constant in the present analysis, $df'/\overline{V} = (1 - f')dN$ so that

$$\int_0^f \frac{df'}{\overline{V}(1 - f')} = \int_0^f (-N_i^0 + C_3 + 2C_4 f')\, df'. \tag{5.14}$$

On carrying out the integration, we get

$$p = N_i^0 - \frac{\ln\{1 - f\}}{f\overline{V}}. \tag{5.15}$$

It is noteworthy that as $f \to 0$, $p \to N_i^0 + \frac{1}{\overline{V}}$.

A value of $\overline{V}$ can be estimated to be $\sim 20\,\mu\text{m}^3$, on the basis that a typical plate of martensite will have the approximate dimensions $0.2 \times 10 \times 10\,\mu$m. With this assumed value, and the experimentally measured volume fractions of martensite, calculated values of $p - N_i^0$ were plotted against $\text{M}_S - \text{T}_Q$, as illustrated in Fig. 5.10.

It is evident that the relationship between these variables is approximately linear, and may be expressed as follows:

$$p - N_i^0 = C_5 + C_6(M_S - \text{T}_Q) \tag{5.16}$$

where C_5 and C_6 are constants defining the best fit line between the variables. On setting $\text{M} - \text{T}_Q = 0$, or in other words, $f = 0$, it is found that $p \to N_i^0 + \frac{1}{\overline{V}}$ so that

$$C_5 = \frac{1}{\overline{V}}$$

so that

$$p - N_i^0 = \frac{1}{\overline{V}} + C_6(M_S - \mathrm{T}_Q). \tag{5.17}$$

On combining this relationship with equations 5.13, it follows that

$$-\frac{\ln\{1-f\}}{f} = 1 + \overline{V}C_6(M_S - \mathrm{T}_Q) \tag{5.18}$$

or

$$-\frac{\ln\{1-f\}}{f} = 1 + C_7(M_S - \mathrm{T}_Q) \tag{5.19}$$

where $C_7 = \overline{V}C_6$. This equation represents a new law for the development of martensitic transformation as a function of undercooling below the M_S temperature. Its application is considered below. It should be noted that in the analysis, homogeneous and heterogeneous samples are treated alike as previously no remarkable difference was observed in the development of martensite reaction in the two kinds of samples.

The experimental data as fitted to the above equation are represented in Fig. 5.11. A better correlation was obtained when compared with the previous model based on equation 5.8.

Figure 5.12 shows that the new model can accurately predict the kinetics of the martensite reaction at all stages. As the data include directly–quenched samples as well as those partially transformed to bainite and quenched from this isothermal transformation temperature, it can be concluded further that the defects generated by bainitic transformation do not give rise to a large amount of autocatalytic nucleation of martensite.

5.3.3 Variation of $\overline{V}$ with Undercooling

Even with the new model developed above, it was assumed that $\overline{V}$ is constant during the course of the reaction. Fisher's model[44–46] for plate martensite predicts that the average volume of martensite plates decreases strongly as the transformation proceeds. The theory assumes that the transformation is random throughout a specimen and that the plates partition the γ –grains into smaller compartments. As a result, the later forming plates should tend to be smaller. However, the nucleation of martensite may not be random throughout[47], as most martensite plates nucleate in the vicinity of other martensite plates due to the autocatalysis effect. It has been recognised[37] that the first observable transformation is due to several clusters of plates rather than a random distribution of plates.

Magee *et al.* [48] have shown experimentally that for Fe–23.8Ni–0.42C wt.% and Fe–28.5Ni–0.40C wt.% alloys, there is no sensible decrease in $\overline{V}$ at volume fractions up to 0.55. However, at high volume fractions, the geometrical partitioning♣ effect is expected to be important, and $\overline{V}$ will be expected to decrease as volume fraction increases. Guimarães *et al.* [49] used Fullman's stereographic method[50] to determine both the mean plate radius, $\overline{r}$, and volume $\overline{V}$. The mean plate thickness was estimated through the equation proposed by Chen and Winchell[51]:

$$\overline{t} = \frac{V_{\alpha'}}{S_v} \tag{5.20}$$

where $(V_{\alpha'})$ is the volume fraction of martensite and S_v the mean density of martensite midplane in the material. The calculated aspect ratio $\overline{t}/\overline{r}$ was found to reach a maximum at some intermediate fraction transformed. Guimarães[52], investigating the influence of austenite grain sizes on the mean volume of martensite plates in Fe–31.9Ni–0.02C wt.%, found that $\overline{V}$ is constant in materials with finer austenite grain size, but it noticeably decreases as the fraction transformed increases in samples with coarser austenite grain sizes. In the later case, the Fisher's partitioning effect is probably more important when compared with the situation for fine austenite grain structures. His computer modelling shows that a fine grain size favours the formation of clusters of partially transformed grains and also enhances autocatalysis in the grains, so that $\overline{V}$ is not sensitive to the volume fraction transformed.

In the present model particularly good agreement has been observed between calculated and experimental volume fractions of martensite, although it slightly overestimates at low fractions transformed. That may be due to the fact that the model assumes a constant value of $\overline{V}$ at all stages of transformation. Moreover, the model assumes that all nucleation sites have the same activation energy. Magee[53] showed that there is a distribution of effectiveness of nucleation sites. These approximations require much further research and characterisation.

5.4 Conclusions

The development of martensitic transformation has been studied using dilatometry, from both a fully austenitic starting microstructure and from a microstructure

♣ *Geometrical partitioning is based on the observation that the initial martensite plates divide the sample into progressively smaller compartments.*

containing a mixture of upper bainitic ferrite and carbon–enriched austenite. It is found that the presence of bainitic ferrite does not significantly alter the way in which the subsequent transformation to martensite occurs. In fact all the data can be rationalised using a new model of athermal martensite kinetics, which includes an effect of autocatalytic nucleation, subject to the approximation that all that plates of martensite have identical volume.

For the levels of chemical segregation observed in the steel studied, the major effect on martensitic transformation is to extend the range over which the reaction occurs relative to homogenised samples. Otherwise, the same parameters can be used to predict martensitic reaction in all samples, within the limits of experimental error.

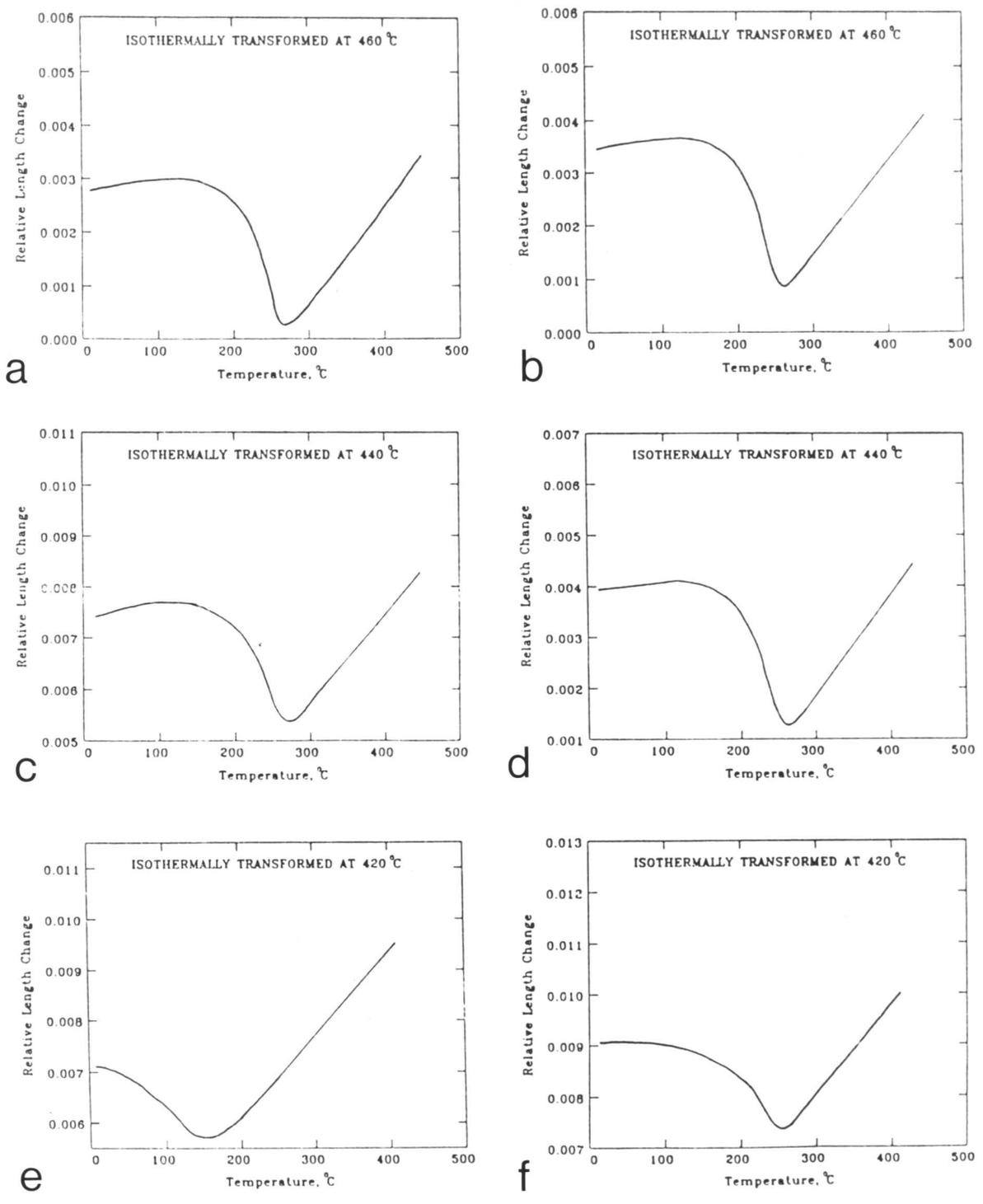

Fig. 5.1: *Dilatometric curves showing the transformation to martensite in heterogeneous and homogeneous steels, after the specimens were isothermally transformed to bainite at different temperatures, with enough time at each isothermal transformation temperature to ensure that bainitic ferrite formation stopped. Graphs (a), (c), (e), (g) and (i) are for homogeneous samples and (b), (d), (f), (h) and (j) are from heterogeneous samples.*

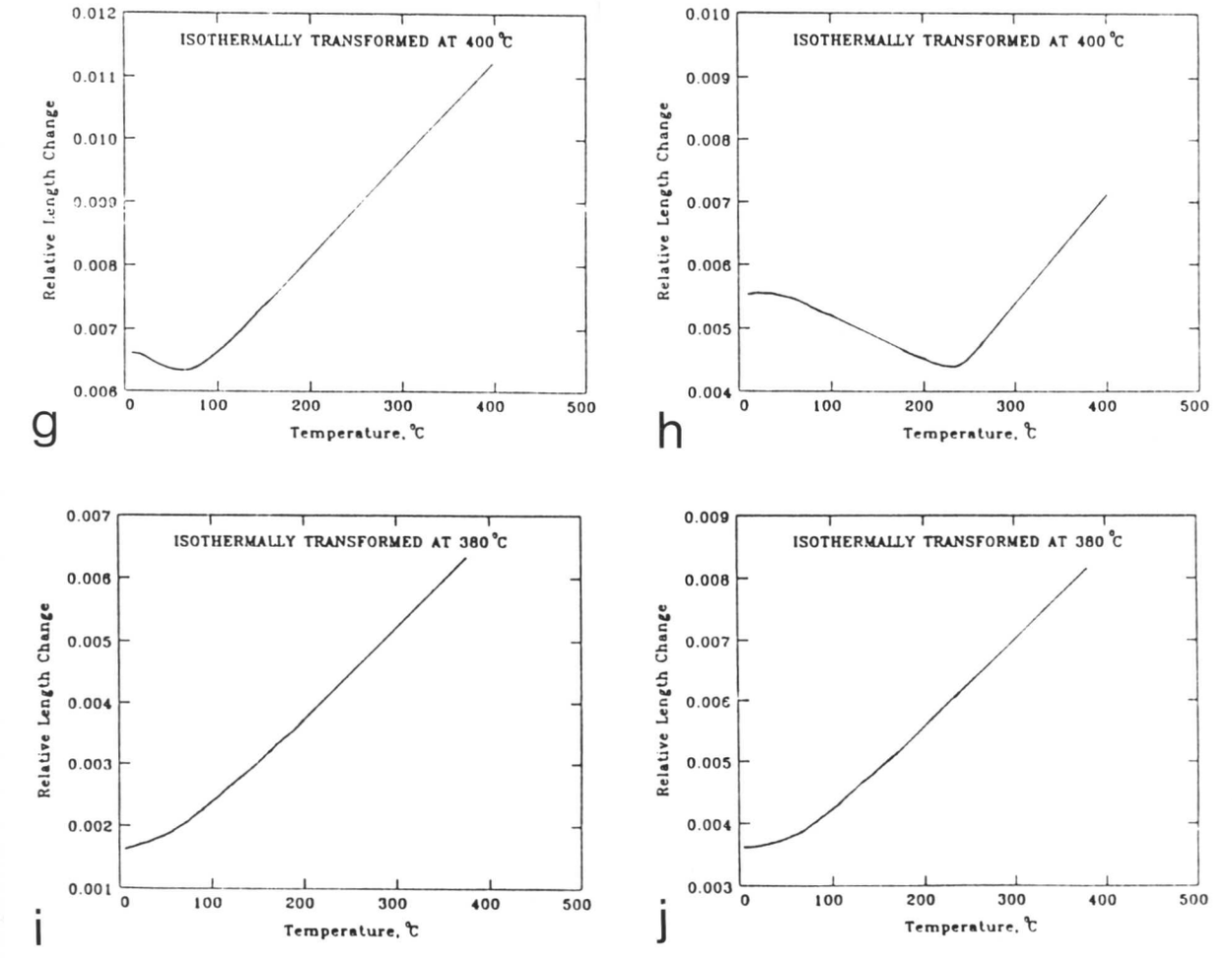

Fig. 5.1: *(continued ....)*

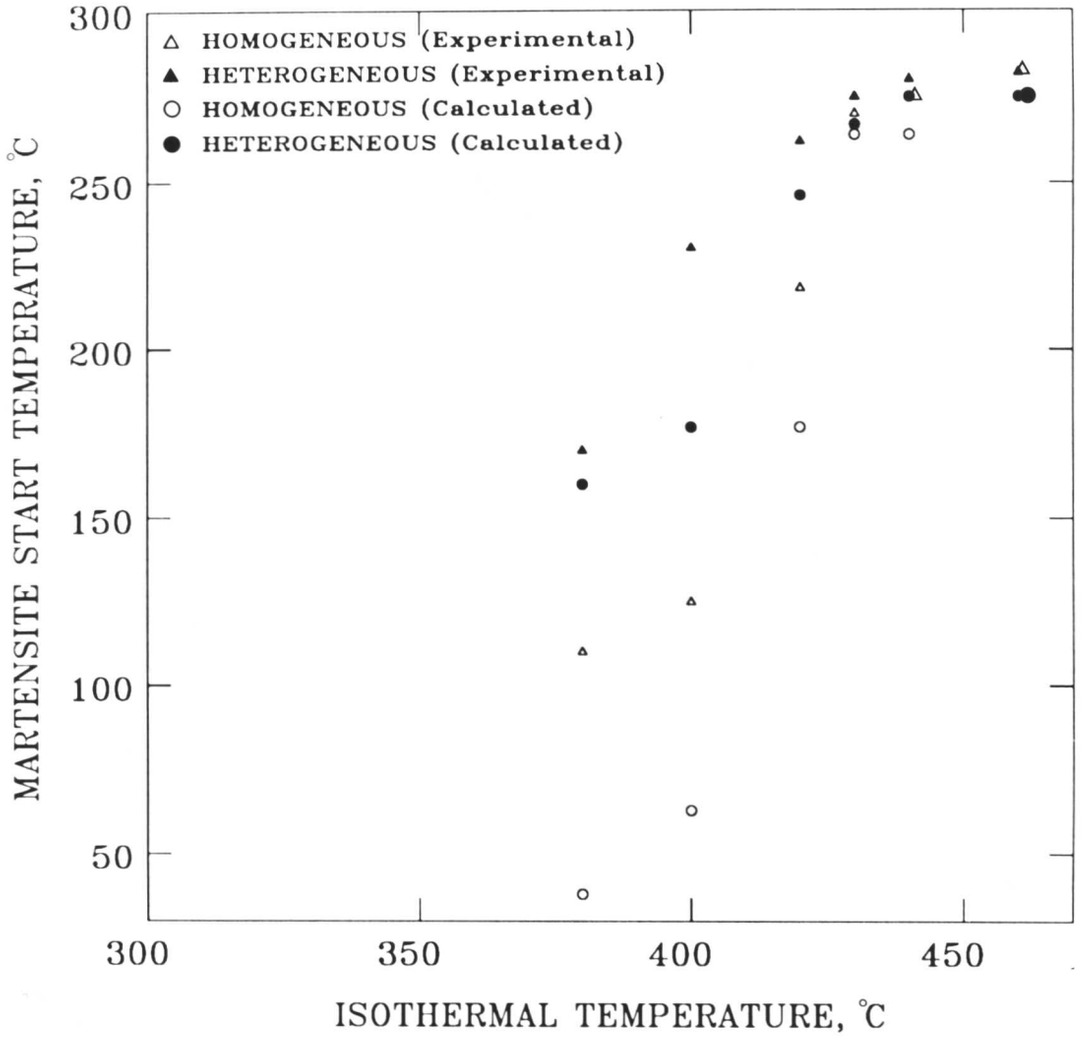

Fig. 5.2: *Thermodynamically calculated*[27,28] *and experimentally determined* M_S *temperatures for homogenised and heterogeneous samples, after partial isothermal transformation to bainite.*

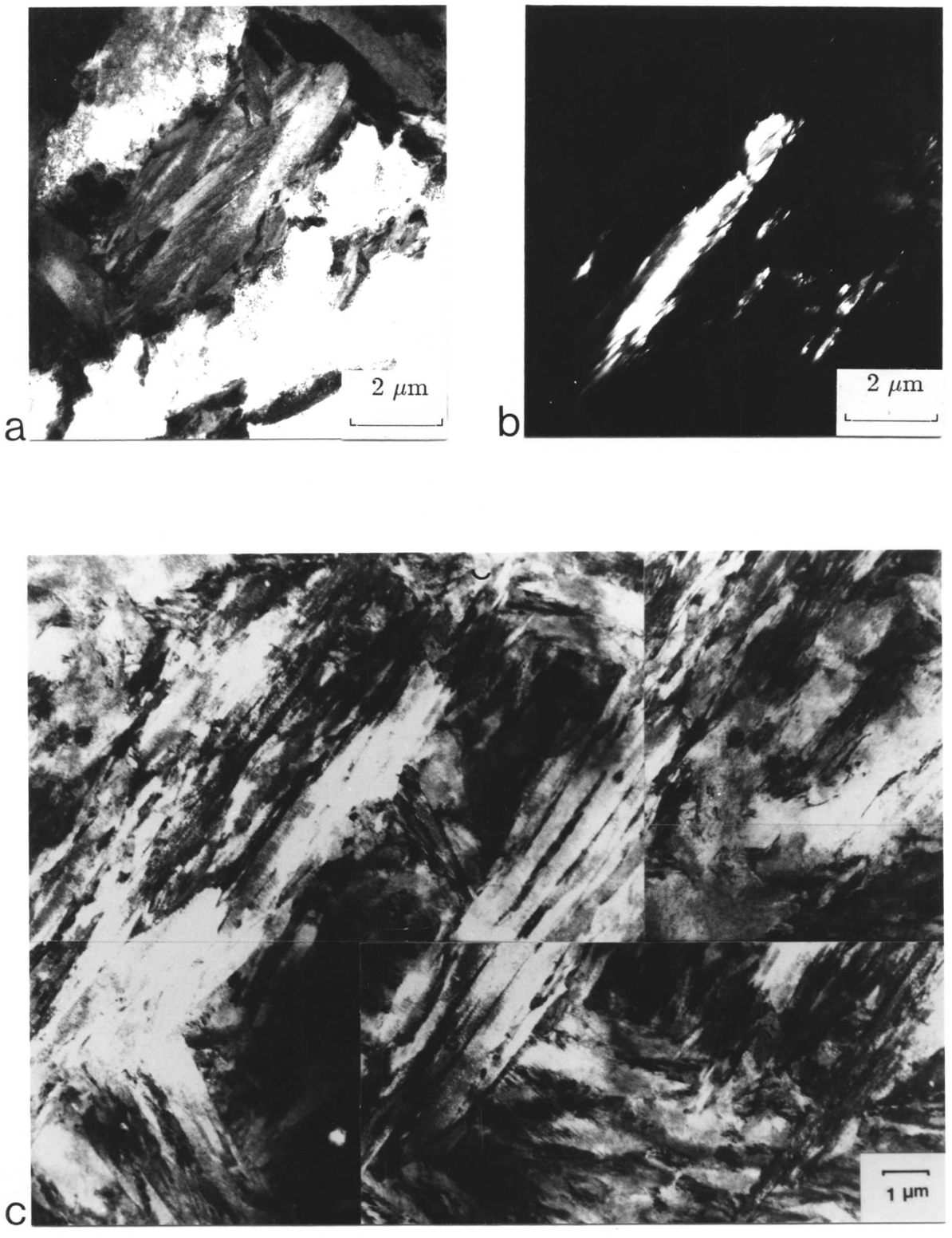

Fig. 5.3: *Transmission electron micrographs showing twinned martensite in a homogenised 300M steel specimen which is isothermally transformed to bainite at 420 °C before quenching to room temperature, (a) bright field image, (b) dark field image, (c) untwinned martensite.*

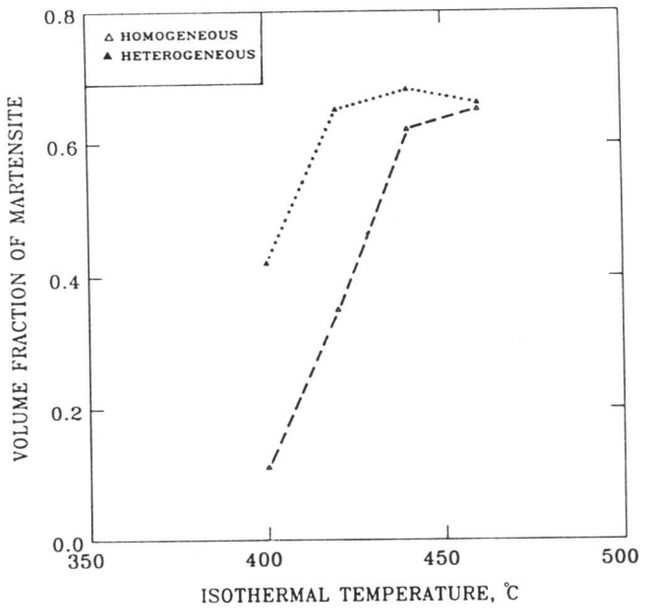

Fig. 5.4: *Volume fraction of martensite obtained for homogeneous and heterogeneous specimens. The specimens were transformed initially to bainite at different isothermal temperatures, as indicated in the diagram. Hence, in each case the residual austenite, i.e., left after transformation to bainite, had a different carbon concentration which decreases as the bainite transformation temperature increases.*

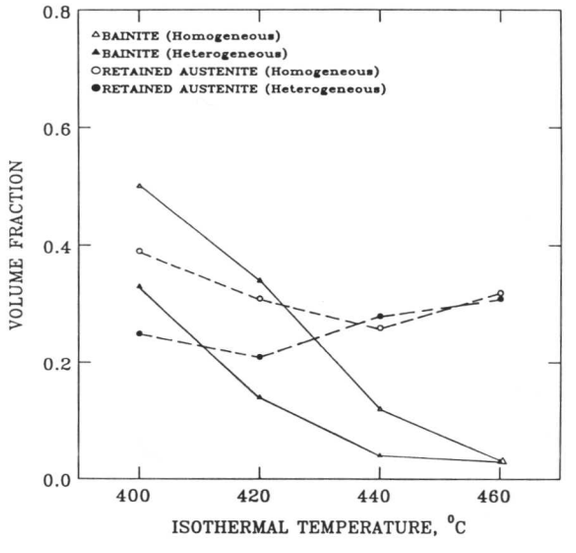

Fig. 5.5: *Volume fraction of austenite retained obtained by difference and experimental volume fraction of bainite, in samples partially transformed to bainite followed by quenching to room temperature.*

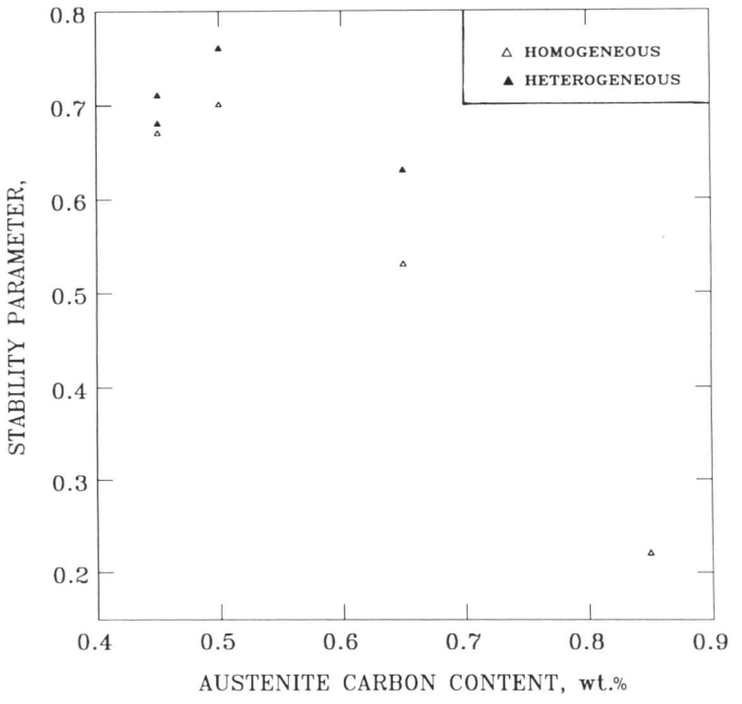

Fig. 5.6: *Variation of the instability of the residual austenite which is left untransformed after the bainite reaction stops, with its carbon content.*

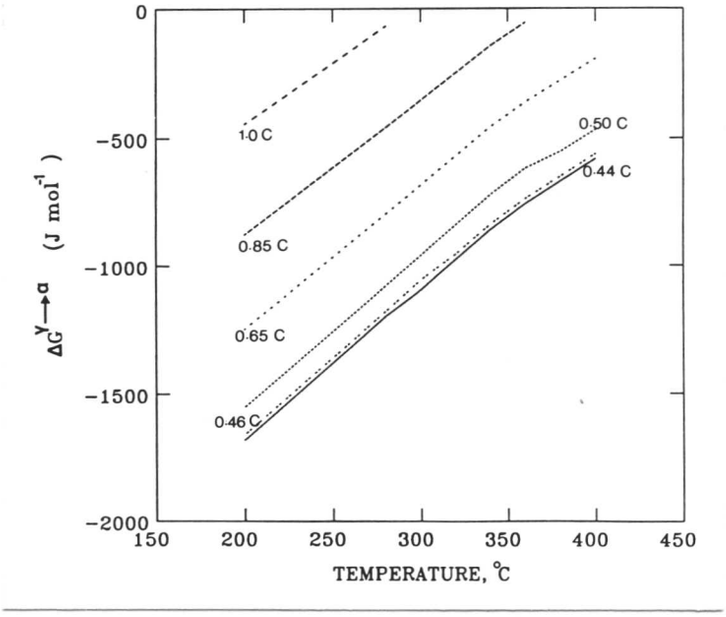

Fig. 5.7: *Plots of* $\Delta G^{\gamma\alpha'}$ *versus* $M_S - T_Q$ *for 300M steel containing a variety of carbon concentrations (wt.%).*

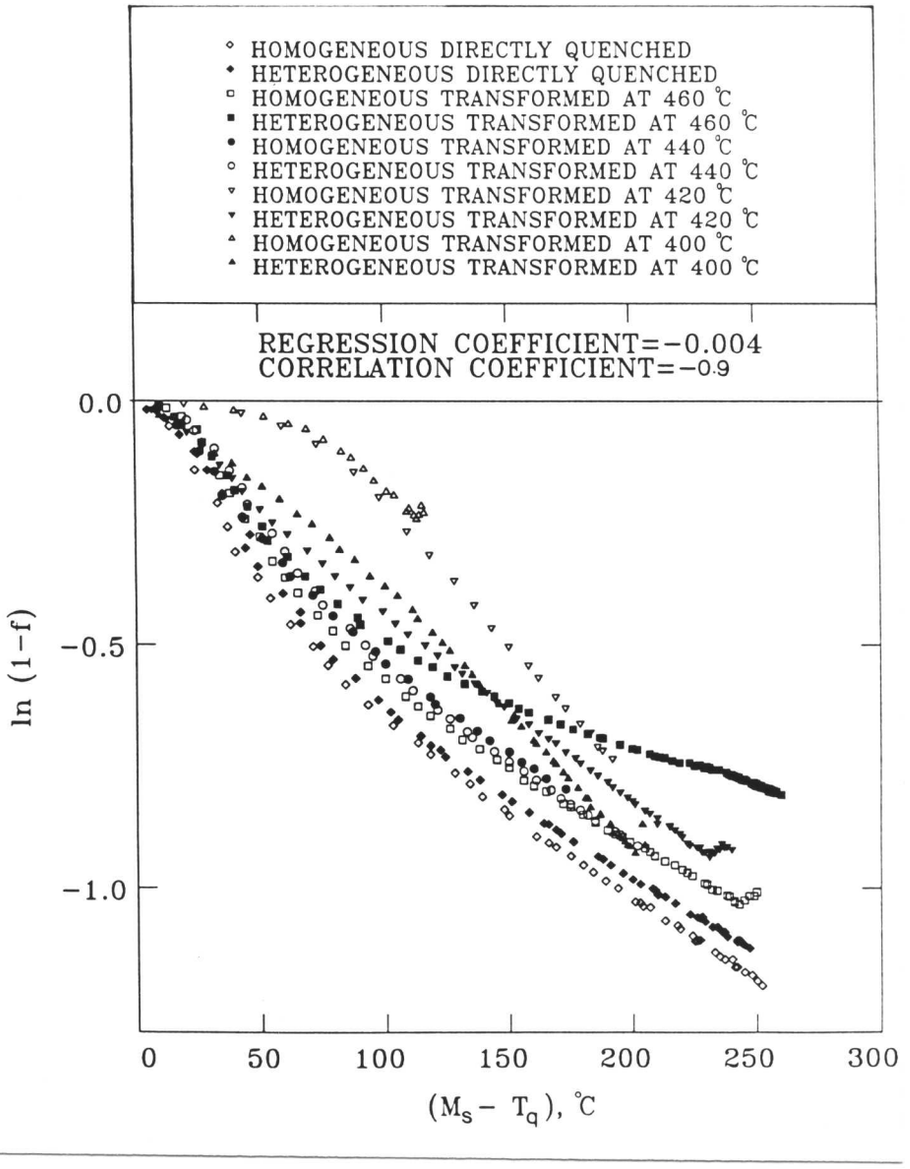

Fig. 5.8: *Results of the regression analysis of the experimental data fitted to Koistinen and Marburger's empirical equation.*

Isothermal Temperature °C	Homogenized		Heterogeneous	
	Correlation Coefficient	Regression Coefficient	Correlation Coefficient	Regression Coefficient
400	-0.98	-0.0019	-0.99	-0.0046
420	-0.98	-0.0031	-0.99	-0.0060
440	-0.99	-0.0051	-0.99	-0.0056
460	-0.98	-0.0050	-0.98	-0.0050
Directly Quenched	-0.98	-0.0055	-0.98	-0.0052

Table 5.1: *Regression constants for the curves shown in Fig. 5.8.*

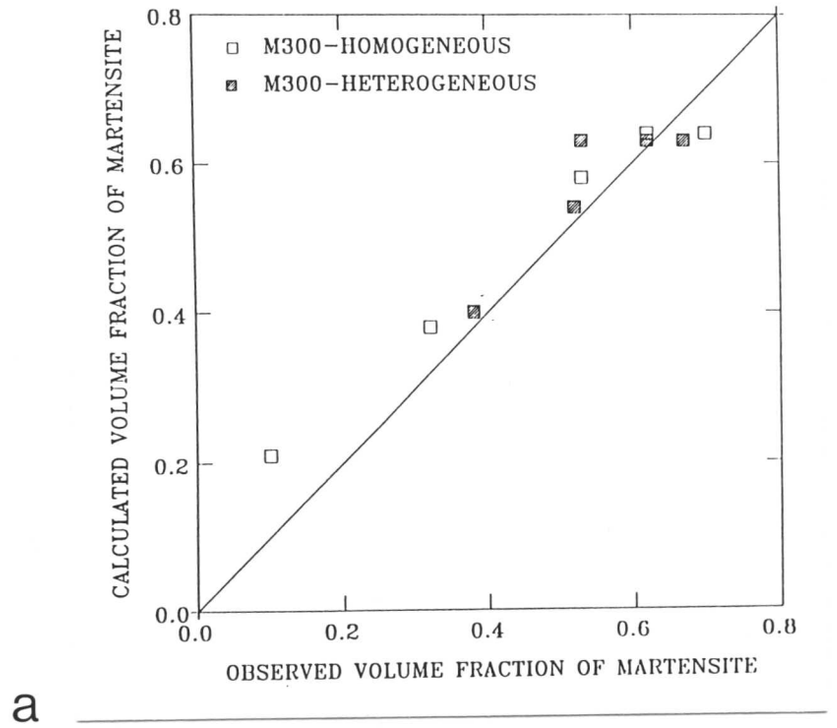

a

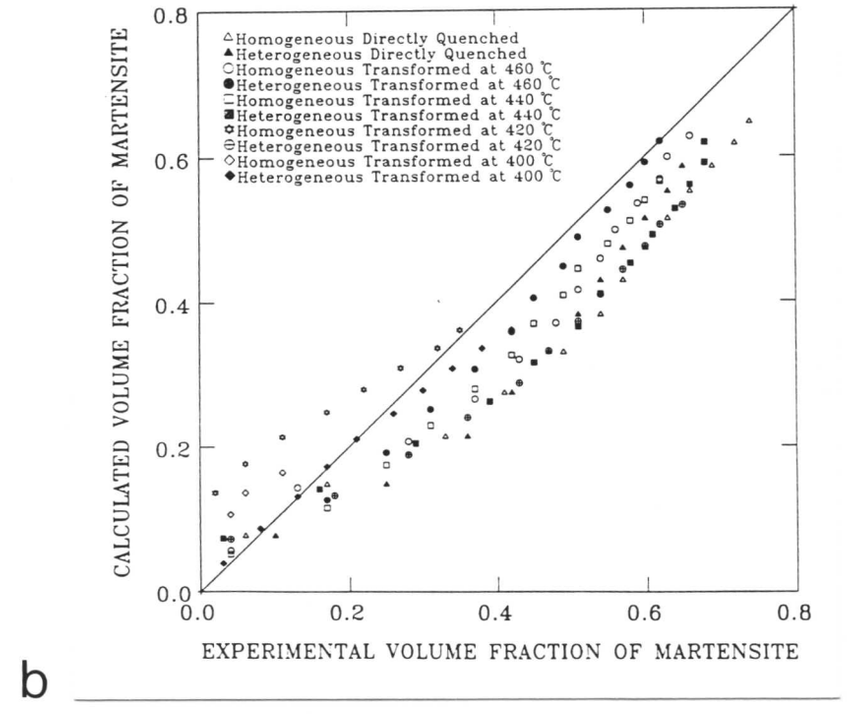

b

Fig. 5.9: *Comparison of the observed and calculated volume fractions of martensite. The calculations utilise the Koistinen and Marburger's equation. A common value of 0.004 was assigned to C_1 for all these calculations. The true volume fraction of martensite (a) at 20 °C only and (b) at all temperatures where measurements were made.*

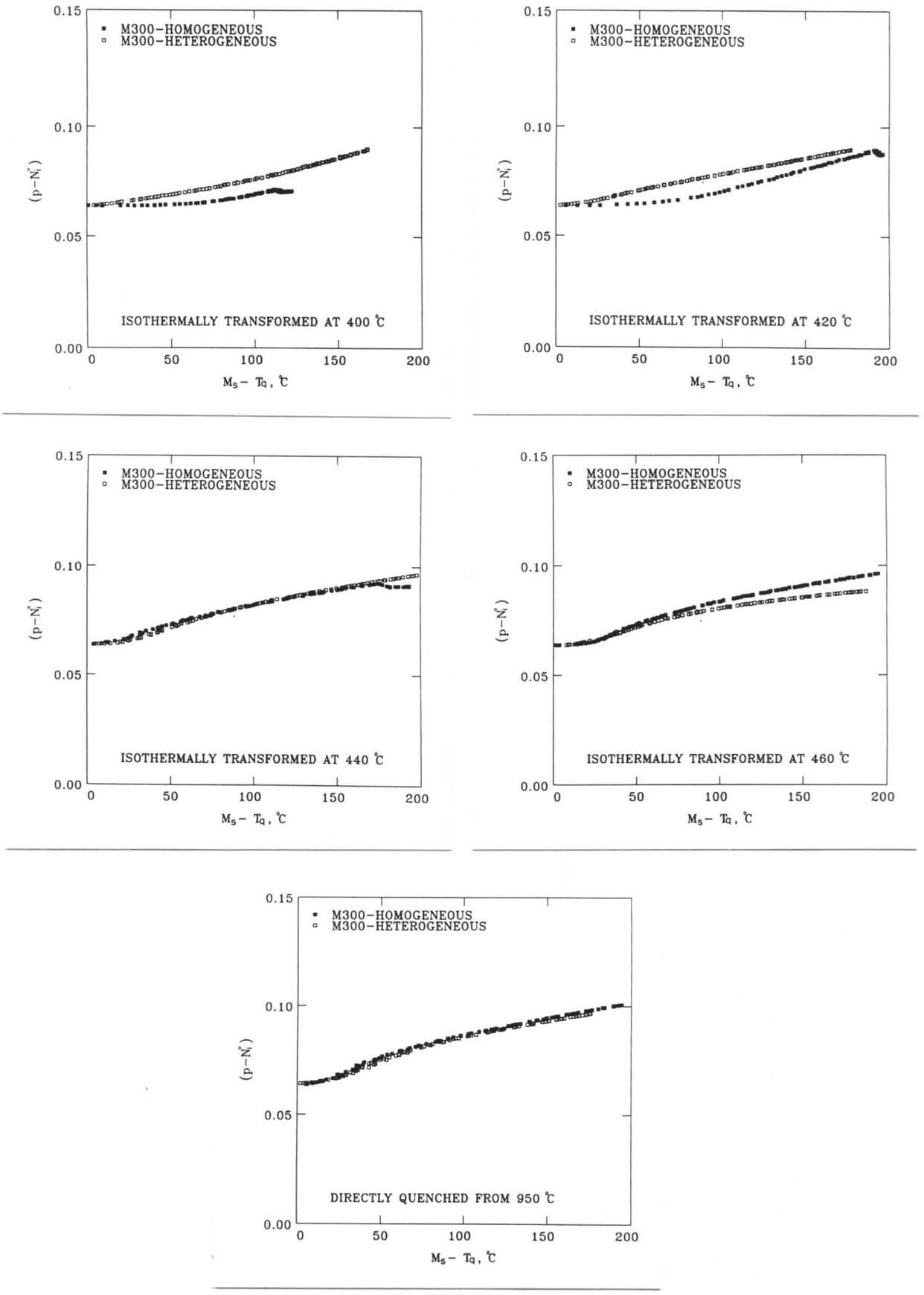

Fig. 5.10: *Graphs illustrating the linear relationship between* $(p - N_i^0)$ *and* $(M_S - T_Q)$.

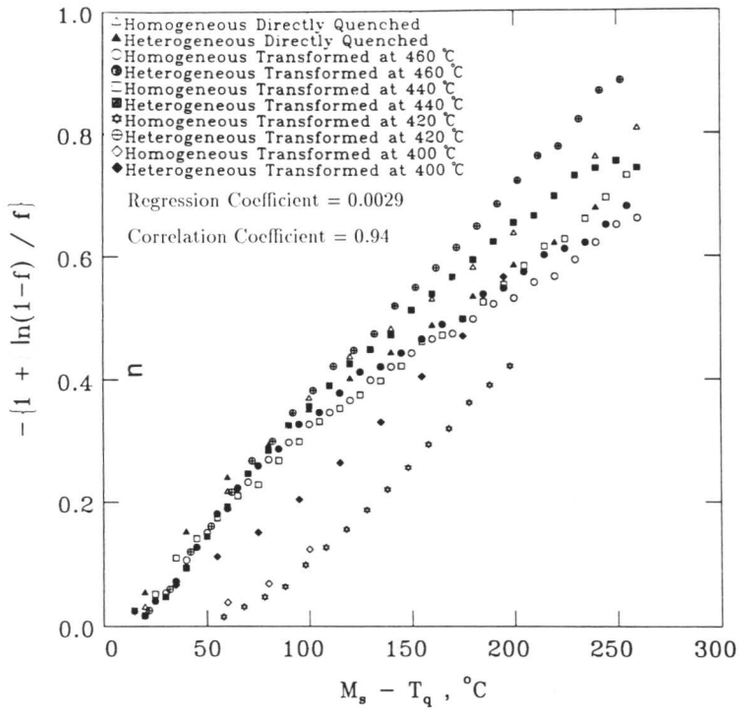

Fig. 5.11: *Results of the regression analysis as the experimental data were fitted to an equation of the form* $-\left[1 + \frac{\ln\{1-f\}}{f}\right] = C_7(M_S - T_Q)$.

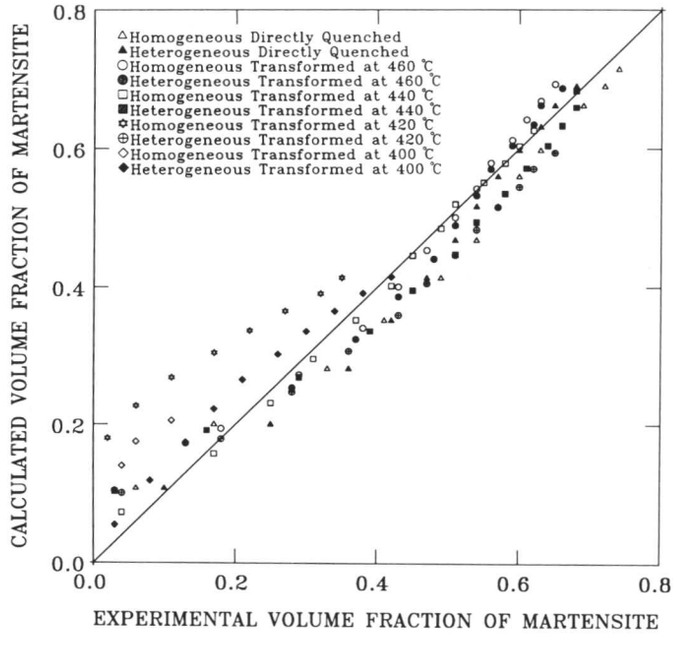

Fig. 5.12: *Comparison of experimental results with those calculated by the new model based on equation 5.18.*

REFERENCES

1. E. F. Bailey: *Trans. A. S. M.,* 1954, vol. 46, p. 830.
2. R. F. Hehemann, V. J. Luhan and A. R. Troiano: *Trans. A. S. M.,* 1957, vol. 49, p. 409.
3. A. R. Troiano and L. J. Klinger: *Trans. A. S. M.,* 1952, vol. 44, p. 775.
4. Y. Tomita and K. Okabayashi: *Metall. Trans. A,* 1983, vol. 14A, p. 485.
5. Y. Tomita and K. Okabayashi: *Metall. Trans. A,* 1985, vol. 16A, p. 73.
6. S. A. Khan and H. K. D. H. Bhadeshia: *Phase Transformations '87,* Institute of Metals, London, edited by G. W. Lorimer, 1988, p. 207.
7. S. A. Khan and H. K. D. H. Bhadeshia: *Metall. Trans. A,* 1990, in press.
8. H. K. D. H. Bhadeshia and D. V. Edmonds: *Metal Science,* 1983, vol. 17, p. 411.
9. H. K. D. H. Bhadeshia and D. V. Edmonds: *Metal Science,* 1983, vol. 17, p. 420.
10. V. T. T. Miihkinen and D. V. Edmonds: *Materials Science and Technology,* 1987, vol. 3, p. 422.
11. V. T. T. Miihkinen and D. V. Edmonds: *Materials Science and Technology,* 1987, vol. 3, p. 432.
12. V. T. T. Miihkinen and D. V. Edmonds: *Materials Science and Technology,* 1987, vol. 3, p. 441.
13. C. F. Jatczak, D. J. Girardi and E. S. Rowland: *Trans. A. S. M.* , 1956, vol. 48, p. 279.
14. J. S. Kirkaldy, V. D. Forstmann and R. J. Brigham: *Cand. Metall. Quart.*, 1962, vol. 1, p. 59.
15. P. G. Bestien: *J. I. S. I.*, 1957, vol. 187, p. 281.
16. J. G. Garland and P. R. Kirkwood: *International Institute of Welding Document*, IX–92–74, 1974.
17. J. G. Garland: *BSC Report*, Prod/500/1/73/A, 1973.
18. E. S. Davenport: *Trans. A. S. M.*, 1939, p. 837.
19. R. A. Farrar: *Stainless steels '84*, p. 336, Institute of Metals, London, 1985.
20. G. R. Speich and R. L. Miller: *Mechanical Properties of Dual Phase Steels,* eds. R. A. Kot and J. W. Morris, Trans. Metall. Soc. AIME, New Orleans, 1979, p. 145.

21. H. K. D. H. Bhadeshia: *Scripta Metall.*, 1983, vol. 17, p. 857.

22. H. K. D. H. Bhadeshia: *Metal Science,* 1982, vol. 16, p. 167.

23. R. B. McLellan and W. W. Dunn: *J. Phys. Chem. Solids,* 1969, vol. 30, p. 2631.

24. A. Schrader and F. Wever: *Arch Eisenhuttenwesen,* 1952, vol. 23, p. 489.

25. S. J. Matas and R. F. Hehemann: *Trans. Met. Soc. A. I. M. E.,* 1961, vol. 221, p. 179.

26. H. K. D. H. Bhadeshia and A. R. Waugh: *Acta Metallurgica,* 1982, vol. 30, p. 775.

27. H. K. D. H. Bhadeshia and A. R. Waugh: *Solid →Solid Phase Transformations*, eds. H. I. Aaronson *et al.,*, published by the Metallurgical Society of the AIME, Warrendale, Pennsylvania, (1981) p. 993.

28. H. K. D. H. Bhadeshia: *Metal Science,* 1981, vol. 15, p. 175.

29. H. K. D. H. Bhadeshia: *Metal Science,* 1981, vol. 15, p. 178.

30. Y. Inokuti and B. Cantor: *Scripta Metall.,* 1976, vol. 10, p. 655.

31. Y. Inokuti and B. Cantor: *J. Mat. Sci.,* 1977, vol. 12, p. 946.

32. H. K. D. H. Bhadeshia: *J. De. Physique,* 1982, vol. 43, p. C4–443.

33. P. Self, H. K. D. H. Bhadeshia and W. M. Stobbs: *Ultramicroscopy*, 1981, vol. 6, p. 29.

34. H. K. D. H. Bhadeshia and A. R. Waugh: *Acta Met.*, 1982, vol. 30, p. 775.

35. W. W. Gerberich, G. Thomas, E. R. Parker and V. F. Zackay: *2nd Int. Conf. on the Strength of Metals and Alloys,* 1970, A. S. M., Ohio, U. S. A., vol. 3, p. 894.

36. P. P. Koistinen and R. E. Marburger: *Acta Met.,* 1959, vol. 7, p. 59.

37. C. L. Magee: *Phase Transformations,* p. 115, ASM, Metals Park, Ohio, 1959.

38. H. K. D. H. Bhadeshia: *Metal Science,* 1982, vol. 16, p. 159.

39. H. K. D. H. Bhadeshia: *Acta Metallurgica,* 1981, vol.29, p. 1117.

40. G. B. Olson and M. Cohen: *Ann. Rev. Mater. Sci.*, eds. R. A. Huggins, R. H. Bube and D. A. Vermilyea, Annual Reviews Inc., California, U. S. A., 1981, p. 1.

41. C. H. Shih, B. L. Averbach and M. Cohen: *Trans. AIME.*, 1955, vol. 203, p. 183.

42. S. R. Pati and M. Cohen: *Acta Met.*, 1971, vol. 19, p. 1327.

43. M. Lin: *Research Proposal for Ph.D Thesis entitled "Autocatalytic Kinetics of Martensitic Transformations",* 20, Massachusetts Institute of Technology, 1987.

44. J. C. Fisher, J. H. Hollomon and D. Turnbull: *Trans. AIME,* 1949, vol. 185, p. 691.

45. J. C. Fisher: *Acta Met,* 1953, vol. 1, p. 32.

46. J. C. Fisher: *Trans. AIME,* 1953, vol. 197, p. 918.

47. V. Raghavan and A. R. Entwisle: *Iron and Steel Inst. Report No.93,* p. 30, 1969.

48. D. G. Mcmurtrie and C. L. Magee: *Metall. Trans.,* 1970, vol. 1, p. 3185.

49. J. C. R. Guimarães and J. C. Gomes: *Met. Trans. A,* 1979, vol. 10A, p. 109.

50. R. L. Fullman: *Trans. AIME,* 1953, vol. 197, p. 447.

51. W. Y. C. Chen and P. G. Winchell: *Met. Trans. A,* 1976, vol. 7A, p. 1177.

52. J. C. R. Guimarães and A. Saavedra: *Private communication with Olson, referred to by M. Lin [42]*, 1984.

53. C. L. Magee: *Metall. Trans.*, 1971, vol. 2, p. 2419.

Chapter 6

REAUSTENITISATION IN HETEROGENEOUS STEELS

6.1 Introduction

There has been a lot of research on the decomposition of austenite but the same is far from true for the reverse transformation, *i.e.* , the formation of austenite during the heating of steels. In the heat-affected zone of a multirun weld, the layers deposited initially are reheated by the deposition of subsequent layers and consequently may experience complicated thermal cycles which result in several modifications of the initial microstructure[1]. It is necessary to understand the variety of stages of annealing and reaustenitisation to be able to calculate the microstructure of the heat affected zones of such welds. The situation is in fact even more complex, as the material being annealed and reaustenitised in a multirun weld is usually chemically heterogeneous since the welds almost always solidify under nonequilibrium conditions[2].

The reaustenitisation process under industrial conditions (and indeed, for all reported studies) is known to depend on the details of the corresponding nucleation and growth process[3]. The nucleation site, growth rate and austenite morphologies depend strongly on the initial microstructure of the steel[3–8]. Once the reverse transformation is complete, the austenite thus produced coarsens, reducing its total grain boundary energy per unit volume. The rate of grain coarsening is in general known to depend on the alloy chemistry, the temperature and on the amount of grain surface per unit volume of sample[9]. The maximum grain size thus obtained again depends on the composition and the annealing temperature, although normal grain growth usually becomes impossible before a metal has become converted into a single crystal. When dispersed particles are present in the material, a limiting grain size exists, beyond which grains cease to grow[9]. The limiting size is determined approximately by the ratio of the mean radius and volume fraction of the particles. Hence, the ultimate austenite grain diameter will be determined by both the reverse transformation kinetics, and any grain growth which occurs after the completion of the transformation. The whole subject of austenite formation is fascinating and complicated by the awesome variety

of starting microstructures which can be heated into the austenite+ferrite phase field. This work is limited to isothermal reaustenitisation experiments in which the starting microstructure consists of a two-phase mixture of bainitic ferrite and residual austenite.

6.2 Isothermal Reaustenitisation

Isothermal reaustenitisation experiments were carried out on the as-received (heterogeneous) specimens, austenitised at 950 °C for 10 minutes, and then isothermally transformed to bainite at $T_B = 320$ °C and $T_B = 400$ °C for approximately 45 minutes in each case. Fig. 6.1 illustrates the heat-treatment schematically. The period of 45 minutes is long enough to permit the formation of bainitic ferrite to cease (Fig. 6.2). After completion of the isothermal heat treatment at T_B, the samples were heated rapidly to a temperature T_γ to promote the growth of austenite. It has already been shown (Fig. 6.3) that for the alloy used, the bainitic reaction terminates when the carbon concentration of the residual austenite, x_γ, reaches the concentration given by the T_0 curve on the phase diagram. The relatively high silicon content of the alloy helps to retard the precipitation of cementite[10–15] from austenite and the microstructure then contains only bainitic ferrite and carbon enriched residual austenite at the isothermal transformation temperature (T_B). The carbon of residual austenite, x_γ, can be determined readily from a simple mass balance procedure[16]. Furthermore, the lack of any reactions other than the growth of bainitic ferrite makes the interpretation of data easier, since the overlap of reactions does not have to be taken into account. Although bainitic transformation at T_B ceases before all the austenite is consumed, the composition of austenite is still far from equilibrium. Hence, although it is unable to decompose further to bainite, it can, given sufficient time, decompose by reconstructive transformation into more ferrite and carbides[17]. At the temperatures where bainite forms, this secondary reaction can be extremely sluggish, but it was found that when the samples were heated from T_B towards T_γ at slow heating rates (Fig. 6.4), the residual austenite tended to decompose during heating to pearlite♣ and to mixture of ferrite and discrete carbides. This decomposition during heating could be avoided by utilising a faster heating rate, as illustrated in Fig. 6.4. Consequently, for all other experiments, heating rate of 100 °C s^{-1} were used for the temperature range $T_B - T_\gamma$.

♣ *Metallographic evidence for decomposition to pearlite during heating cannot be shown as the sample is then completely reaustenitised at* T_γ *= 770 °C.*

The results obtained using dilatometry are shown in Figs. 6.5 and 6.6. It is evident that there is no decomposition of austenite during heating from T_B to T_γ. It is important to note that the specimens were not cooled below T_B prior to heating to elevated temperatures, in order to avoid any martensitic decomposition of the residual austenite left after the formation of bainite stops. Thus, when the mixed microstructure of just bainitic ferrite and carbon-enriched residual austenite is heated rapidly to T_γ the nucleation of new austenite becomes unnecessary and the growth process can be studied in isolation[18].

During attempts to carry out isothermal reaustenitisation experiments at very high temperatures (greater than about 770 °C), it was found impossible, using the equipment available, to avoid a small degree of austenite formation just before the isothermal reaction temperature T_γ was reached. Hence the data for T_γ were corrected to take this prior austenite formation into account, using the procedure given in reference [19] and is illustrated in Fig. 6.7. If there is no transformation during heating, the length of the specimen should vary linearly with temperature due to the constant thermal expansion coefficients for the phases involved in this study and over the temperature range of interest, as illustrated in Fig. 6.7a. In that case, the maximum relative length change due to austenite growth can be measured directly as the difference between points 'a' and 'b'. Note that curve remains linear until the designated T_γ is reached, indicating no change in microstructure before the sample reaches T_γ. The other typical case is shown in Fig. 6.7b, where because of the high value of T_γ where the kinetics are rapid, reaustenitisation starts during heating in spite of high heating rate used. Therefore, the deviation from the straight line corresponding to the linear thermal expansion of the specimen as extrapolated from low temperatures can be attributed to the growth of austenite which has occurred during heating to T_γ. If the low temperature part of the curve is extrapolated to the reaction temperature, the vertical difference between the extrapolated line and the actual length change curve gives the true length change due to transformation at T_γ, as if no reaction had occurred during heating to isothermal reaustenitisation temperature. The distance $a-a'$ is therefore added to $a'-b$ to correct for prior reaction.

6.3 Results and Discussion

In all the cases transformation rate was rapid at first, but decreased with time until eventually the rate became undetectable. The rate of this reverse transformation to austenite was found to increase monotonically as T_γ was raised. This is because, unlike the transformation of austenite to ferrite, both the diffusion coefficient and driving force increase with superheating. The maximum extent of austenite formation, as deduced from the maximum relative length change (Fig. 6.8), also increases with increasing reaustenitisation temperature, from a volume of zero at the temperature where the carbon concentration of the residual austenite equals that given by A_{e3} curve of the phase diagram, as predicted by Yang and Bhadeshia[18]. It is particularly interesting that the growth of austenite does not begin immediately the temperature is raised above T_B. This is a direct consequence of the incomplete-reaction phenomenon associated with bainitic reaction, in which the reaction stops prematurely before the austenite achieves its equilibrium composition. Hence austenite growth cannot begin until a much higher temperature is reached, giving a large hysteresis between the forward and reverse reactions.

It is interesting to note that there is not much of a difference in the maximum relative length change for the samples transformed initially to bainite at 320 °C and those transformed at 400 °C, for low values of T_γ. But this difference becomes quite significant at T_γ=760 °C (Fig. 6.8) when both types of samples transform completely to austenite. This is due to the fact that the starting microstructure of the samples transformed to bainite at 400 °C prior to reaustenitisation contains a higher volume fraction of residual austenite compared with those initially transformed to bainite at 320 °C. The differences are clear from the representative micrographs of the two cases shown in Fig. 6.9. Those specimens were quenched down to room temperature after transformation to bainite almost ceased; the carbon enriched austenite has to some extent transformed to martensite. For any given isothermal reaustenitisation temperature T_γ, the extent of austenite growth is larger for lower T_B. This expected since the driving force for austenite growth is larger at any T_γ if its carbon concentration is larger when compared with the average concentration $\overline{x}$, *i.e.* , as T_B is reduced. Another way of looking at this is to realise that for lower T_B, there exists a larger volume fraction of bainitic ferrite which can transform back to austenite on superheating.

Any qualitative comparison of the volume fractions of austenite obtained in homogeneous and heterogeneous specimens must be carried out bearing in mind that the two kinds of samples do not have equivalent starting microstructures. The extent of bainitic transformation at T_B is different for the two cases (Table 6.1) so that the residual austenite in the two cases is expected to contain different carbon contents even if the transformation conditions are otherwise identical. Micrographs of partially reaustenitised homogeneous and heterogeneous specimens are shown in Fig. 6.10. Austenite formation is found to occur more uniformly in the homogeneous sample, whereas for the heterogeneous specimens the transformation is more dominant in the solute-enriched bands. It can be seen more clearly in Fig. 6.11.

These bands, being the last to transform to bainite, are expected to have most of the carbon rejected from the neighbouring transformed (bainitic ferrite) areas and as a result will have lower A_{e3} temperatures relative to the remainder of the sample. In most cases reaustenitisation seems to proceed by the "erosion" of the bainitic ferrite without any evidence of the independent nucleation of austenite.

All the reaustenitised (heterogeneous) specimens were helium-gas quenched from T_γ to ambient temperature. Dilatometric curves of the relative length change as a function of temperature for that part of the thermal cycle are presented in Figs. 6.12 and 6.13. In each diagram, any deviation from a straight line during the cooling of the specimen represents the onset of martensitic transformation, so that a martensitic-start temperature (M_s) of any austenite can be determined.

It is clear from Figs. 6.14a and 6.15a that the experimentally measured M_s temperatures of the new austenite increases with increasing reaustenitisation temperature for the specimen initially transformed to bainite at T_B =320 °C. This is exactly as expected since the carbon concentration decreases and volume fraction of the austenite that forms increases as T_γ is raised. However, in case of the specimens initially transformed at T_B =400 °C, the M_s temperature was found to decrease with an increase in T_γ in the small temperature range considered.

A relationship between the carbon concentration of any austenite and its thermodynamically calculated[21,22] martensitic-start temperature was deduced by best fitting a curve to the data (Fig. 6.16) for this particular alloy. The empirical equation thus obtained is found to be

$$x_\gamma = \frac{496 - M_s}{490} \tag{6.1}$$

where x_γ is carbon concentration of austenite in weight percent, and M_s is the martensitic-start temperature in degrees centigrade. If x_γ is expressed in units of mole fraction, then the equation becomes:

$$x_\gamma = \frac{503 - M_s}{11360} \tag{6.2}$$

Equation 6.1 was used to calculate the carbon concentration of austenite that forms at T_γ from the M_s temperatures measured using dilatometry and the results are shown in Figs. 6.14b and 6.15b.

As expected, Fig. 6.14b shows a decrease in the carbon content of austenite with increasing reaustenitisation temperature for T_B = 320 °C. On the other hand, an increase in the carbon content of austenite with increasing T_γ is observed in the case T_B = 400 °C as in shown in Fig 6.15b. This unusual behaviour can be explained as follows.

For the samples whose initial microstructure was generated at T_B =320 °C, due to higher driving forcefor the $\gamma \rightarrow \alpha_b$, the bainitic ferrite (and regions of residual austenite) is distributed uniformly in the solute-depleted as well as in solute-rich regions (Fig. 6.9). Due to homogeneous distribution of the austenite, the specimen behaves, more or less, as a chemically homogeneous sample and the effective A_{e3} curve determining the growth of austenite will be that of a homogeneous alloy. When such a microstructure is reaustenitised the growth of austenite takes place uniformly all over the sample.

At the lower reaustenitisation temperatures, a large amount of carbon is tied-up in a relatively small volume fraction of austenite; as the reaustenitisation temperature is increased, more austenite forms and consequently gets diluted in carbon. The carbon content of austenite for a homogeneous alloy should follow the path '$d - d'$' with increasing reaustenitisation temperature as shown in Fig. 6.17. Hence, we can see, Fig. 6.14a shows an increase in the M_s temperature with increasing reaustenitisation temperature.

But the situation for T_B =400 °C is rather different, when most of the austenite in the starting microstructure being confined eventually to substitutional solute-enriched regions (Fig. 6.9). Consequently, the effective A_{e3} curve controlling austenite growth will not be a single curve, but rather a range of A_{e3} curves will be at work. This is represented in Figs. 6.17 and 6.18. At the lower reaustenitisation temperatures, the reaction is much more restricted to solute-enriched regions with the lower A_{e3} temperatures. The growth of austenite will stop at a point 'c' on the A_{e3} curve for the solute-enriched regions. With an increase in T_γ, austenite bands thicken and advance into regions of relatively lower A_{e3} temperature, *i.e.* the relevant A_{e3} curve moves towards the solute-depleted regions, following the path '$c - d'$' as shown in Figs. 6.17 and 6.18. The growth of austenite will then stop at a point somewhere away from the A_{e3} curve of solute enriched region but near the A_{e3} curve of solute depleted region on the phase diagram. In this way, the carbon concentration of austenite is expected to increase with an increase in T_γ, as is observed experimentally via the M_s temperatures.

The volume fraction $V_{\gamma s}$ of austenite in a heterogeneous sample transformed at a temperature T_γ is given by the lever rule of the phase diagram shown in Fig. 6.17.

$$V_{\gamma s} = \frac{ab}{ac} \tag{6.3}$$

At the same T_γ, volume fraction $V_{\gamma h}$ of austenite formed in a homogeneous alloy (or in a heterogeneous sample which transforms uniformly to bainite at T_B) should be

$$V_{\gamma h} = \frac{ab}{ad} \tag{6.4}$$

As $ac < ad$, hence, $V_{\gamma s} > V_{\gamma h}$ for the samples reaustenitised at the same temperature T_γ.

6.3.1 Experimental Confirmation of the "Yang and Bhadeshia Model"

Yang and Bhadeshia[18] have investigated the growth of austenite from bainitic ferrite in a matrix of austenite in homogeneous steels. Their model explains the variations in the maximum degree of reaustenitisation to be expected as a function of temperature, the reaction start temperature T_γ, the temperature above which the completion of reaustenitisation occurs, and the equilibrium austenite volume fraction transformed during the isothermal holding as a function of the equilibrium carbon concentration of austenite and the carbon concentration of residual austenite when the isothermal bainite transformation has ceased. Bainite is known to exhibit an incomplete reaction phenomenon[16, 23]; the reaction stops when the carbon concentration of the residual austenite reaches the T_0' curve on the phase diagram and in this sense stops prematurely before an equilibrium volume fraction of bainite is obtained. So, the carbon concentration x_γ of the residual austenite, when the formation of bainite ceases during isothermal holding at the temperature T_B, is given by;

$$x_\gamma = x_{T_0}\{T_B\} \tag{6.5}$$

Where x_{T_0} is the carbon concentration of the residual austenite at a temperature, where ferrite, whose free energy has been raised by a stored energy term associated with the transformation strain, and austenite of identical composition have the same free energy. The experimental data obtained in the present work for x_γ are marked as points 'a' and 'b' on Fig. 6.19, which represent the carbon content of austenite after the specimen were transformed to bainite at T_B =320 °C and T_B =400 °C respectively. In this phase diagram, a set of T_0 and A_{e3} phase boundaries has been calculated for the range of chemical compositions detected experimentally. Since the microanalysis technique draws information from an interaction volume which is about $4.5\mu m^3$, the actual variations in solute concentrations may be underestimated. It should be noted that the values of x_γ for cases 'a' and 'b' are much less than the equilibrium carbon concentration (x_{Ae3}) at the respective transformation temperatures. Hence, the reverse transformation cannot be expected to happen immediately the temperature is raised above that at which the bainite grows (*i.e.* T_B). The formation of austenite will occur first at a temperature where $x_{T_0} = x_{Ae3}$ for the austenite whose carbon content is given by the points 'c' and 'd' in the Fig. 6.19.

These temperatures have been marked as $T_{\gamma a}$ and $T_{\gamma b}$ on the A_{e3} phase boundary. The experimental results support the prediction[18] that at any temperature greater than $T_{\gamma a}$ and $T_{\gamma b}$ for cases 'a' and 'b' respectively (Fig. 6.19), reaustenitisation should cease as soon as the residual austenite carbon concentration reaches the A_{e3} curve, *i.e.* when

$$x_\gamma = x_{Ae3}\{T_{\gamma a}\} \tag{6.6}$$

Also, a temperature $T_{\gamma f}$ (Fig. 6.19) above which the alloy can transform completely into austenite satisfies the condition

$$x_{Ae3}\{T_{\gamma f}\} = \overline{x} \tag{6.7}$$

It can be established from the Fig. 6.19 as the average carbon content of the alloy $\overline{x}$ predicted that the specimen should transform completely to austenite at 760 °C and the metallographic confirmation of this can be seen in Fig. 6.20 and 6.21.

6.4 Conclusions

Reaustenitisation from a mixture of bainite and austenite has been studied isothermally under conditions where the nucleation of austenite is not necessary. The dilatometric results can be explained well by a theory for reaustenitisation proposed by Yang and Bhadeshia[18]. Specimens partially transformed to bainitic ferrite and carbon enriched residual austenite, comparison of the volume fractions of austenite obtained in homogeneous and heterogeneous samples bearing in mind that the two kinds of samples do not have equivalent starting microstructures and hence carbon content of austenite is different in the two cases. As previously (Table 3.4) higher volume fractions of bainite were obtained in the homogeneous alloy its reaustenitisation start temperature will be lower than the heterogeneous alloy. The temperature at which the completion of reaustenitisation occurs, being dependent on average carbon content of the alloy $\overline{x}$, should be the same for homogeneous and heterogeneous alloys.

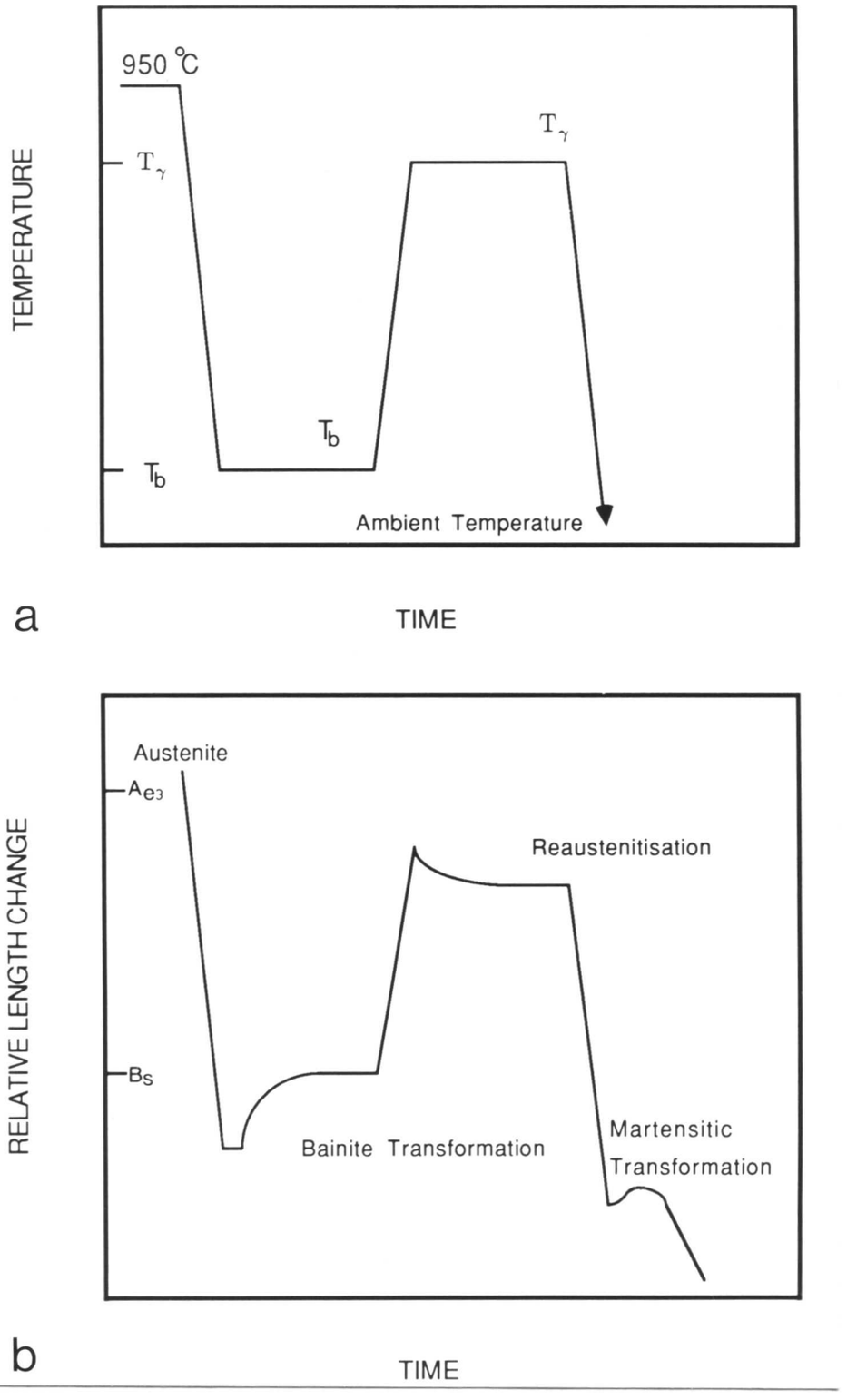

Fig. 6.1: *Schematic illustration of heat treatments used in the experiments.*

(a) Time versus temperature curve.

(b) Time versus relative length change curve.

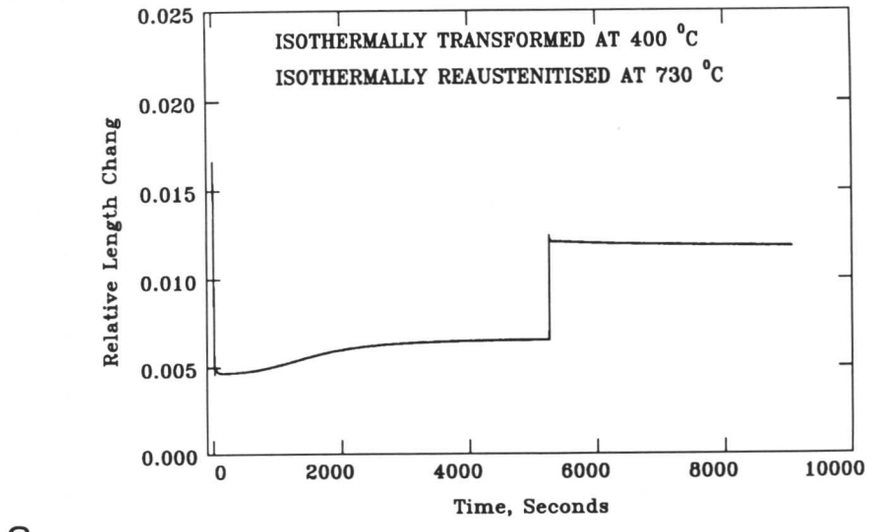

a

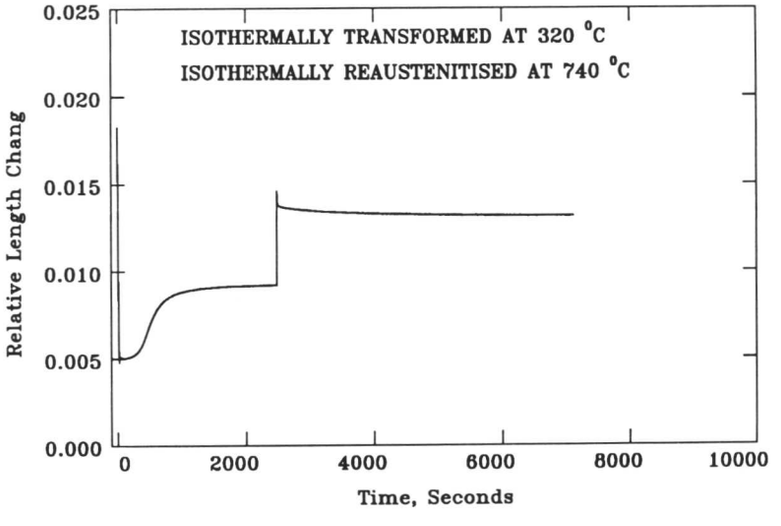

b

Fig. 6.2: *Typical dilatometric curves showing firstly the partial decomposition of austenite to the maximum amount of bainitic ferrite that can form at the transformation temperature concerned. In the second stage, the mixture of bainitic ferrite and carbon enriched austenite is rapidly heated to a temperature where it is thermodynamically possible for the austenite to grow.*

(a) Sample transformed initially to bainite at T_B*=400 °C and then it is isothermally reaustenitised at* T_γ*=730 °C.*

(b) Sample transformed initially to bainite at T_B*=320 °C and then it is isothermally reaustenitised at* T_B*=740 °C.*

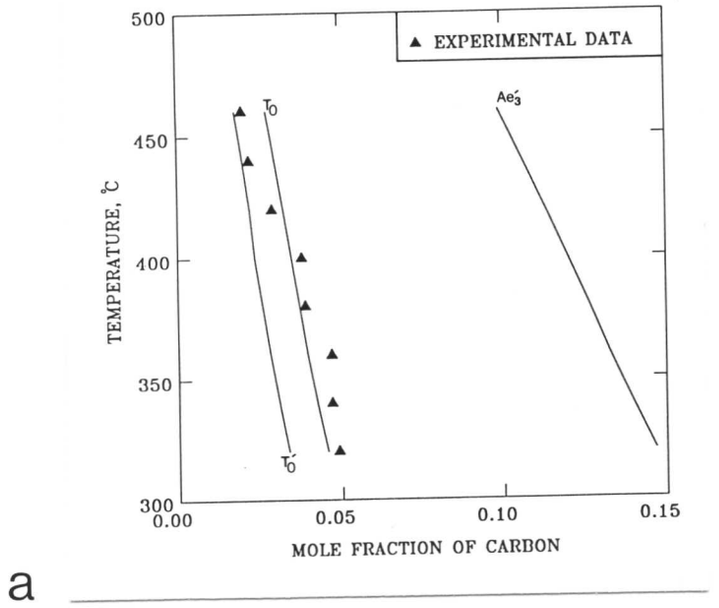

a

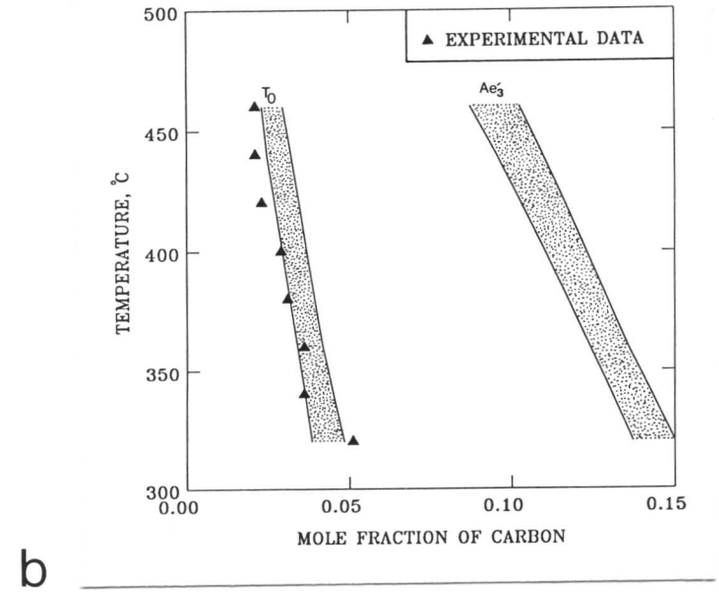

b

Fig. 6.3: *Calculated*[16,20] *phase boundaries for 300M steel along with the experimental data for samples transformed isothermally to upper bainite until the reaction ceased.*

(a) Calculated T_0, T'_0 *and* A'_{e3} *phase boundaries assuming a chemically homogeneous alloy. All the points on the diagram are experimental data.*

(b) Calculated T_0 *and* A'_{e3} *phase boundaries for the heterogeneous alloy, the shaded regions covering the range of chemical compositions detected experimentally.*

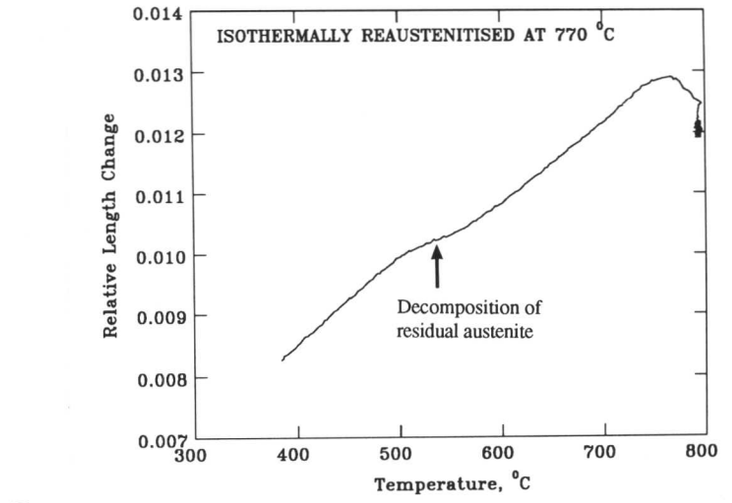

a

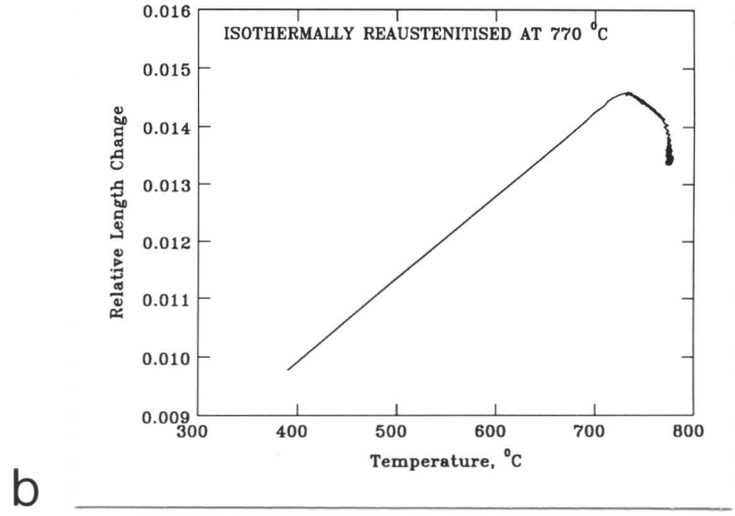

b

Fig. 6.4: *The effect of heating rate in suppressing any decomposition of residual austenite, prior to the sample reaching* T_γ.

(a) Heating rate $= 11\ ^\circ C s^{-1}$.

(b) Heating rate $= 100\ ^\circ C s^{-1}$.

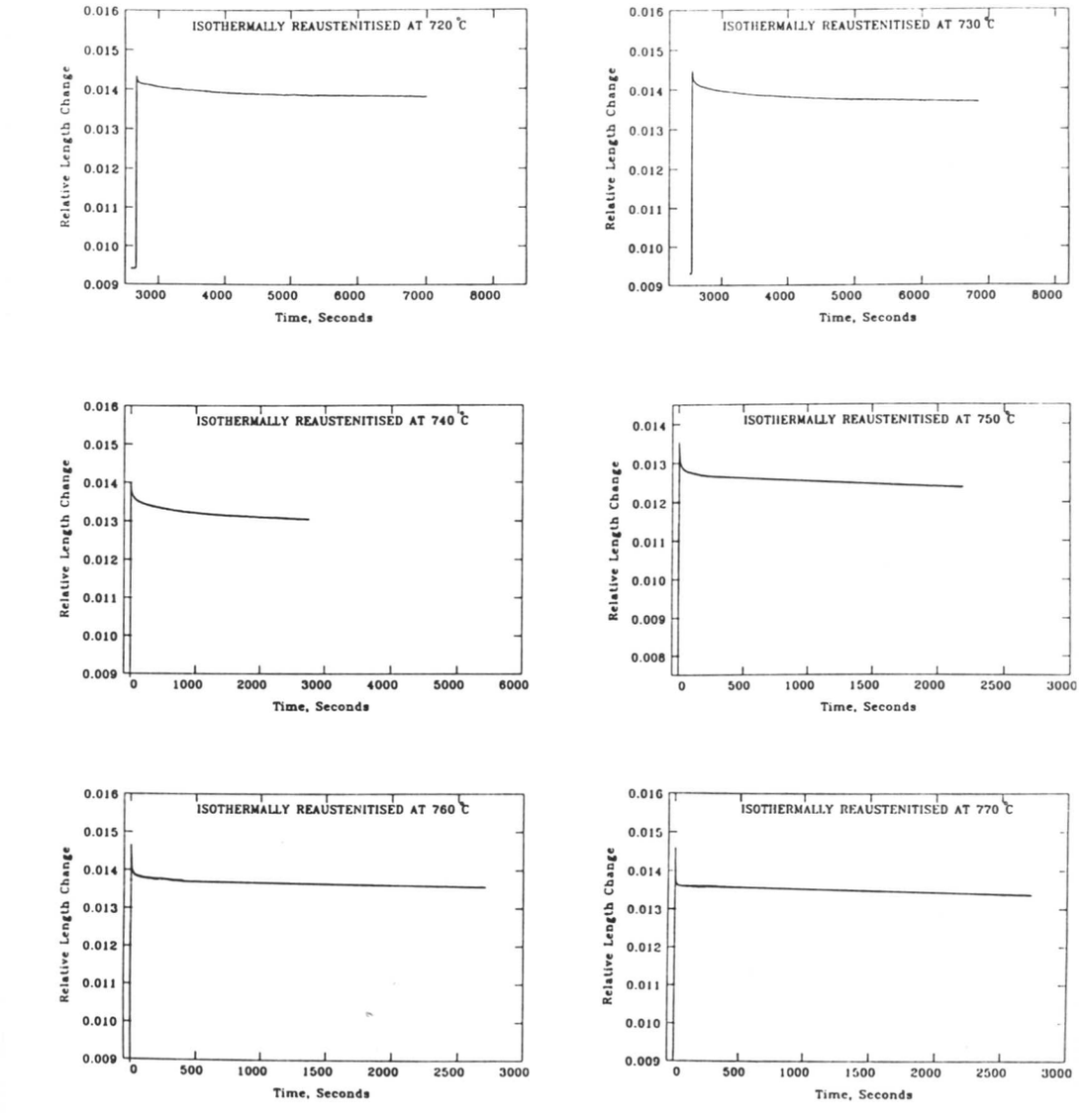

Fig. 6.5: *Graphs showing the relative length change obtained as a function of time during isothermal reaustenitisation at a variety of temperatures. The samples were all initially transformed at 320 °C to obtain a mixed starting microstructure of bainitic-ferrite and carbon-enriched residual austenite.*

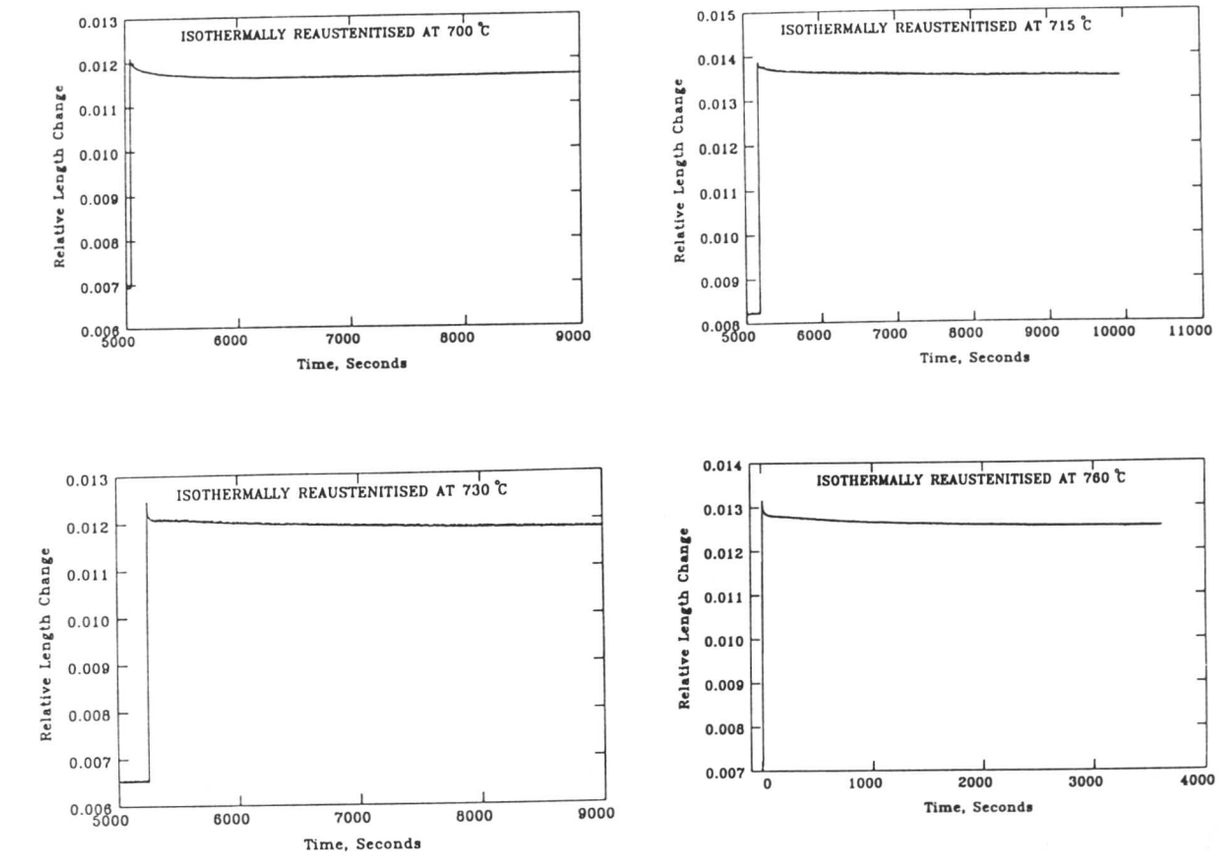

Fig. 6.6: *Graphs showing the relative length change obtained as a function of time during isothermal reaustenitisation at a variety of temperatures. The samples were all initially transformed at 400 °C to obtain a mixed starting microstructure of bainitic-ferrite and carbon-enriched residual austenite.*

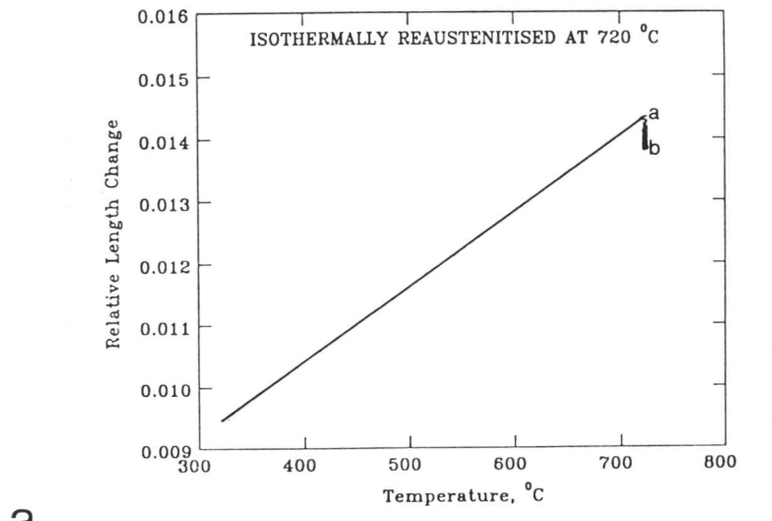

a

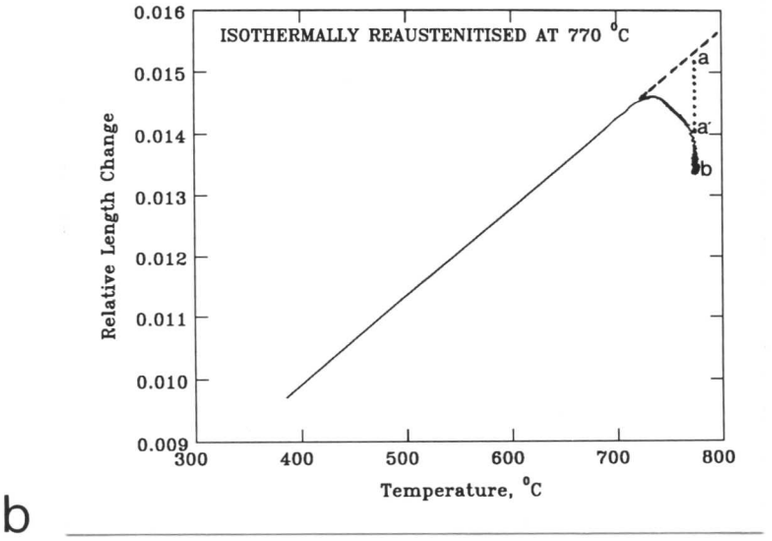

b

Fig. 6.7: *The relative length change versus temperature curves, of samples which were transformed initially to a mixture of bainitic ferrite and austenite at* T_B*=320 °C, prior to reaustenitisation at a variety of temperatures.*

(a) Isothermal reaustenitisation at 720 °C, from a starting microstructure of bainitic ferrite and austenite. The maximum relative length change can in this case be measured directly as the difference between points 'a' and 'b'.

(b) Isothermal reaustenitisation at 770 °C from a starting microstructure of bainitic ferrite and austenite. Because of the high value of T_γ*, some austenite is seen to form during heating before the sample reached its designated isothermal reaustenitisation temperature. The distance 'a−a'' is therefore added to 'a'−b' (the relative length contraction at* T_γ*) to correct for this prior reaction.*

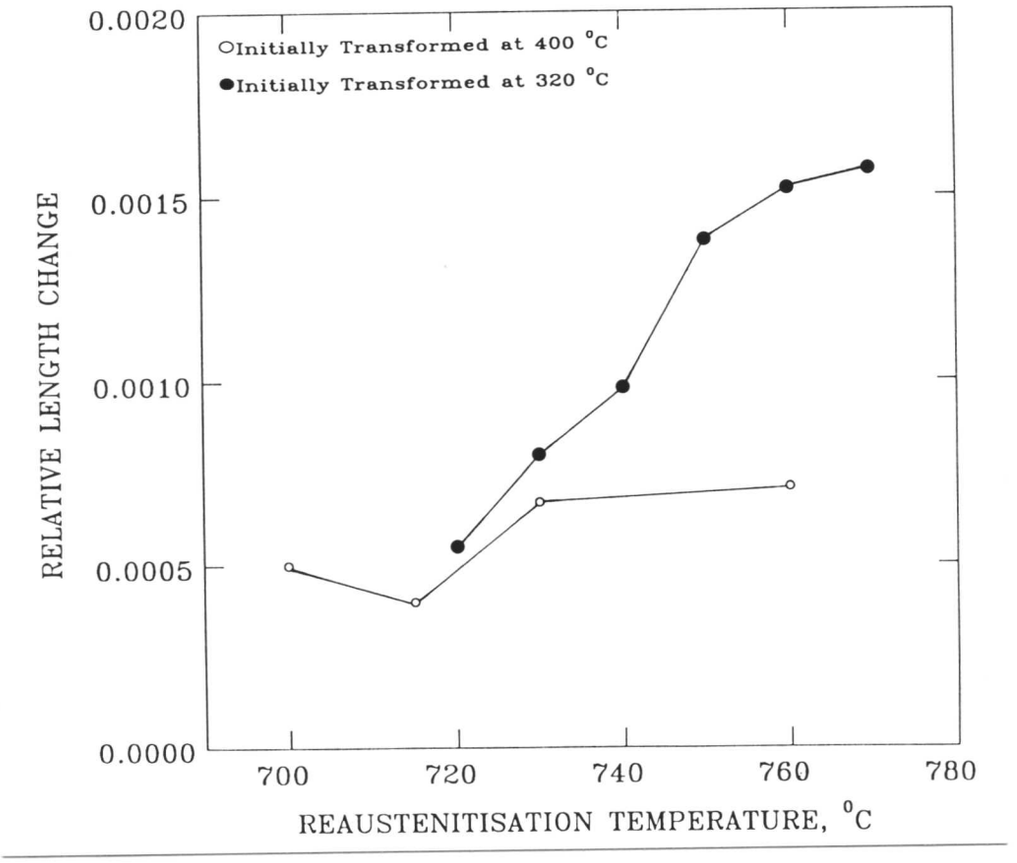

Fig. 6.8: *Magnitudes of the maximum relative length change obtained during isothermal reaustenitisation of heterogeneous samples, as a function of the isothermal reaustenitisation temperature* T_γ. *The absolute relative length changes given here are, in fact, negative as the growth of austenite at the expense of ferrite results in an increase in density. Data from two different starting microstructures, contain different amounts of residual austenite, are presented.*

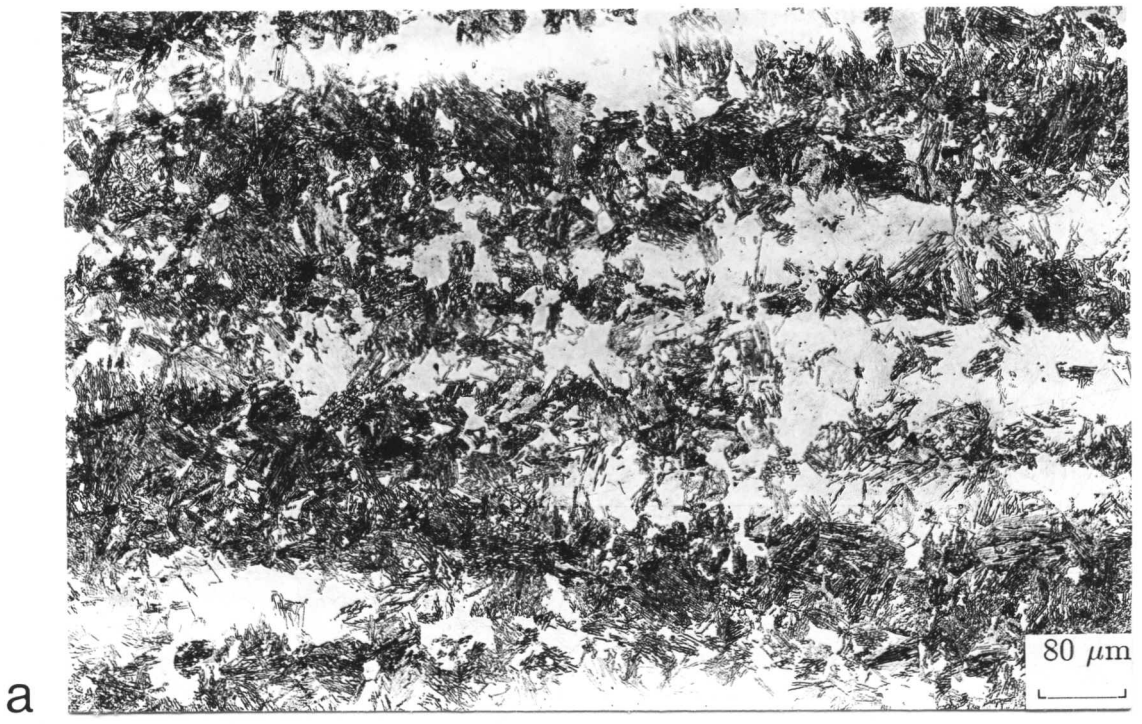

a

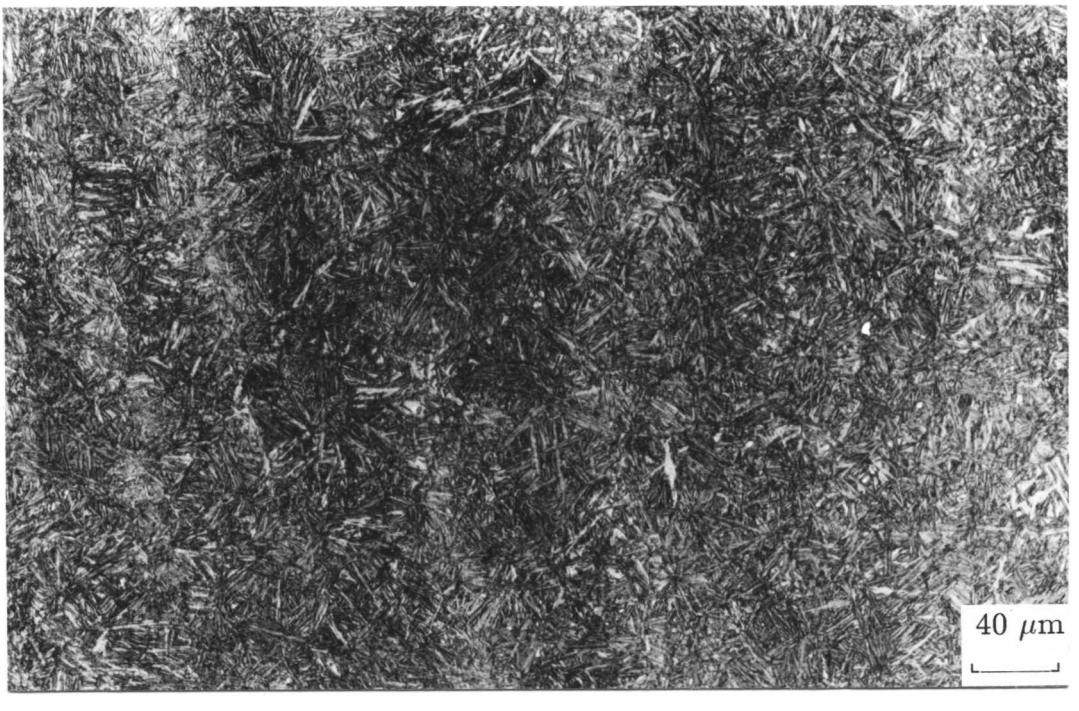

b

Fig. 6.9: *Micrographs showing the extent of bainitic-ferrite formation and the amount of carbon enriched residual austenite obtained by reaction at* T_B*, before rapid heating to different reaustenitisation temperatures.*

(a) Optical micrograph of a heterogeneous specimen isothermally transformed at T_B*=320 °C.*

(b) Optical micrograph of heterogeneous specimen isothermally transformed at T_B*=400 °C, where the amount of bainitic ferrite that can form is much more limited.*

Isothermal Transformation Temperature °C	Experimental Volume Fraction	
	Homogeneous	Heterogeneous
320	0.63	0.64
340	0.60	0.48
380	0.45	0.40
400	0.50	0.33
420	0.34	0.14
430	0.06	0.04
440	0.11	0.07
450	0.02	0.03
460	0.03	0.05

Table 6.1: *Dilatometrically determined maximum volume fractions of bainitic ferrite obtained by isothermal transformation at the temperatures indicated, for both the as-received and the homogenised samples of 300M steel.*

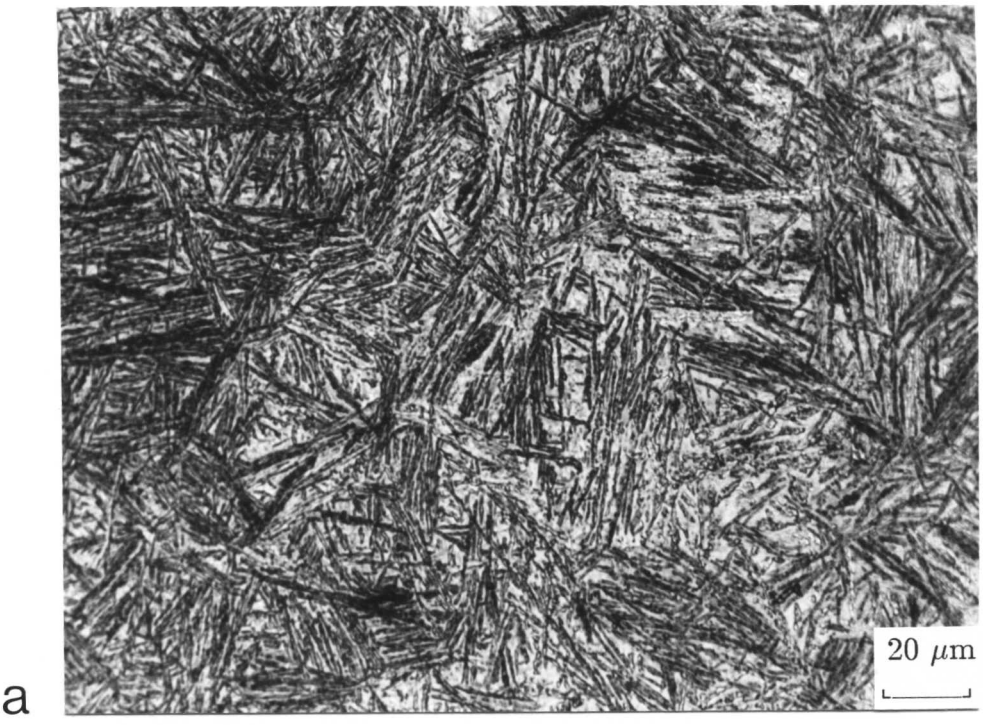

a

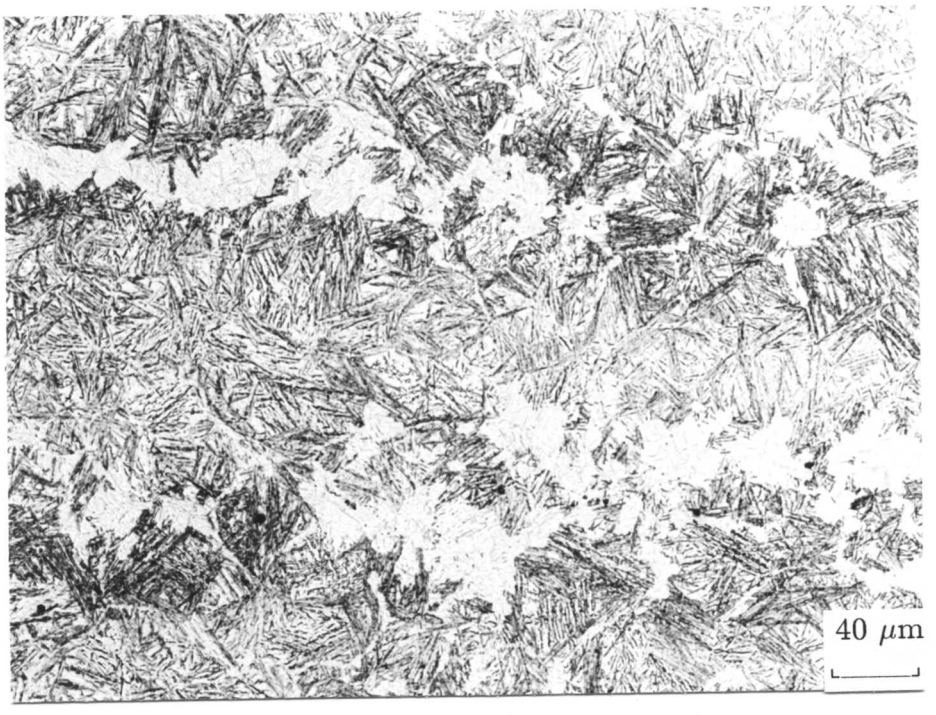

b

Fig. 6.10: *Comparison of homogeneous and heterogeneous samples after partial reaustenitisation at 740 °C. Both the samples were initially transformed at 320 °C to obtain a mixed starting microstructure of bainitic-ferrite and carbon-enriched residual austenite.*

(a) Homogeneous alloy.

(b) Heterogeneous alloy.

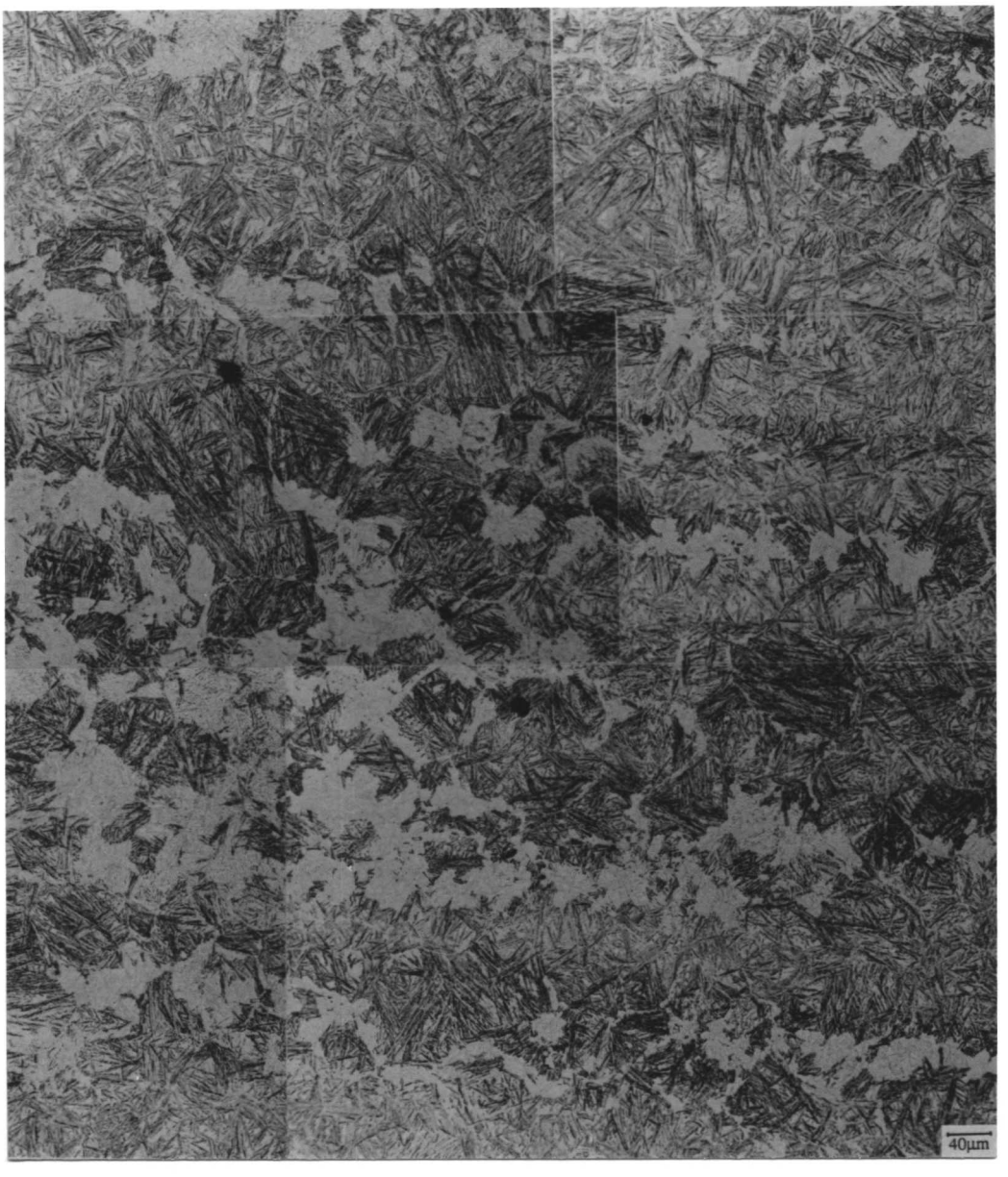

Fig. 6.11: *A partially reaustenitised heterogeneous sample showing differences in the extent of the reaction. The reaction has proceeded to a larger extent along the solute enriched bands, whose lower* A_{e3} *temperature causes them to transform first.*

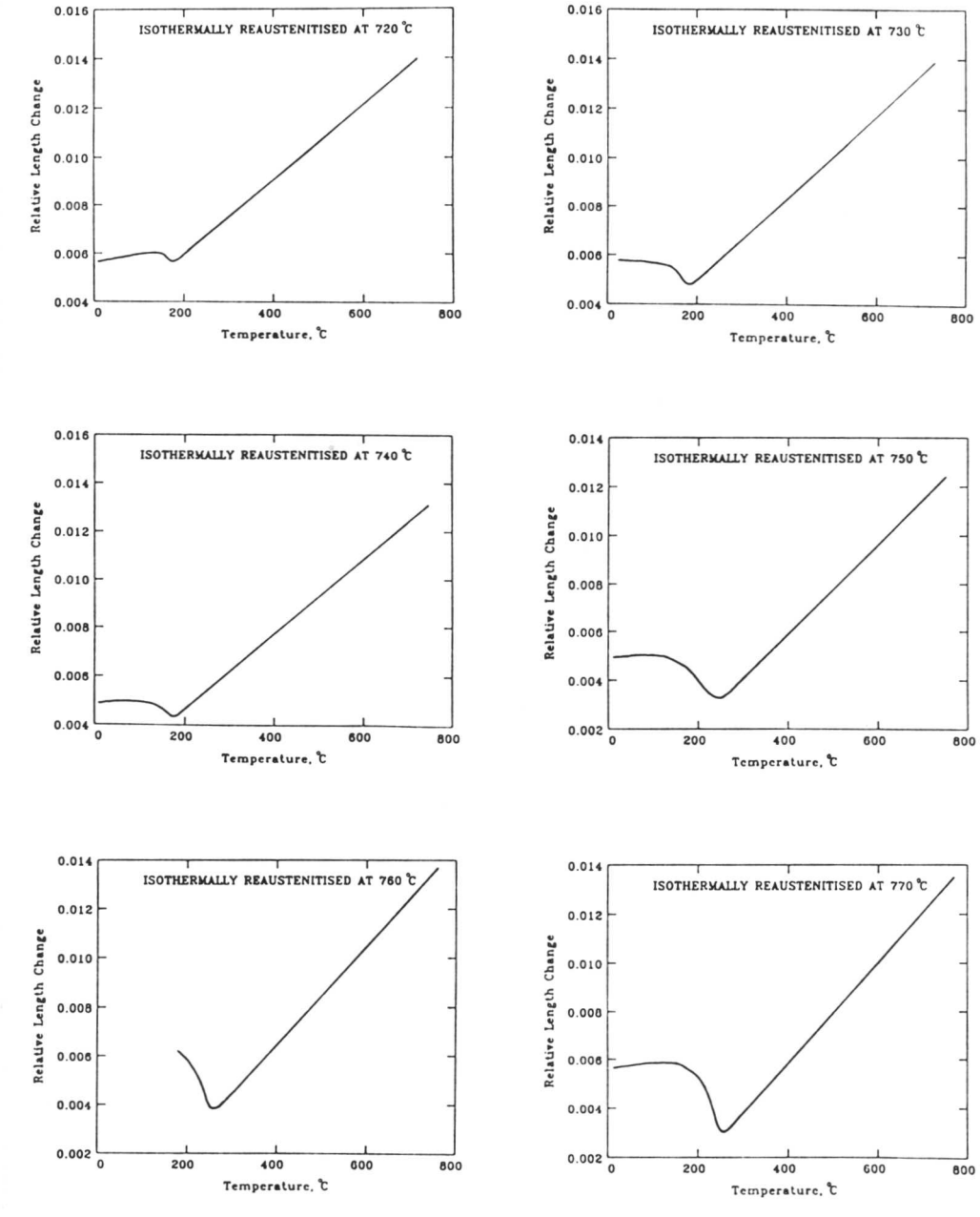

Fig. 6.12: *Relative length changes recorded during the quenching of heterogeneous samples after isothermal reaustenitisation at the temperature* T_γ *indicated in each diagram. The specimens were transformed to bainitic ferrite and carbon enriched residual austenite formed at* T_B*=320 °C prior to reaustenitisation.*

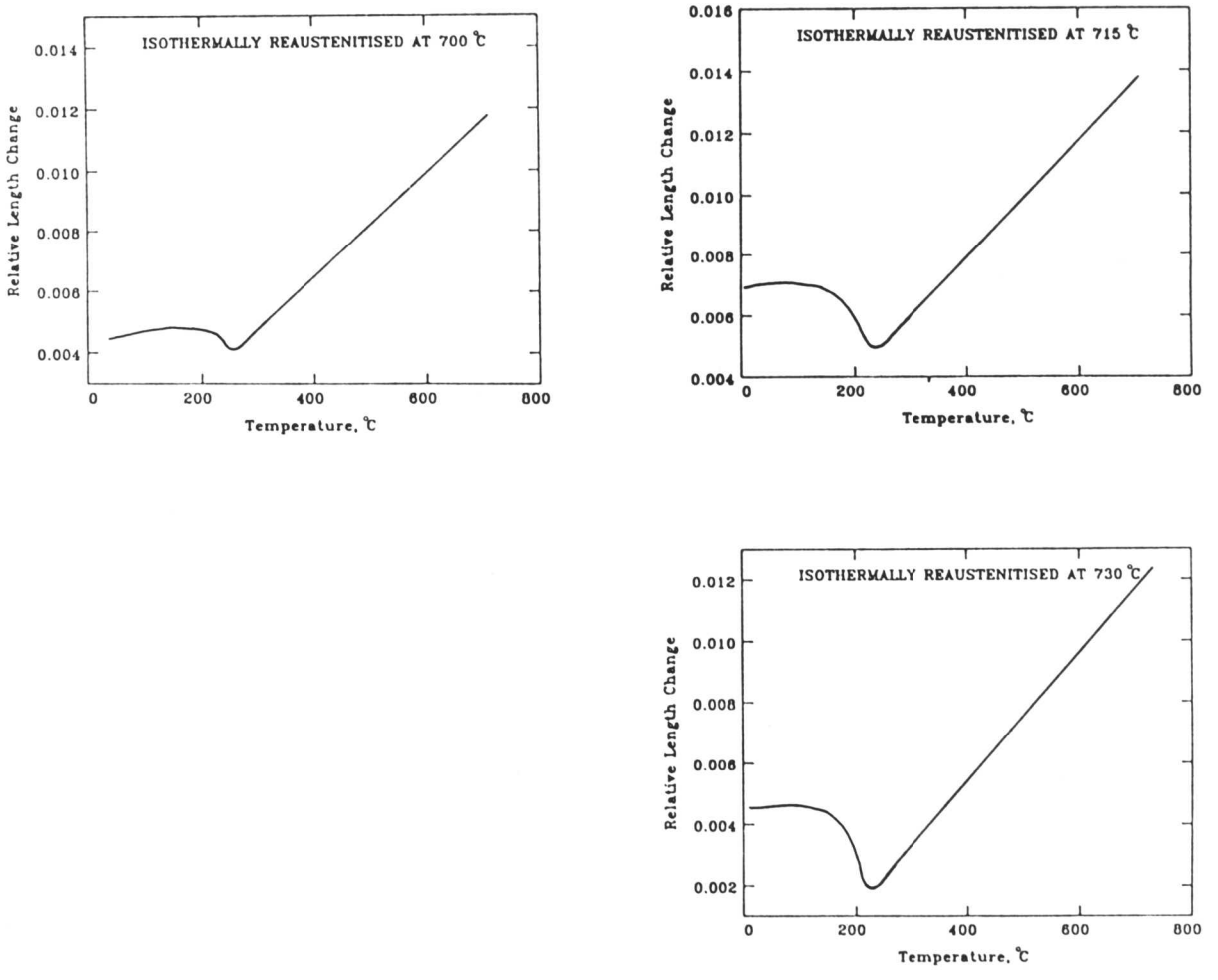

Fig. 6.13: *Relative length changes recorded during the quenching of heterogeneous samples after isothermal reaustenitisation at the temperature* T_γ *indicated in each diagram. The specimens were transformed to bainitic ferrite and carbon enriched residual austenite formed at* T_B*=400 °C prior to reaustenitisation.*

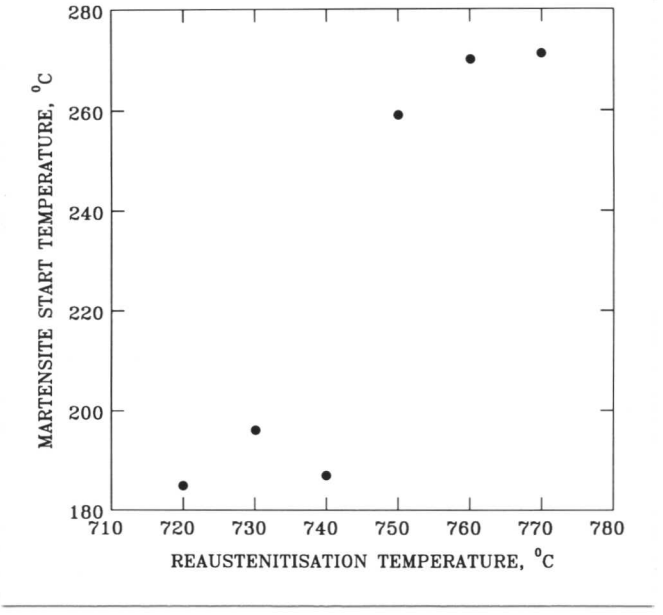

Fig. 6.14: *Dilatometrically measured martensitic-start temperatures as the heterogeneous samples reaustenitised at different temperatures were quenched to ambient temperature. The specimens were transformed to bainitic ferrite and carbon enriched austenite at 320 °C prior reaustenitisation.*

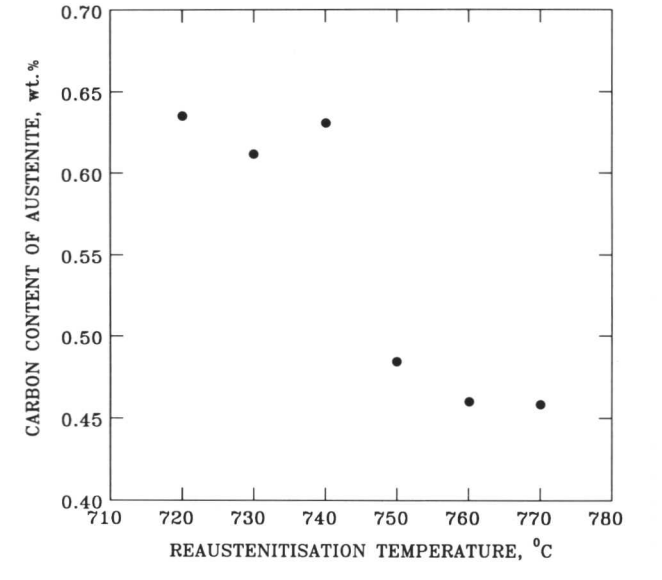

Fig. 6.15: *Calculated carbon concentrations of austenite formed after the heterogeneous specimens were reaustenitised at a variety of temperatures. The calculations are based on dilatometrically measured values of martensitic-start temperatures as shown in Fig. 6.14.*

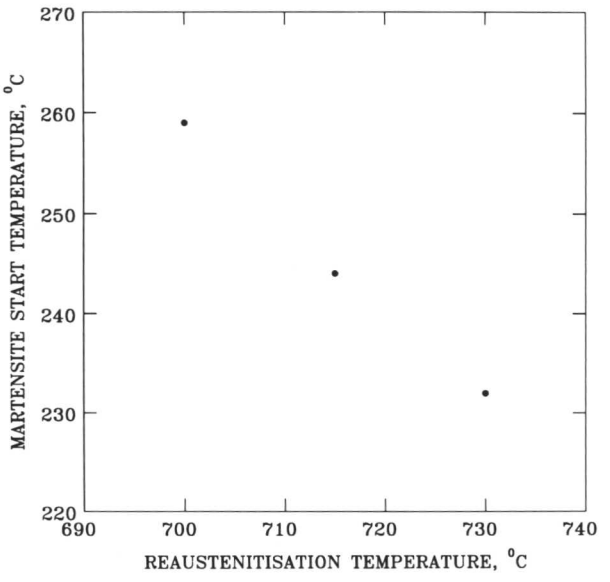

Fig. 6.16: *Dilatometrically measured martensitic-start temperatures as the samples reaustenitised at different temperatures were quenched to ambient temperature. The specimens were transformed to bainitic ferrite and carbon enriched austenite at 400 °C prior to reaustenitisation.*

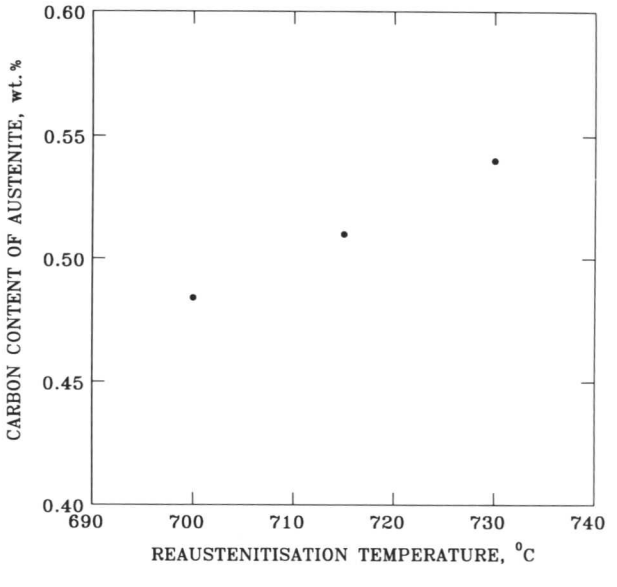

Fig. 6.17: *Calculated carbon concentrations of austenite formed after specimens were reaustenitised at different temperatures. The calculations are based on dilatometrically measured values of martensitic-start temperatures shown in Fig. 6.16*

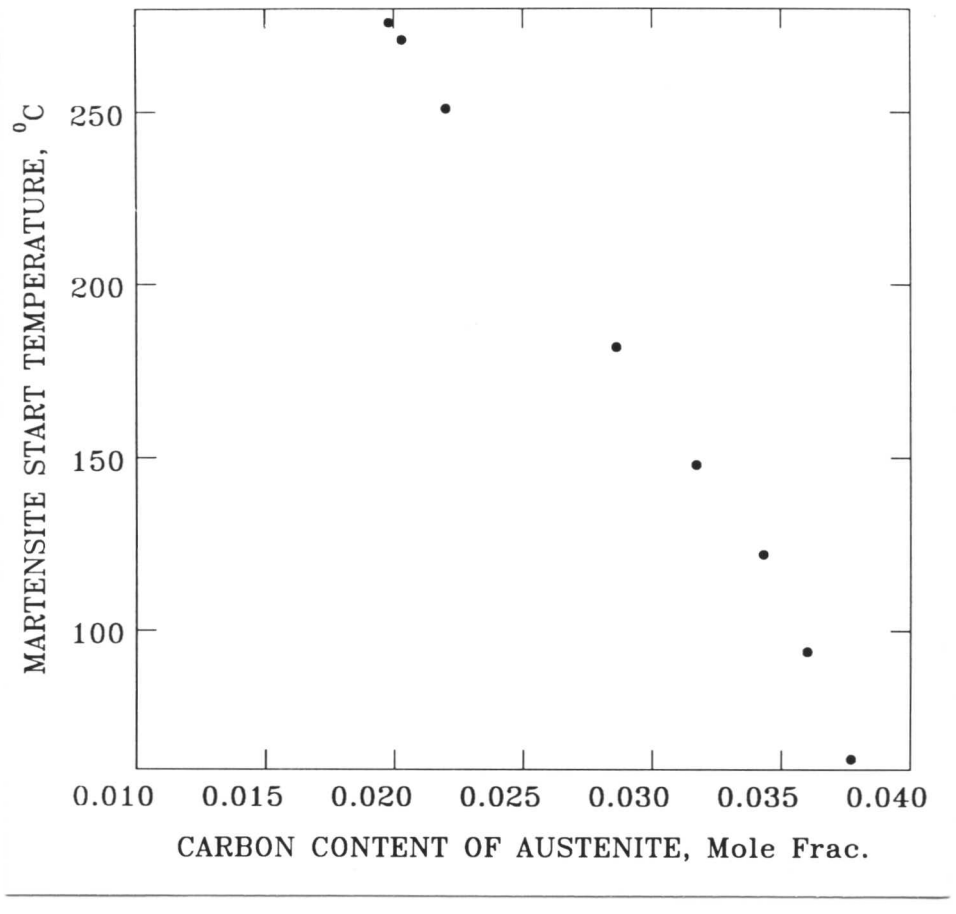

Fig. 6.18: *Calculated*[21,22] *martensite start temperatures of austenite with different carbon content for 300M steel. A linear relation (eq. 6.1) was obtained by fitting a curve to this data with correlation coefficient of -0.99.*

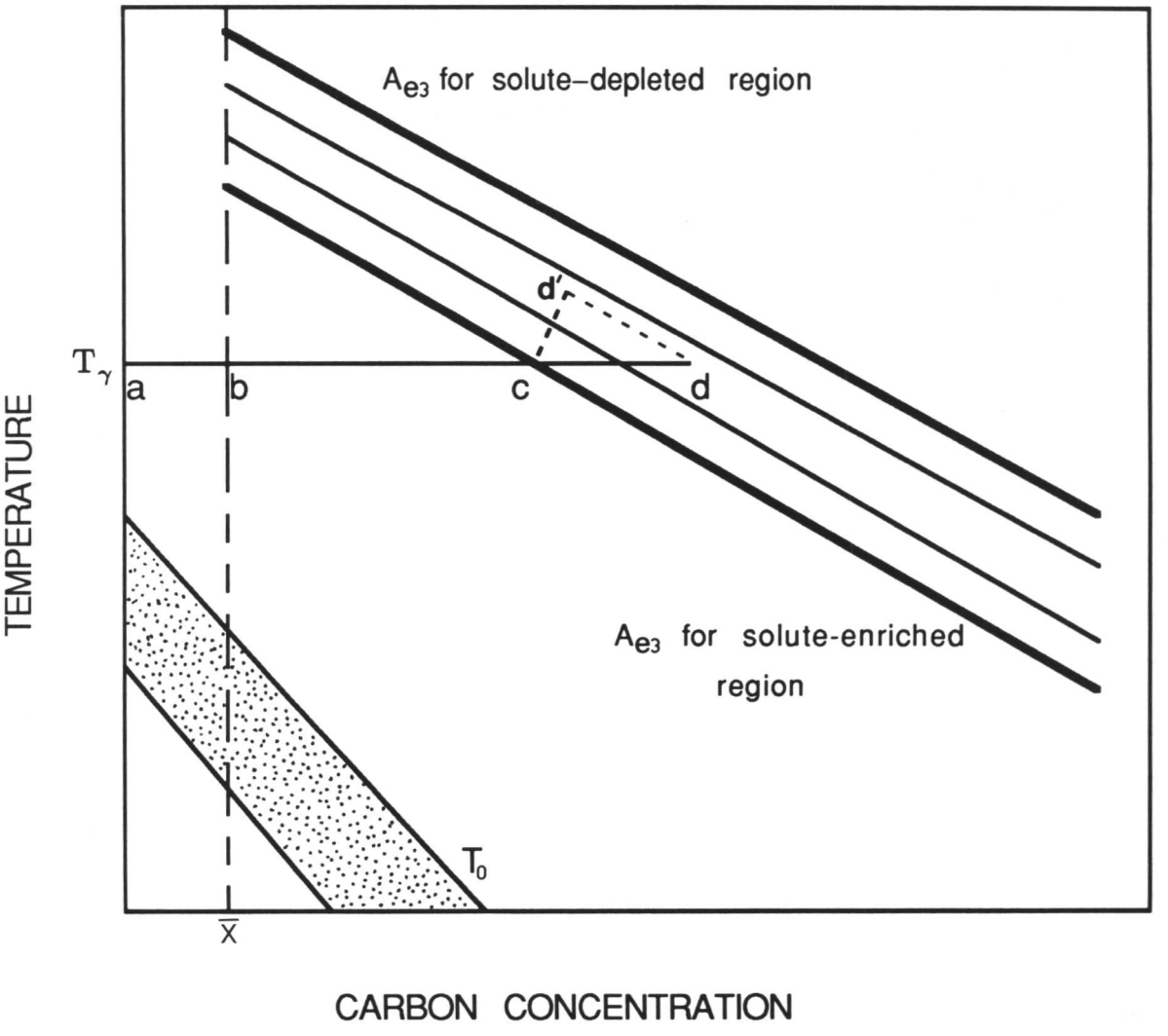

Fig. 6.19: *Schematic phase diagram of a heterogeneous material with average carbon content* $\overline{X}$. A_{e3} *and* T_0 *curves have been represented by a set of lines covering a composition range.*

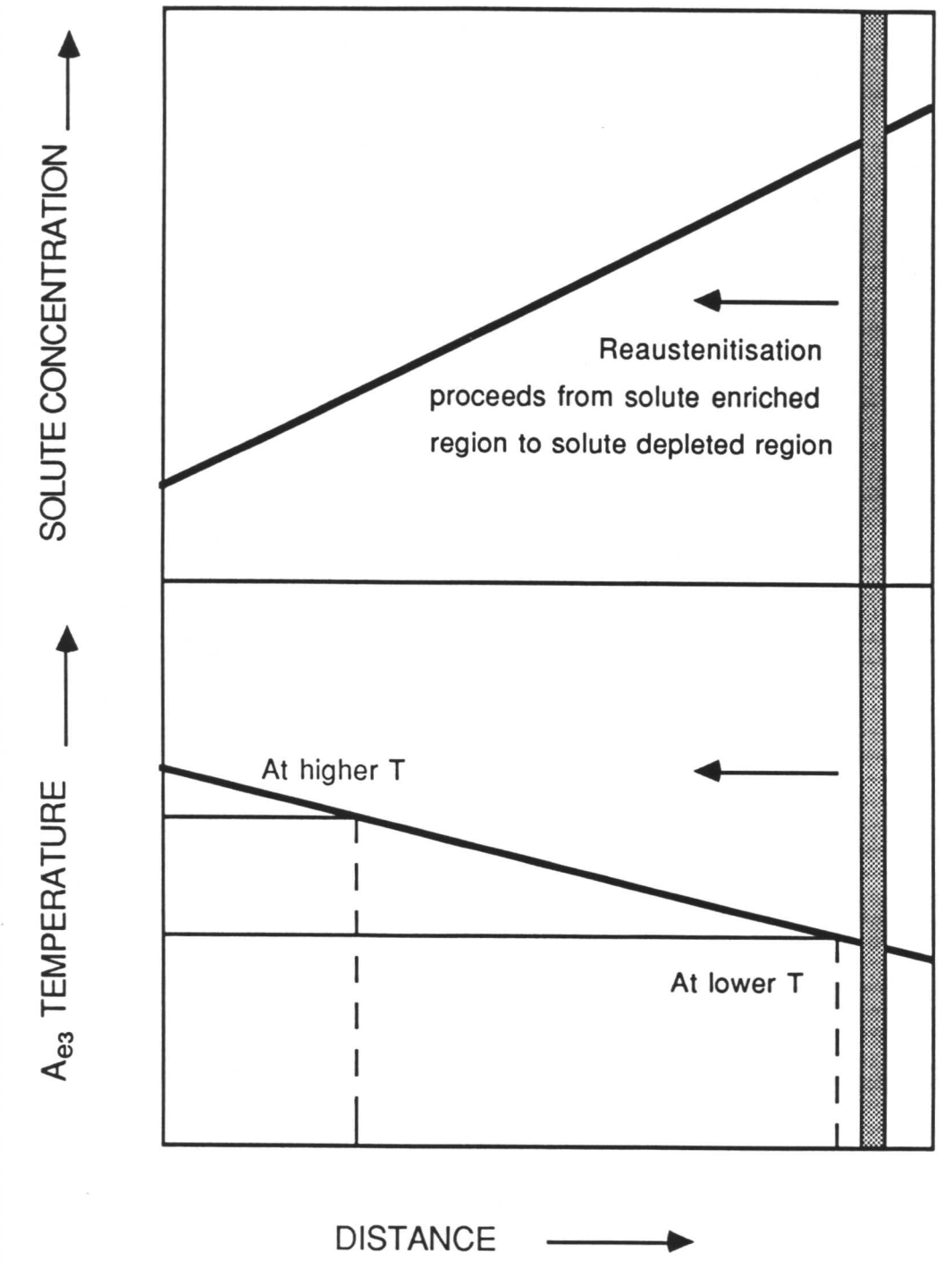

Fig. 6.20: *Schematic diagram showing the variation of A_{e3} temperature in a heterogeneous alloy and its effect on growth of austenite.*

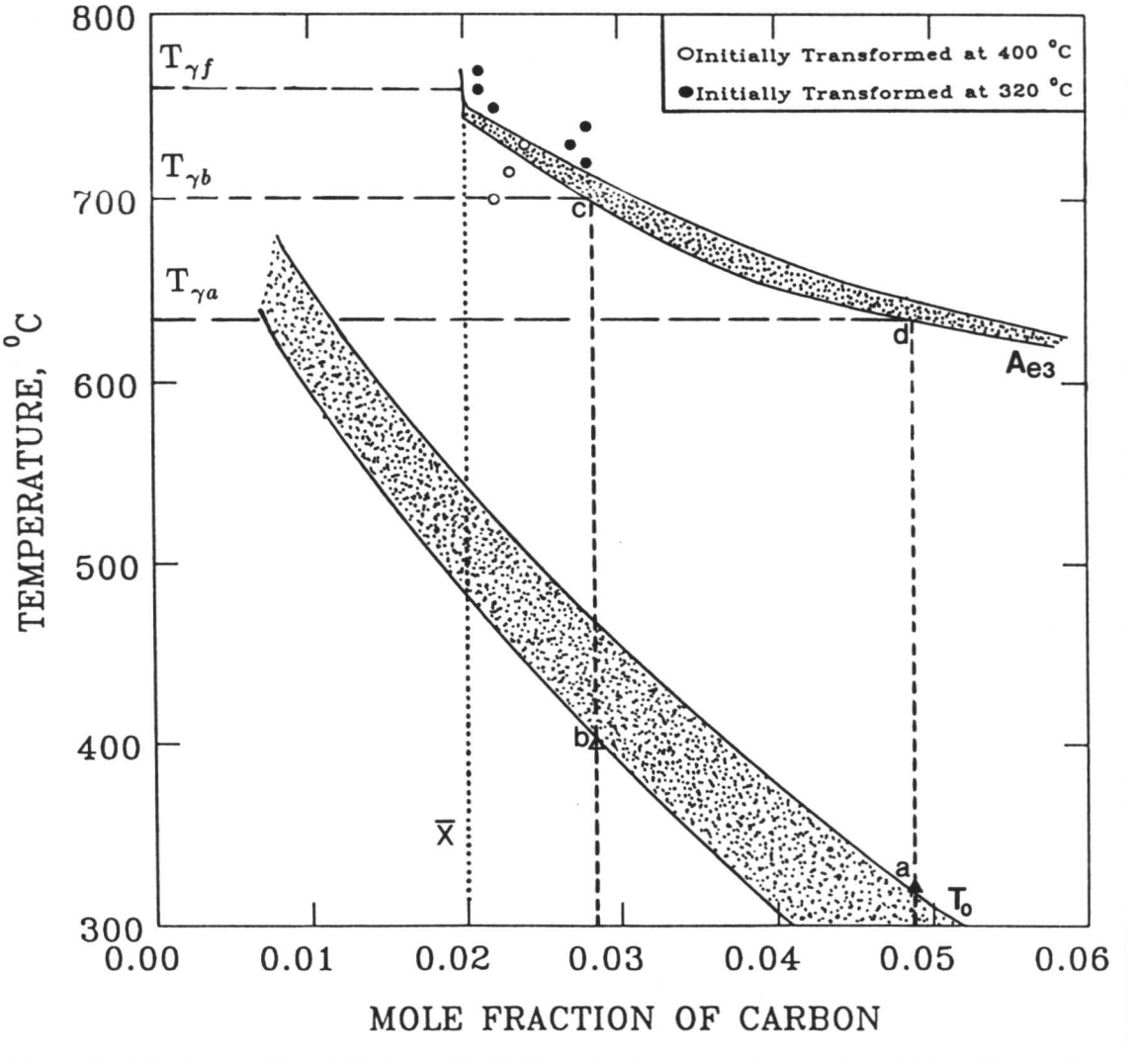

Fig. 6.21: *Calculated* A_{e3} *and* T_0 *phase boundaries for heterogeneous 300M steel, covering the range of chemical compositions detected experimentally.* T_0 *curve is calculated as in Refs. [16,20] and the* A_{e3} *curve is calculated as in Ref. 24.*

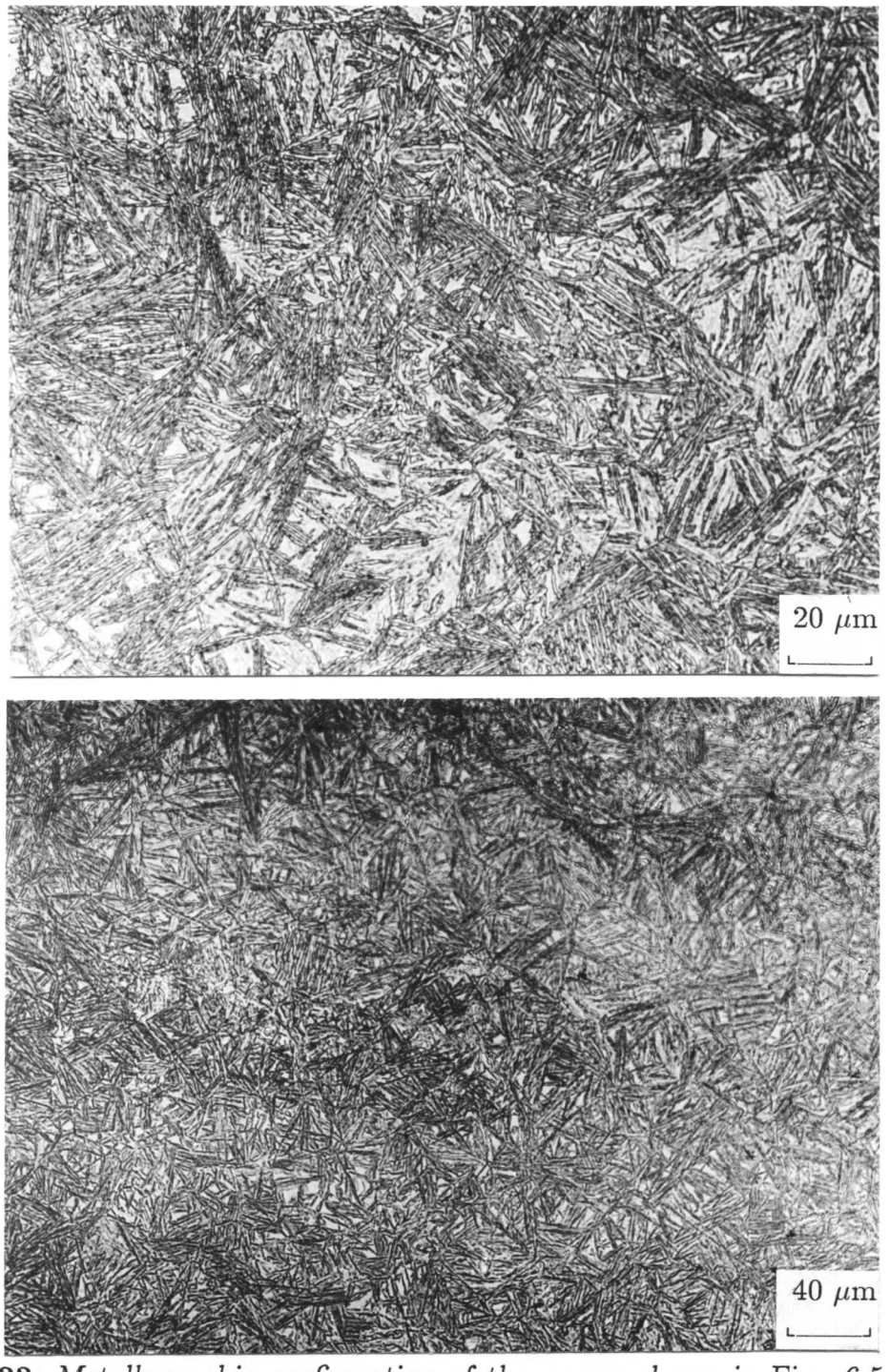

Fig. 6.22: *Metallographic confirmation of the curves shown in Fig. 6.5. The samples were initially transformed to bainitic ferrite and carbon enriched residual austenite at 320 °C.*

(a) Optical micrograph of the heterogeneous specimen isothermally reaustenitised at 720 °C.

(b) Optical micrograph of the heterogeneous specimen isothermally reaustenitised at 730 °C.

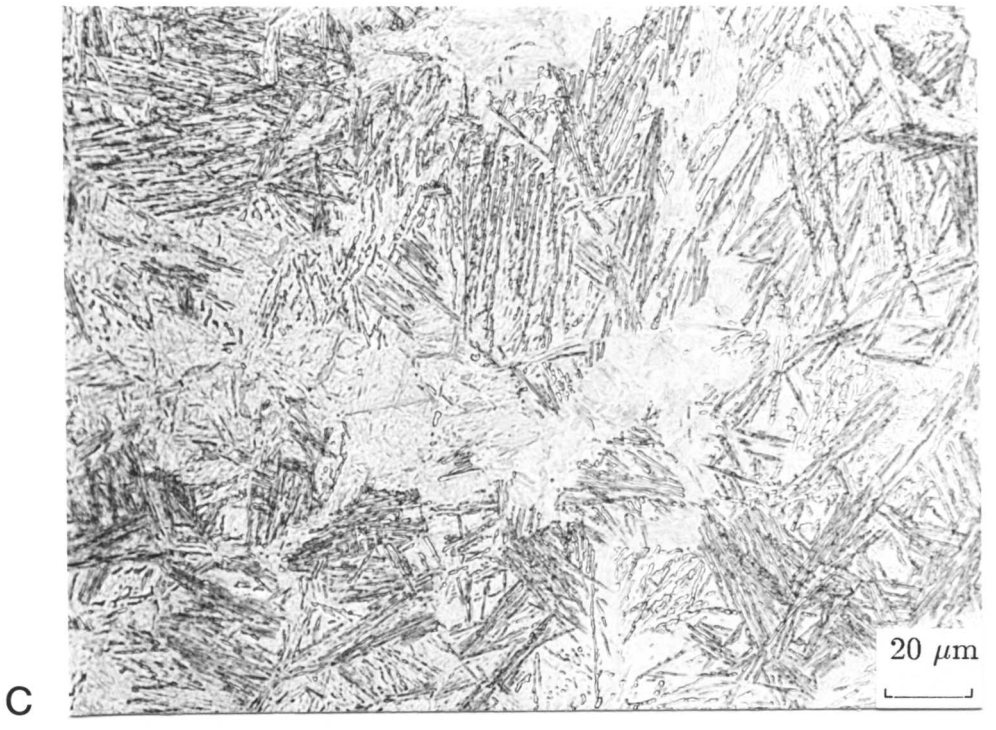

c

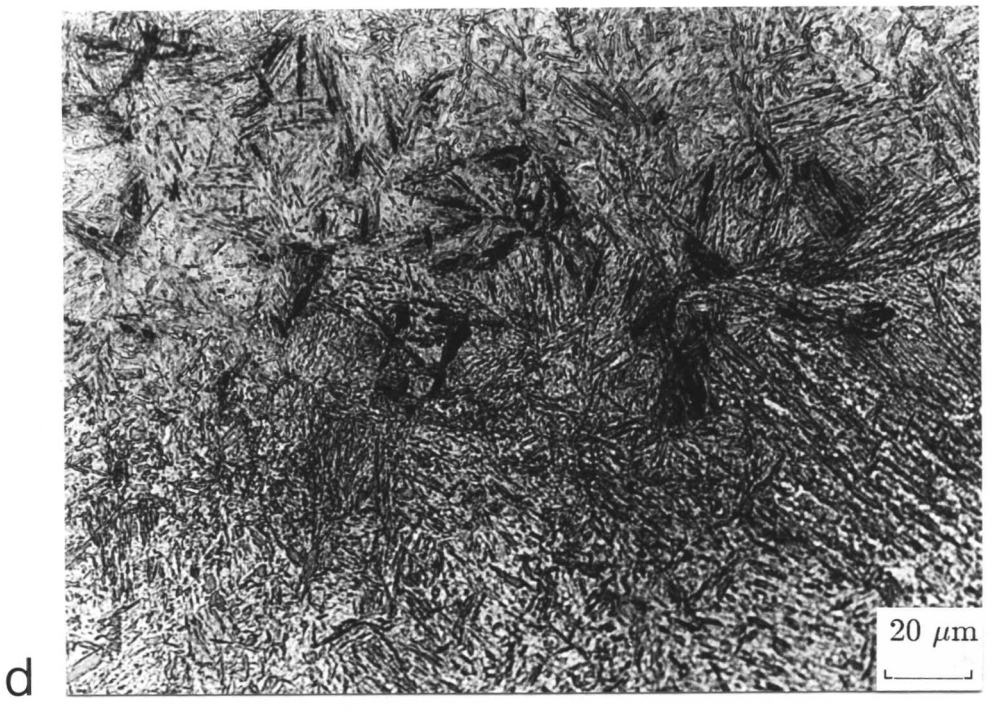

d

Fig. 6.22: *(continued .....)*

(c) Optical micrograph of the heterogeneous specimen isothermally reaustenitised at 740 °C.

(d) Optical micrograph of the heterogeneous specimen isothermally reaustenitised at 750 °C.

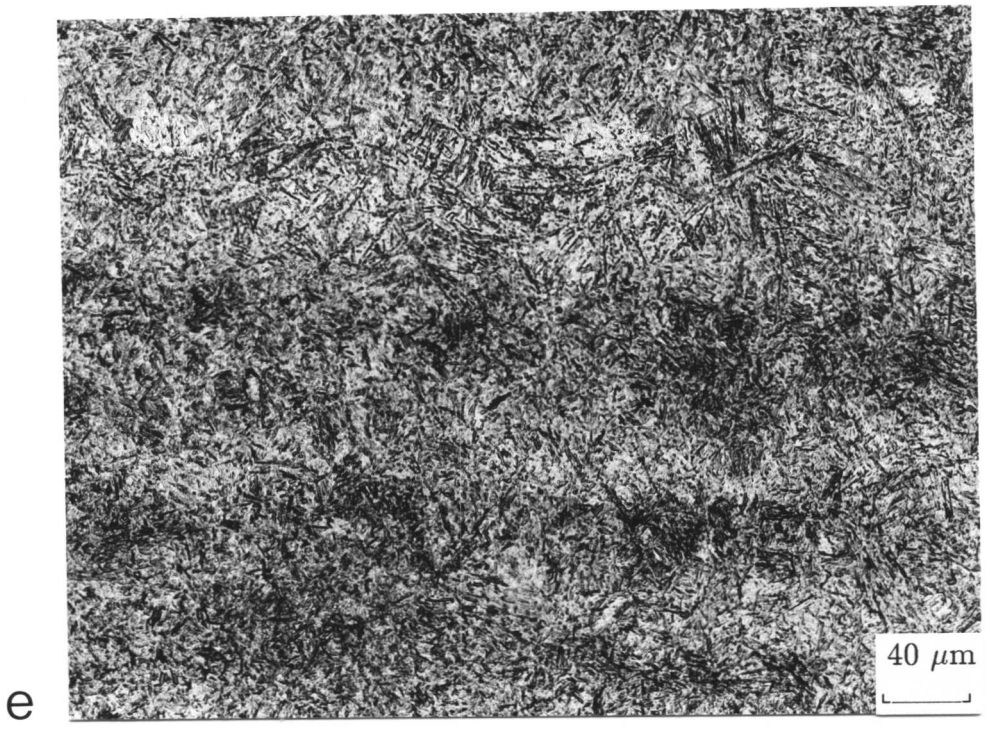

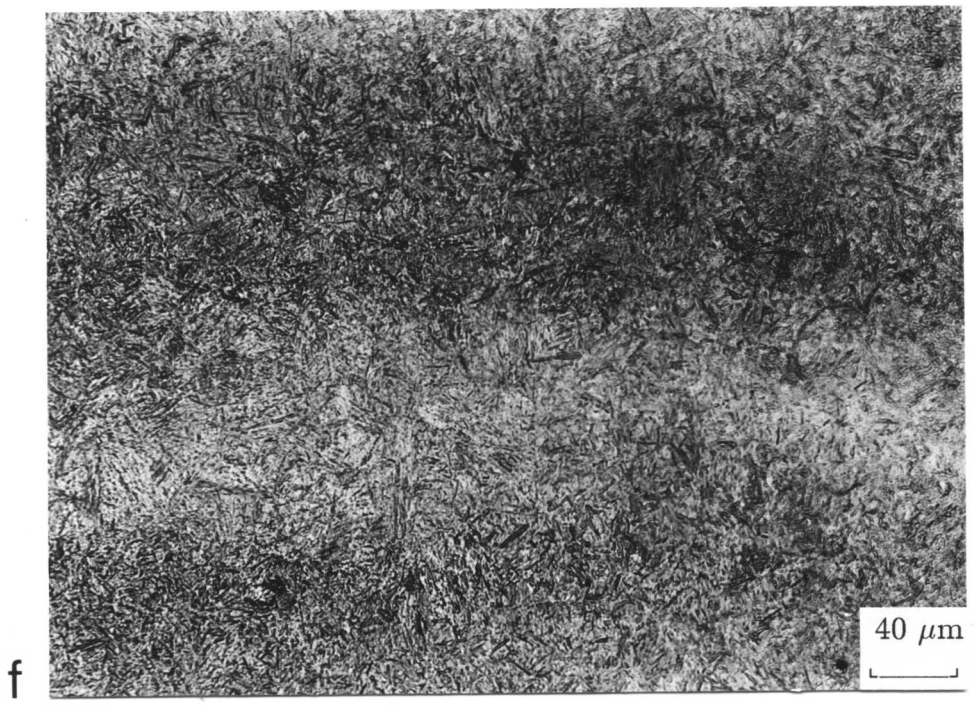

Fig. 6.22: *(continued .....)*

(e) Optical micrograph of the heterogeneous specimen isothermally reaustenitised at 760 °C.

(f) Optical micrograph of the heterogeneous specimen isothermally reaustenitised at 770 °C.

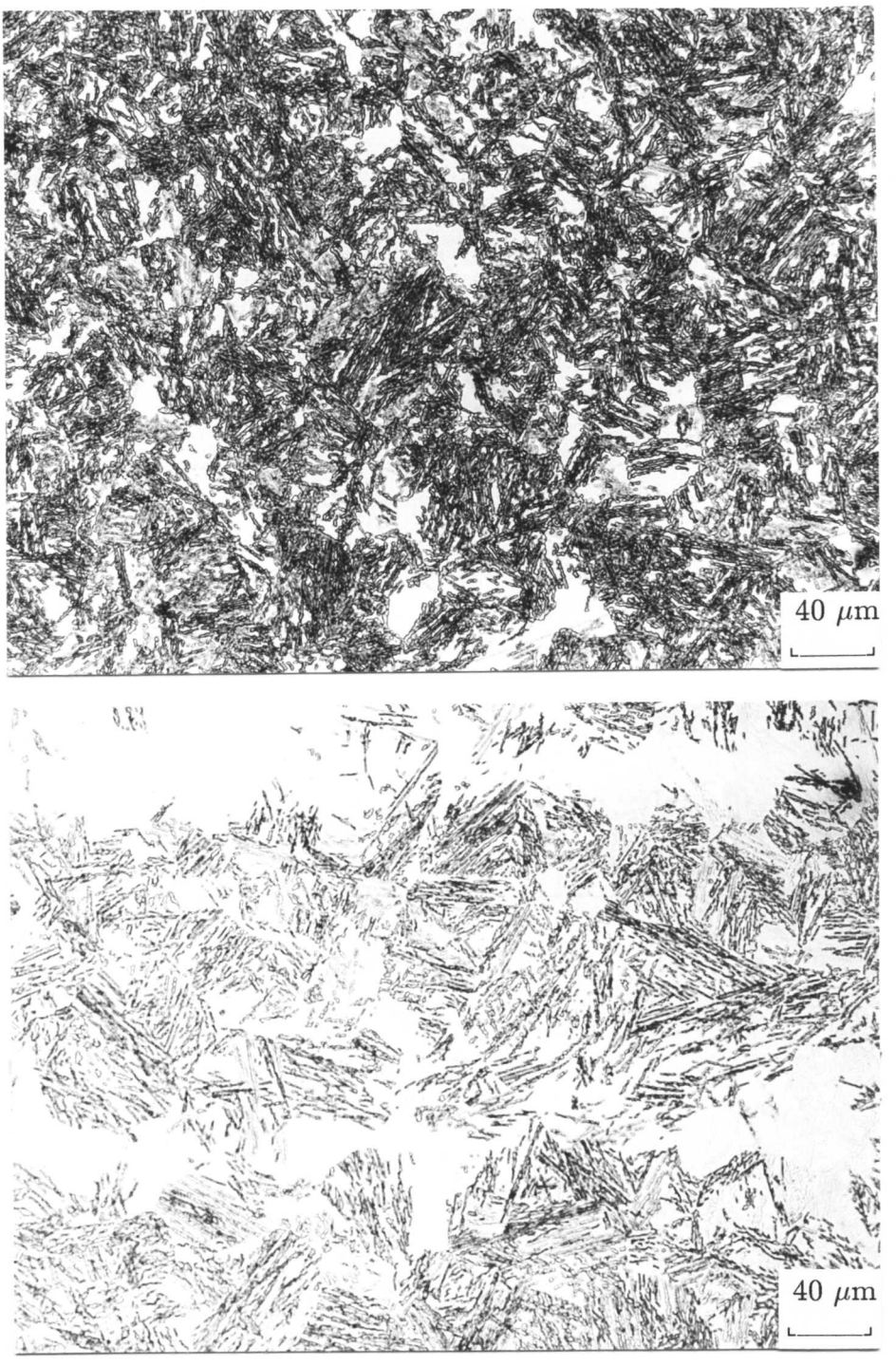

Fig. 6.23: *Metallographic confirmation of the curves shown in Fig. 6.6. The samples were initially transformed to bainitic ferrite and carbon enriched residual austenite at 400 °C.*

(a) Optical micrograph of the heterogeneous specimen isothermally reaustenitised at 700 °C.

(b) Optical micrograph of the heterogeneous specimen isothermally reaustenitised at 715 °C.

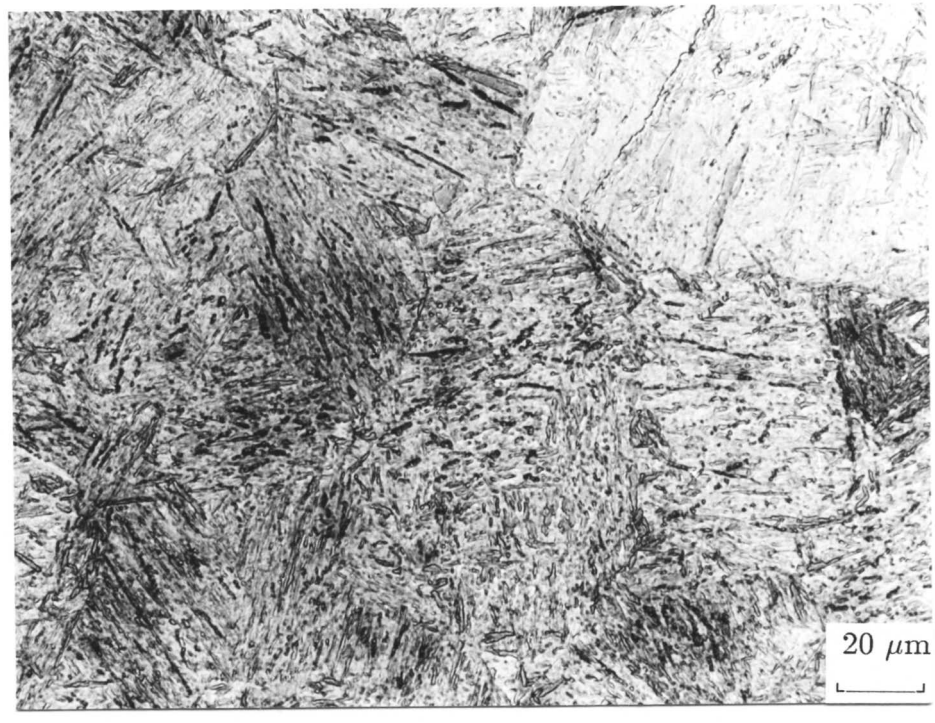

c

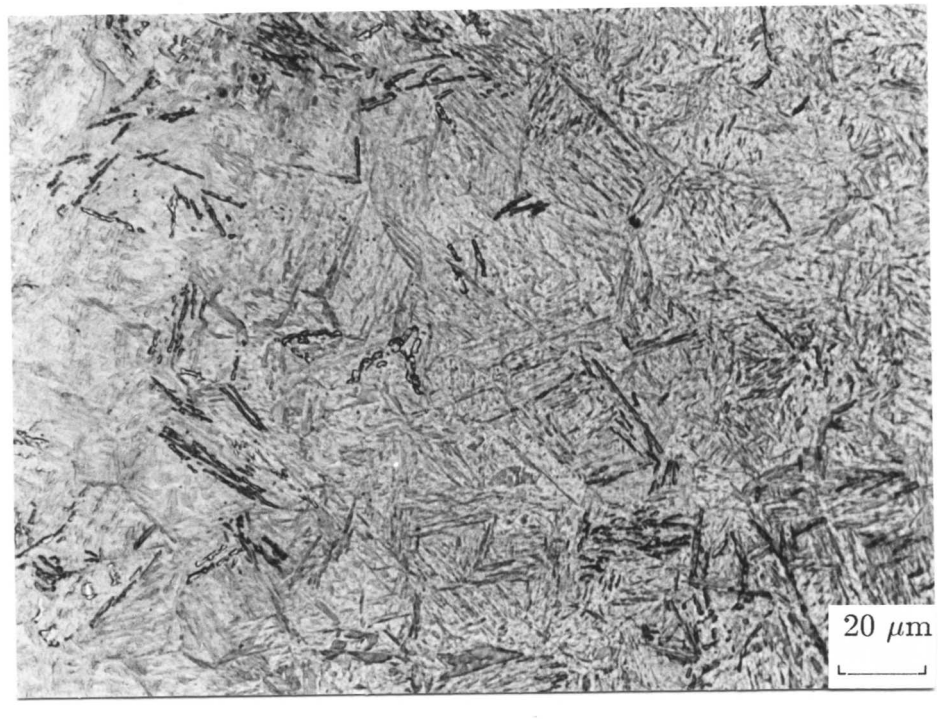

d

Fig. 6.23: *(continued .....)*

(c) Optical micrograph of the heterogeneous specimen isothermally reaustenitised at 730 °C.

(d) Optical micrograph of the heterogeneous specimen isothermally reaustenitised at 760 °C.

REFERENCES

1. H. K. D. H. Bhadeshia: *Advances in the Science and Technology of Welding*, Eds. S. David and S. Vitek, ASM International, Ohio, USA, 1990, in press.
2. G. J. Davies and J. G. Garland: *Int. Met. Rev.*, 1975, vol. 20, p. 83.
3. R. A. Roberts and R. F. Mehl: *Trans. ASM.*, 1943, vol. 31, p. 613.
4. G. R. Speich and A. Szirmae: *Trans. TMS-AIME*, 1969, vol. 245, p. 1063.
5. G. R. Speich, V. A. Demarest and R. L. Miller: *Metall. Trans.*, 1981, vol. 12A, p. 1419.
6. X-L. Cai, A. J. R-Garratt and W. S. Owen: *Metall. Trans.*, 1985, vol. 16A, p. 543.
7. C. I. Garcia and A. J. DeArdo: *Metall. Trans.*, 1981, vol. 12A, p. 521.
8. U. R. Lenel and R. W. K. Honeycombe: *Metal Science*, 1984, vol. 18, p. 201.
9. P. Cotterill and P. R. Mould: *Recrystallization and Grain Growth in Metals*, 1976, Surrey University Press, London.
10. E. C. Bain: *Alloying Elements in Steel*, ASM, Cleveland, OH, 1939.
11. W. S. Owen: *Trans. ASM*, 1954, vol. 46, p. 812.
12. J. Gordine and I. Codd: *JISI*, 1969, vol. 207.1, p. 461.
13. R. M. Hobbs, G. W. Lorimer and N. Ridely: *JISI*, 1972, vol. 210.2, p. 757.
14. A. G. Allten and P. Payson: *Trans. ASM,* 1953, vol. 45, p. 498.
15. A. S. Keh and W. C. Leslie: *Mater. Sci. Res.,* Plenum Press, New York, NY, 1963, vol. 1, p. 208.
16. H. K. D. H. Bhadeshia and D. V. Edmonds: *Acta Metall.*, 1980, vol. 28, p. 1265.
17. H. K. D. H. Bhadeshia: *Proceedings of the International Solid-Solid Phase Transformations Conference,* Pittsburgh, p. 1041, 1981.
18. J. R. Yang and H. K. D. H. Bhadeshia: *Phase Transformations '87*, p. 203, Ed. G. W. Lorimer, Institute of Metals, London, 1988.
19. J. R. Yang: *Ph.D. Thesis*, University of Cambridge, 1988.
20. H. K. D. H. Bhadeshia: *Acta Metall.*, 1981, vol. 29, p. 1117.
21. H. K. D. H. Bhadeshia: *Metal Science*, 1981, vol. 15, p. 175.
22. H. K. D. H. Bhadeshia: *Metal Science*, 1981, vol. 15, p. 178.